POLITECNICO DI MILANO
DIPARTIMENTO DI CHIMICA, MATERIALI E INGEGNERIA CHIMICA
"GIULIO NATTA"

Doctoral Program in
Materials Engineering

YIELD AND POST-YIELD BEHAVIOUR OF SEMICRYSTALLINE POLYMERS: OPEN ISSUES OF PRACTICAL INTEREST

Doctoral dissertation of
Nadia PERILLO

Supervisor
Prof. Claudia MARANO

Tutor
Prof. Marta RINK

The Chair of the Doctoral Program
Prof. Chiara CASTIGLIONI

XXVII Cycle

to Marcello and my family

Nadia

Summary

This PhD thesis covers three different research topics in the field of science and technology of polymeric materials. They all have in common the fact that the knowledge of the yield and/or the post yield behavior is necessary for their analysis. Further, they all deal with semicrystalline polyolefins.

The first one regards the study of the yield and post-yield behavior of syndiotactic polypropylene in relation to the strain-induced structural changes.

The second one regards a methodology to characterize fracture toughness of polymeric films, the Essential Work of Fracture. The validity of this method requires that the fracture propagation occurs within plastically deformed material.

The last topic concerns a method to predict the long term failure of polymeric materials under creep loading when the plasticity controlled failure occurs.

This PhD thesis is divided in four chapters. In the first one a brief description of the main deformation mechanisms of semicrystalline polymers, as concerns polyolefins, is presented. The next three chapters deal with the topics just presented.

Contents

Index of tables

Chapter 2.

Chapter 3.

Chapter 4.

Index of figures

Chapter 1.

Chapter 2.

Chapter 3.

Chapter 4.

Chapter 1

Semicrystalline polymers and their deformation mechanisms

Semicrystalline polymers are biphasic materials in which the crystalline phase consists of stacks of crystalline lamellae embedded in a disordered entangled amorphous phase. [1] A highly interconnected network (the crystalline domains are connected by "tie molecules") is characteristic of semicrystalline polymers. The lamellar crystals are formed by mostly folded chains as in Figure 1b. They are generally twisted along their long axis and organized in a radial superstructure, a polycrystalline aggregate known as "spherulite" (Figure 1a).

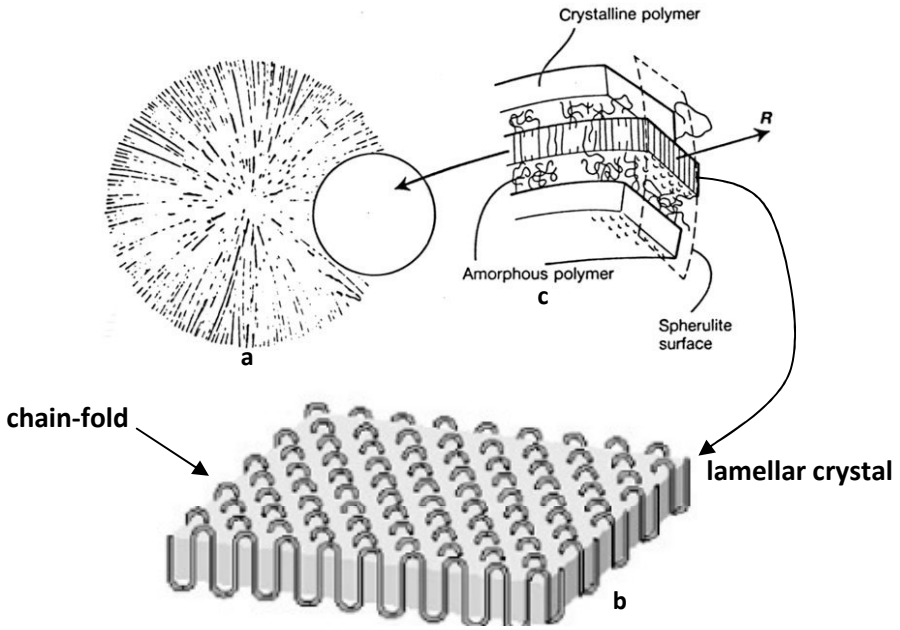

Figure 1. ***(a) Spherulite composed of lamellar crystals characterized by a chain-folded structure (b) and of the amorphous inter-lamellar phase (c)***

The peculiar features of the final resulting microstructure in a semicrystalline polymer depend both on the type of polymer and its molecular microstructure (tacticity, molar mass, amount of chain branching etc…) but also on crystallization conditions as the cooling rate, the presence of orientation in the melt, the melting temperature, etc….

The investigated semicrystalline polymers in this thesis work are α-polyolefins (polyethylene and polypropylene). Their glass transition temperatures (T_g) are lower than T_{room} (T_{g_HDPE}≈-100°C, T_{g_iPP}≈-10°C, T_{g_sPP} ≈ 0°C) and their amorphous phase is mainly characterized by rubber-like behavior.

Deformation of semicrystalline polymers is a complex multistage process involving spherulites, crystalline lamellae, amorphous phase network, etc….[1] The highly interconnected microstructure in a semicrystalline polymer implicates that the deformation process in the crystalline phase has to be considered simultaneous and consistent with that of the amorphous phase. [1]

At low strains (elastic range) the change in shape of the spherulites present in a semicrystalline polymer is affine. The amorphous layers between crystals would deform earlier than any crystallites but their deformation is quickly prevented by the highly interconnected network between the amorphous and the crystalline phase. [1] In correspondence of the yield point at which the plastic deformation initiates, irreversible shear deformations in the amorphous and in the crystalline phases take place. At higher strains the initial spherulitic morphology is destroyed and a microfibrillar structure, where the macromolecules are aligned along the stretch direction, forms.[1]

Basic deformation mechanisms include crystallographic slips at all strain levels while a melting-recrystallization process, accompanied by the chain-unfolding of crystalline lamellae, is restricted at high applied strains. [1]

Polymeric crystals can deform plastically by mainly crystallographic slips which are similar to deformation mechanisms of non polymeric materials.

A crystallographic slip is the sliding of a crystal along a specific crystallographic plane (slip plane) in a specific direction within this plane (slip direction).[1] In Figure 2 an example of slip direction and of slip plane is reported. ψ is the angle between the force ***F*** and the normal direction of the slip plane while λ is the angle between the force ***F*** and the slip direction.

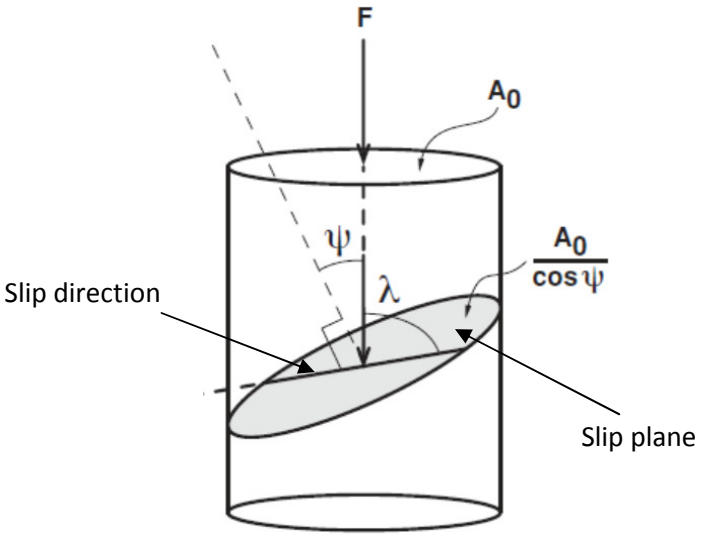

Figure 2. An example of slip direction and of a slip plane along with a crystallographic slip occurs

The slippage of crystals is not isotropic because there are crystallographic planes where slip is easier. A crystallographic slip occurs through a progressive gliding of linear defects or dislocations, along the slip plane.[1]

The macromolecular structure of polymers implicates some peculiarity in the crystallographic slips. The most important one is the fact that only some slip planes are available for the crystal slips. [1] Actually chain rupture has to be prevented and the lattice symmetry as well as the chain folded structure have not to be disrupted. [1] Due to the presence of the chain folding the slips are preferred in the planes which contain the folds. Therefore in polymer crystals the most typical slippage modes are: the longitudinal slip and the transversal slip reported schematically in Figure 3. The first mechanism occurs along the direction of chain axis while the second displays in the direction perpendicular to it, both in the same plane of chain axis.[1]

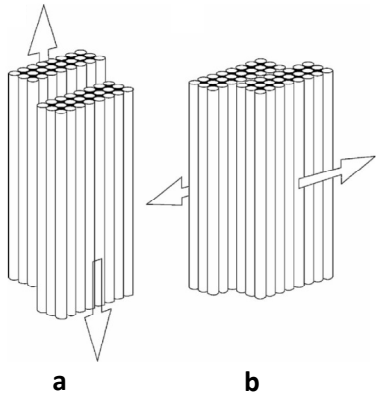

Figure 3. Two types of crystallographic slip in macromolecular crystals: (a) longitudinal slip (b) transversal slip[1]

These mechanisms, occurring within the lamellae, can be either homogeneous (fine) or heterogeneous (coarse).[1-5] The fine slip takes place through the nucleation and propagation of so-called “screw dislocations”: when a shear stress acts on a crystal and reaches a critical value it initiates the propagation of a dislocation that moves along the chain in a wormlike manner causing locally a shortening of the chain and, eventually, when it exits from the crystal,

a translation of the chain.[2-4] The propagation of these defects is responsible of the so-called α-crystalline relaxation. This mechanism causes a change in the angle between the chain axis and the axis normal to lamella: the chain axis rotates in the direction of maximum extension while the axis normal to lamella rotates in the opposite direction (Figure 4b).[1] It also causes the thinning of lamellae.

The heterogeneous slip occurs through defective interfaces within the crystalline blocks and causes the formation of blocks of chains (Figure 4c). [2-4] It causes the rotation of the chain axis and of the axis normal to lamella towards the direction of maximum extension. [1]

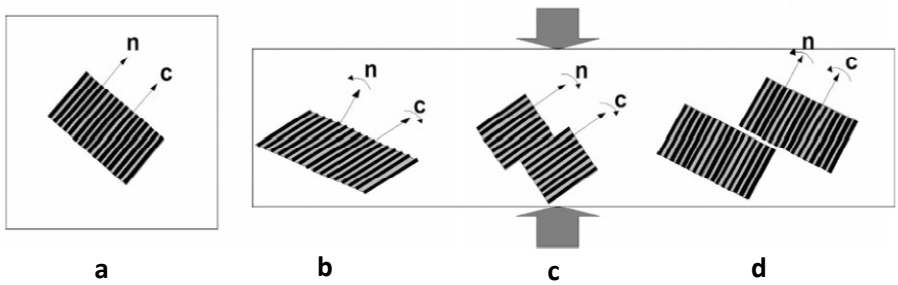

Figure 4. ***Rotation of the chain axis, c and of the axis normal to lamella n produced by fine slip (b), coarse slip (c) and inter-lamellar shear (d). In (a) orientation of both vectors in lamella prior to deformation is shown*** [1]

These two intra-lamellar slip processes (fine and coarse slips) are competitive in the range of temperatures and strain rates usually adopted in studying the mechanical behavior of semicrystalline polymers. The homogeneous slip, which is thermally activated, occurs when the applied strain rate is comparable to the rate of screw dislocations propagation. [2-4] It is generally observed at low strain rates or at high temperatures. The second is activated at high strain rates or at low temperatures.[2-4]

When the heterogeneous crystal slip occurs a sharp neck forms while in the case of fine slip the localization of the plastic instability is less pronounced.[4] Figure 5 shows the macroscopic effect of the two slip mechanisms for a quenched i-PP drawn at T_{room} (a) and 60°C (b). The pronounced neck observed in (a) indicates that localized crystal slips occurred while in (b) the diffuse neck suggests that homogeneous crystal slips occurred.

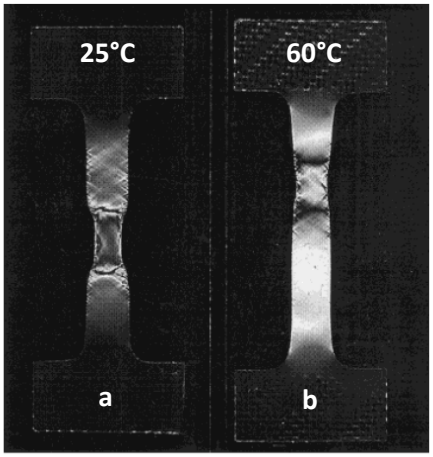

Figure 5. ***Images of dumbbell specimens of quenched isotactic polypropylene drawn at 25°C (a) and at 60°C (b) up to $\varepsilon_N = 0.3$ ($\dot{\varepsilon}$ = 1.05*10^{-3}s^{-1} crossed polarizers)[4] (See text)***

In Figure 4d it is also shown the inter-lamellar shear mechanism which is characteristic of the amorphous phase. It causes the rotation of both the chain axis and the axis normal to lamella away from the direction of maximum extension.[1] It was reported in literature that the reversible inter-lamellar slip has the main role in the strain recovery due to the rubber-like mechanical behavior of the "tie molecules".[1]

Performing X-ray measurements allows to understand what kind of mechanism occurs observing the rotation of the chain axis and of the axis normal to lamellar plane.

Strobl et al. have performed a systematic study of the mechanical behavior of polyolefins tested through loading-unloading tests in tensile loading conditions and have determined at the end of unloading of each cycle the residual and the recovered strain components. [6-9]

The main finding of these studies was that the strains at which different deformation mechanisms become active are characteristic of the polymers irrespective of crystallinity degree, temperature and strain rate. [6-9]

The invariance of these strains indicates a fairly homogeneous deformation in a semicrystalline polymer. Actually, as previously reported the crystalline and the amorphous phase have to deform consistently. This behavior is guaranteed by the presence of a highly interconnected structure in which crystallographic slips and the inter-lamellar shear modes act together.[1,5]

The onsets of these mechanisms were determined by the authors through X-ray measurements performed on stretched samples and are referred to as points A,B,C,D.

They correspond to:

- ***A***: onset of isolated shears (inter-lamellar slips) and intra-lamellar (fine and coarse) slip processes.[6] In Figure 6 a schematic representation of the inter-lamellar slips (shear) and intra-lamellar slips (fine and coarse slips) is reported. These mechanisms are the same reported in Figure 4b-d.It is the limit of the linear elastic behavior above which a residual strain can be measured. In Figure 7 the applied (step cycle), the recovered (cyclic) and the residual (basic) strains are reported as function of the applied true stress. The data are relevant to loading-unloading tensile tests performed on a PEVA12.[6] It can be observed

that up to point A the applied strain and the recovered strain component are identical.

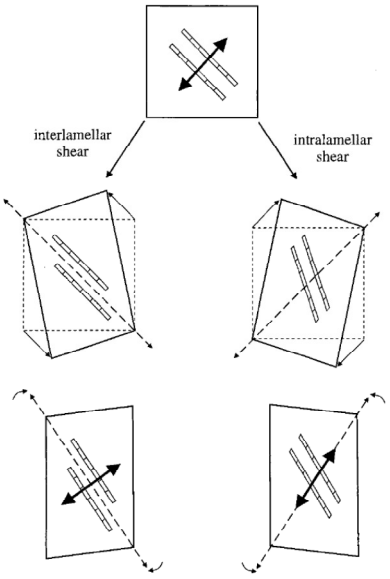

Figure 6. ***Schematic representation of shear (inter-lamellar slips) and intra-lamella slips (fine and coarse slips)*** [6]

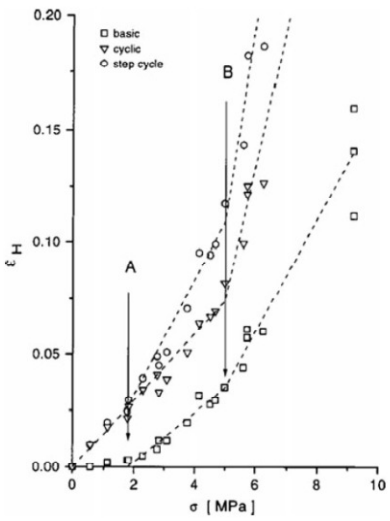

Figure 7. ***Applied (step cycle), recovered (cyclic) and residual (basic) strains as function of the applied true stress. Data relevant to loading-unloading tensile tests performed on a PEVA12. Arrows indicate location of the points A and B*** [6]

- ***B***: the yield point at which inter-lamellar shears and intra-lamellar slips occur cooperatively. Actually it is not the onset of the fully plastic flow because the recovered strain (cyclic) increases above this point. [5] (Figure 7).
- ***C:*** the beginning of crystalline lamellae fragmentation when the "tie molecules" reach their maximum extension and the crystalline blocks are not more stable.[5] A microfibrillar structure (macromolecules aligned along the loading direction) begins to form. At this point the recovered strain component assumes a constant value as shown in Figure 8.

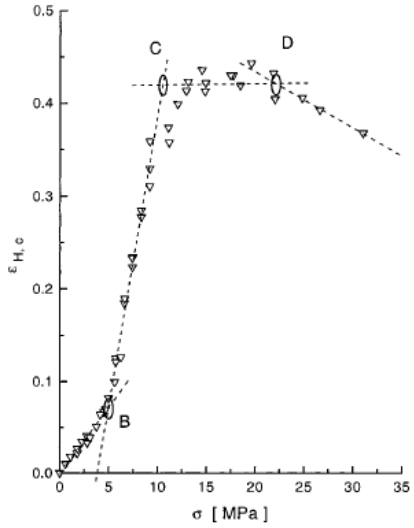

Figure 8. ***Applied (step cycle), recovered (cyclic) and residual (basic)strains as function of the applied true stress. Data relevant to loading-unloading tensile tests performed on a PEVA12. Points C and D are reported*** [6]

- ***D:*** chain disentanglement corresponding to a truly plastic deformation.

  In Figure 9a as an example the residual strain of a HDPE strained up to $\varepsilon_H = 1$ is reported versus the temperature of the thermal treatment applied after the unloading.[6] It can be observed that the residual strain gradually decreases up to about T=100°C and then fast decreases at higher temperatures. An irreversible residual strain component (truly plastic strain) remains after a thermal treatment. Similar results were obtained for other polyolefins as shown in Figure 9b where the residual strain after heating, $\varepsilon_{H,i}$, is plotted as function of the applied strain for HDPE, LDPE 33 and PEVA12.[6] It can be observed that only applying a true strain higher than 1 (point D for polyethylens) a truly plastic strain can be determined also after a thermal treatment.

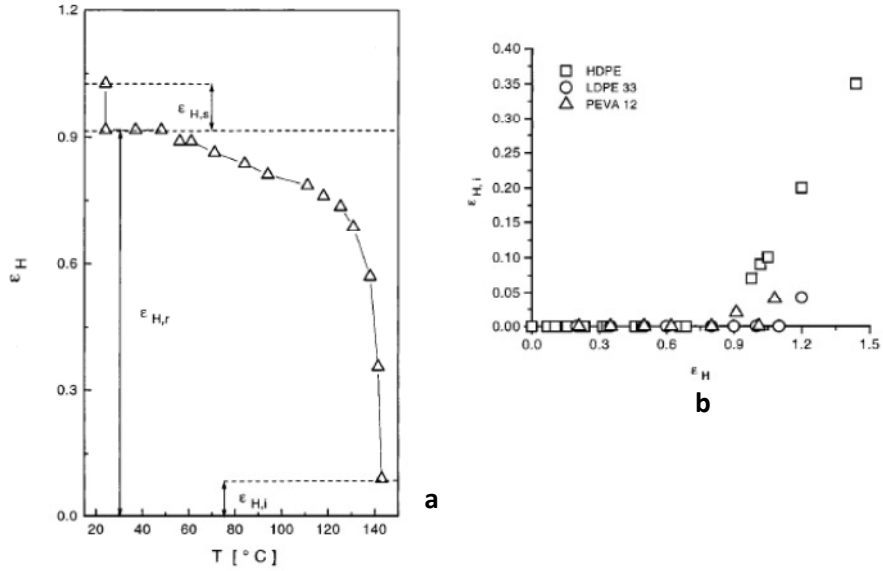

Figure 9. ***(a) Residual strain versus the temperature of the thermal treatment applied after the unloading for a HDPE. The recovered and the residual strain components at T_{room} at the end of unloading , $\varepsilon_{H,s}$ and $\varepsilon_{H,r}$,and the truly irreversible plastic deformation found at the highest temperature, $\varepsilon_{H,i}$ are reported*** [6]

(b) Residual strain component after heating , $\varepsilon_{H,i}$ as function of the applied strain for HDPE, LDPE 33 and PEVA12 [6]

This scheme is also valid in plane strain compression of semicrystalline polymers.[5]

As example Figure 10 shows the true stress-strain curves for three different polyethylenes and polyethylenvinilacetates differing in their crystallinity degree. The characteristic points B-D as reported in literature are indicated.[6]

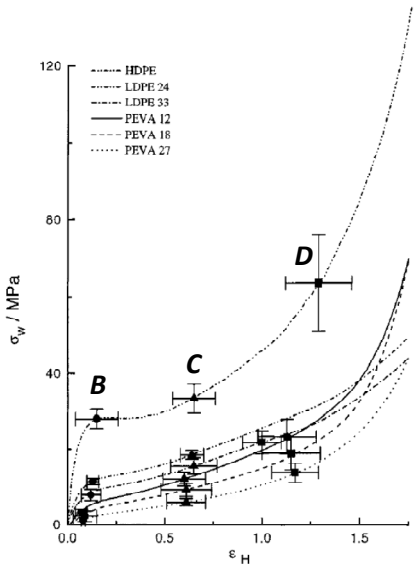

Figure 10. ***True stress-strain curves for three different polyethylenes and polyethylenvinilacetates differing in their crystallinity degree. The characteristic points B-D are reported*** [6]

It can be observed that in correspondence of these characteristic points the strains are equal for all the tested materials while the stresses depend on the crystallinity degree (temperature and strain rate are the same for all the tests).

Bibliography

1. Z. Bartczak, A. Galeski, *Macromol. Symp* **2010**, *294-1*, 67-90
2. R. Séguéla, V. Gaucher-Miri, S. Elkoun, *J. Mater. Sci.* **1998**, *33*, 1273-1279
3. R. Séguéla, S. Elkoun, V. Gaucher-Miri, *J. Mater. Sci.* **1998**, *33*, 1801-1807
4. R. Séguéla, E. Staniek, B. Escaig, B. Fillon, *J. Appl. Polym Sci.***1999***, 71,*1873-1885
5. S. Patlazhan, Y. Remond, *J. Mater. Sci.* **2012**, *47*,6749-6767
6. R. Hiss , S. Hobeika, C. Lynn, G. Strobl, *Macromolecules* **1999**, *32*, 4390-4403
7. K. Hong, A. Rastogi, G. Strobl, *Macromolecules* **2004,** *37***,**10265-10173
8. Y. Men, J. Rieger, G. Strobl, *Phys. Rew. Lett*. **2003**, *91*, 095502-1.
9. S. Hobeika, Y. Men, G Strobl, *Macromolecules* **2000**, *33*, 1827-1833.
10. Y. Men, G. Strobl, *J. Macromol. Sci.-Physics* **2001**, *B40*, 775-796.

Chapter 2

A study of the yield and post-yield behavior of syndiotactic polypropylene

2.1 Introduction

A recently published paper included in this chapter reports the main results of the study performed to characterize the mechanical behavior of syndiotactic polypropylene (s-PP) in relation to its microstructure. A brief summary is first reported (paragraph 2.2).

In order to make easier the reading of the paper in paragraph 2.3 a more detailed description of the crystalline polymorphism of s-PP is reported.

In paragraph 2.4 the possibility to use s-PP as an “elastomeric material” is discusses referring to literature.

In the paragraph 2.5 tests performed to characterize the “elastomeric” behavior of s-PP are described and relevant results discussed.

2.2 Paper abstract

Loading-unloading tensile tests were performed to study the residuals strain dependence of the applied strain for three commercial s-PP differing in pentad [rrrr] percentage content. Note 1

A suitable experimental method was set up: it allowed to confirm literature results relevant to s-PP and to investigate a wider strain range.

The results obtained were analyzed referring to literature as concerns strain-induced structural modifications.

The lamellae fragmentation onset, which is attributed to an heterogeneous crystal slip, occurs at a material dependent strain value: nevertheless the residual strain due to this microstructural change resulted to be the same irrespective of the material.

Note 1: Pentad [rrrr] content is a stereoregularity index (for a fully syndiotactic polypropylene is equal to 100%). It is the percentage of the sequences of chiral carbon atoms in alternating configuration (racemic diad, r).

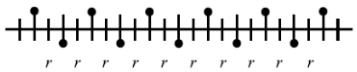

fully syndiotactic polypropylene [1]

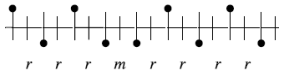

presence of a meso diad [1]

2.3 s-PP polymorphism

Syndiotactic polypropylene is characterized by a very complex polymorphism. It shows different crystalline structures depending on the crystallization conditions, strain rate and temperature. In literature four different polymorphic forms named I, II,III and IV and a mesomorphic disordered form are reported.[1] In Figure 1 models of packing of chains in s-PP are reported. Table 1 summarizes the unit cell dimensions for the different s-PP's forms.

The most stable form of s-PP is the form I. When slowly cooled from the melt state or when crystallized from solution, s-PP shows a crystalline phase in form I consisting of an antichiral packing (right-handed and left-handed chains alternating along a and b axis of the unit cell) in which the macromolecular chains show a two-fold helical conformation in an orthorhombic unit cell (Figure 1a). [1] When s-PP is quickly crystallized at low temperatures disordered form I is present. The form I is stabilized at temperature higher than 60°C.[1]

Form II is a metastable form of s-PP characterized by a C-center orthorhombic unit cell in which the macromolecular chains arranged in a helical conformation are packed with the same chirality (Figure 1b). [1] When s-PP is crystallized from the melt state at elevated pressure (above 2kbar) crystals of form II are obtained.[1] Also in the case of the melt-crystallization process of low stereoregular s-PPs a mixture of crystals in form I and II is obtained. The form II can be obtained also in annealed stretched s-PP.[1]

Form III is a metastable form of s-PP, characterized by a orthorhombic unit cell where the macromolecular chains arranged in a trans-planar conformation are packed (Figure 1c). [1]

Form III is characterized by a conformation energy higher with respect to that of form I and form II.

Form IV is a metastable form of s-PP, in which the helical chains are packed with the same chirality in a C-center monoclinic unit cell with β_m=108.8° (Figure 1d). [1] Others authors state that the form IV unit cell is triclinic. [2] Form IV was firstly obtained exposing stretched s-PP originally in trans-planar form III to organic solvents. It is metastable and readily transforms into the twofold helical forms by annealing above 50°C.

s-PP can present also a metastable mesomorphic form characterized by a disordered packing of chains in trans-planar conformation. When s-PP is quenched under quiescent conditions from the melt state to 0°C and kept at this temperature for a quite long time (at least 20h) s-PP crystallizes in this trans-planar mesomorphic form. [1] The higher the stereoregularity degree the shorter the time the polymer has to be kept at 0°C to stabilize the mesomorphic form and to inhibit the formation of form I when the material is heated from 0°C to 25°C. If present at T_{room} the mesomorphic form transforms into form I by annealing at 90°C.[1] For a highly stereoregular s-PP ([rrrr]=96%) the crystallinity degree that can be obtained quenching from the melt to 0°C and maintaining the material at 0°C for a long time is at maximum 30%.

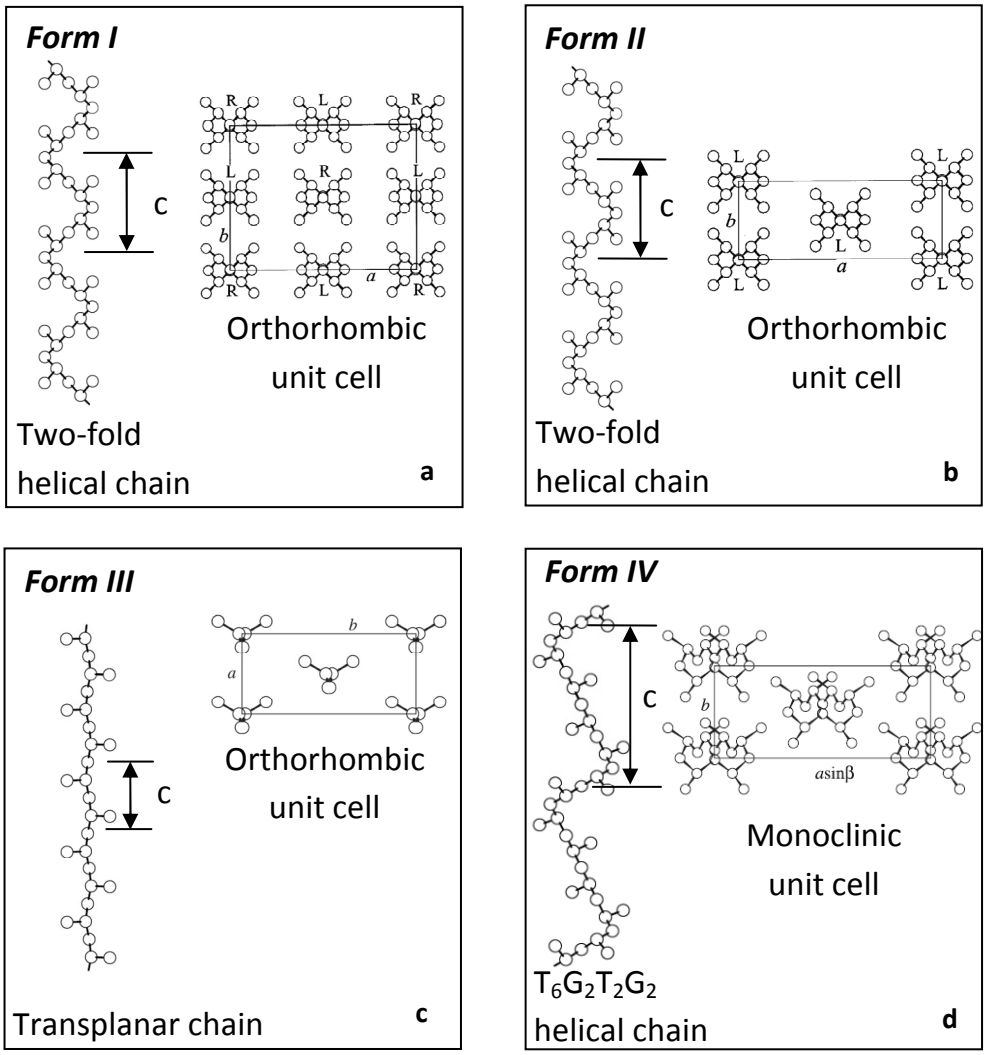

Figure 1. ***Models of packing of chains in syndiotactic polypropylene*** [1]

Crystallographic Axes (Å)	***Form I*** *Orthorhombic unit cell*	***Form II*** *Orthorhombic unit cell*	***Form III*** *Orthorhombic unit cell*	***Form IV*** *Monoclinic unit cell*
a	14.5	14.5	5.22	14.17
b	11.2	5.6	11.17	5.72
c	7.4	7.4	5.06	11.60

Table 1. ***Unit cell dimensions for the different forms of s-PP*** [1]

By performing X-ray measurements on strained samples De Rosa et al.[1,3-16] observed that the s-PP polymorphic form I transforms into trans-planar form III, when the polymer is stretched up to high strains. This form transition is irreversible. When s-PP is unloaded, form III transforms in the metastable form II. The form III -> form II transition is reversible and the process occurs at the same time scale of the deformation applied on the material. A significant fraction of the applied strain is recovered during the unloading. The distance between four monomeric units which constitute the structural unit in the helical form changes from 7.4 Å, in the helical form, to 10.2 Å, in the transplanar from, as shown in Figure 2 for the reversible form II/form III transformations. Crystal dimensions increase of about 38% along their c axis during the stretching. When unloaded the crystals recover their initial dimensions in a fast structural transition.

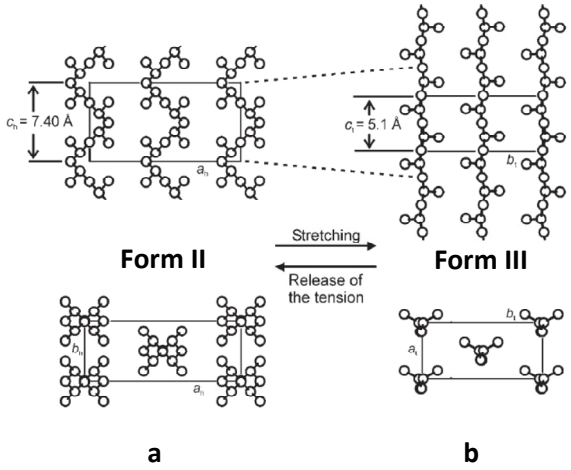

Figure 2. Reversible crystal-crystal transition between form II (a), stable after unloading , and form III (b), stable at high applied strains

According to De Rosa et al.,[1,6,11] at least a part of the recovered strain in the unloading can be attributed to the form III -> form II transition.

The authors state also that these crystal form transitions do not cause any change in the polymer crystallinity degree.

De Rosa et al.[1,3-16] also measured the strain at which the transformation of form I into form III starts and is completed: it resulted to be dependent on the pentad [rrrr] content. The appearance of a mesophase in place of form III or previous to form III formation is also controlled by the syndiotactic pentad [rrrr] content. In Figure 3, the deformation ranges, where the different polymorphic forms have been observed in several s-PP differing in the pentad [rrrr] concentration are reported. All the studied materials had been slowly cooled from the melt state: in the unstrained samples, a disordered form I was observed in the case of the lower [rrrr] pentad percentage content (46,54,60%); for the higher [rrrr] pentad percentage considered (91.8%) only the ordered form I was observed; in the s-PP with 72,78 and 87 [rrrr] pentad percentage both form I and form II were present (form I was predominant).

It could be useful for the reader to know that the materials considered in the paper included in this chapter are those corresponding to [rrrr] percentage of 91.5, 78 and 54%, highlighted in Figure 3 with arrows.

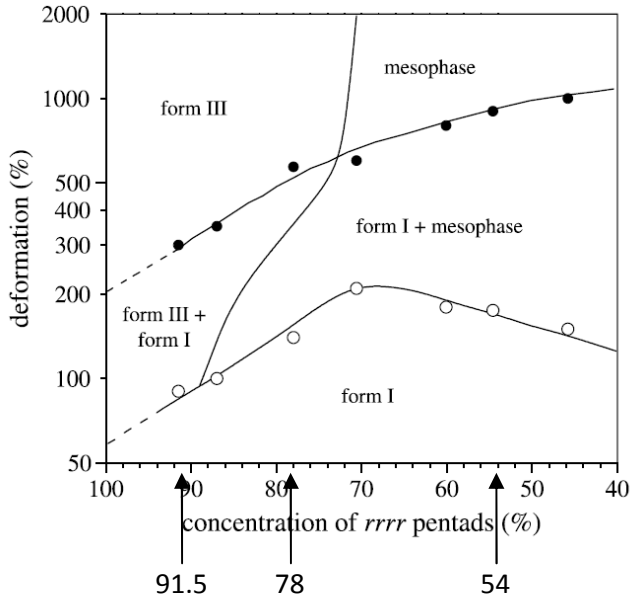

Figure 3. ***Strain values at the onset (open cyrcle) and at the end (full cyrcle) of the form I -> form III transformation as a function of [rrrr] pentad content*** [16]

For s-PP with a pentad content [rrrr] of 91.8 the form I gradually transforms into form III in the strain range of 90-300%. For s-PP with pentad [rrrr] percentage of 72, 78 and 87, form I firstly transforms into the mesomorphic form and then, at higher strains, the more ordered form III appears. The transformation is complete at a strain of 600%. For the lower [rrrr] pentad content (45, 54 and 60%) the ordered form III can never form because of the regioirregularities present along the chains: an oriented mesomorphic form forms. During the unloading form III transforms into form II, while the mesomorphic form transforms in form I.

According to De Rosa et al. the transformation of form I into form III or into mesophase is a mechanically induced melting of the form I crystals and a fast recrystallization into the trans-planar form with a negligible crystallization of the amorphous phase.[15]

The scheme reported in Figure 4 summarizes the crystals form transitions occurring in s-PP under straining or as a consequence of annealing.

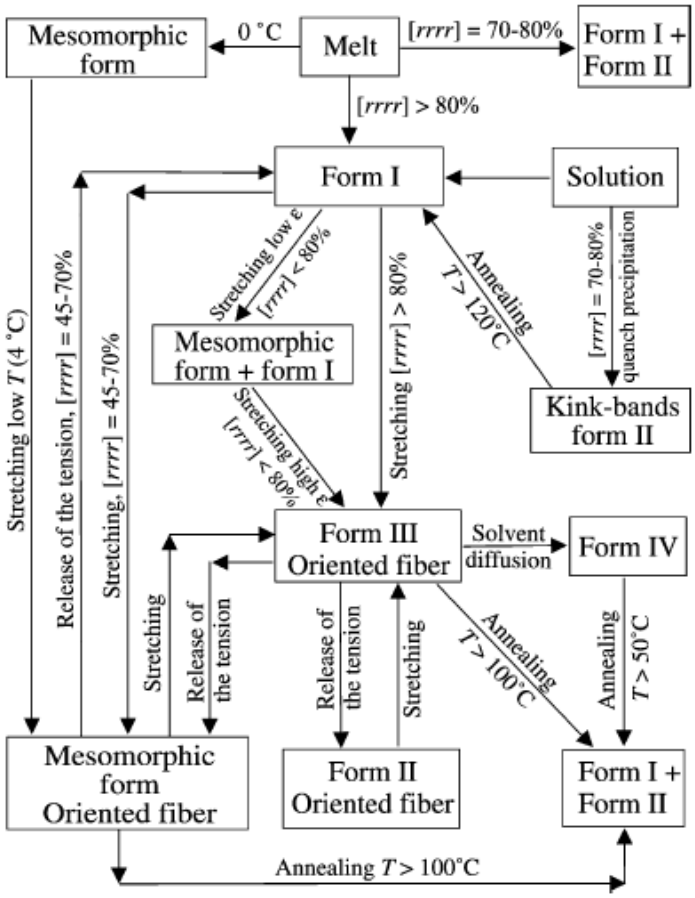

Figure 4. A scheme of the crystal form transitions observed in s-PP induced by annealing or straining [1]

2.4 s-PP: a thermoplastic elastomer?

The research activity performed on the characterization of the mechanical behavior of syndiotactic polypropylene (s-PP), finalized to the paper publication, started within a collaboration with the research group of Prof. De Rosa of the Chemical Science Department of Università degli Studi di Napoli "Federico II". This research group has performed a wide structure characterization of semicrystalline polyolefins (among which s-PP) since '80s and, as reported in paragraph 2.3, they also studied the strain-induced crystal form transitions of s-PP. As reported in literature (see for example 1) they proposed the use of s-PP as a thermoplastic "elastomer". As observed in Figure 5a (blue curve) and also reported in the paper included in the chapter, when s-PP is strained well beyond the yield point and then unloaded, it recovers a quite large part of the applied strain. This behavior is significantly different from that of the isotactic polypropylene in which the strain recovery is negligible as shown in Figure 5a where the true stress-strain curve relevant to the loading-unloading test performed on a i-PP is reported for comparison (black curve). The test on i-PP was performed by the author of this thesis in the same conditions adopted for s-PP.

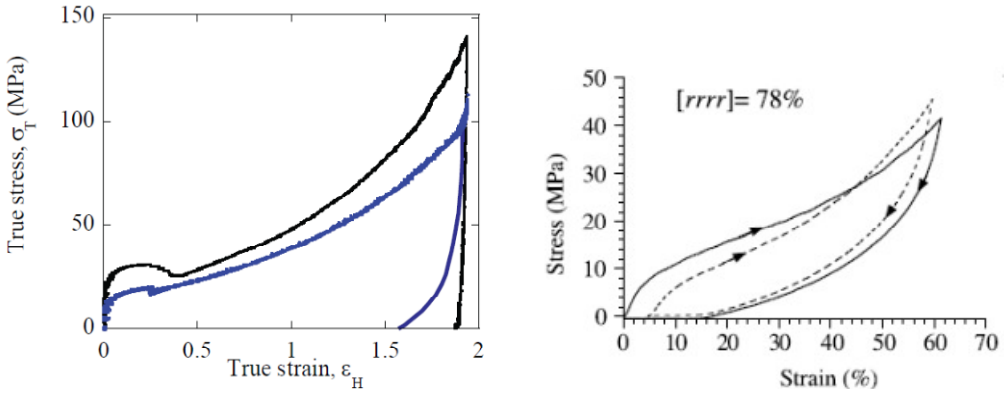

Figure 5. ***(a)True stress-strain curves of a iPP (black) and s-PP78 (blue). Uniaxial tensile tests performed on dumbbell specimens (gauge length of 33mm) at a constant displacement rate of 5mm/min at T_{room}.(b) Nominal stress-strain curves of "plastically" deformed s-PP78 (1° cycle after the plastic deformation process – solid line-; 4° cycle after the plastic deformation process - dotted line -)[1]***

As reported in literature[1] if s-PP is "plastically" deformed (i.e. strained above its yield point), and strained again after the unloading, it will show an "elastomeric" behavior: it will recover almost completely the applied strain when unloaded, as shown in Figure 5b. The strain range within s-PP will show this "elastomeric behavior" is upper limited by the value of the strain that was recovered during the unloading of the "plastically" deformed s-PP. Referring to the example in Figure 5a this range is equal to the difference between the applied strain ε_H=1.88 and the residual strain ε_{H_res}= 1.6 that is $\varepsilon_H - \varepsilon_{H\_res} = \varepsilon_{H\_rec} = 0.28$. If the "plastically" deformed s-PP is strained above this limit, a further plastic deformation will occur.

Within the collaboration with De Rosa group the possibility to produce s-PP fibers or films with an "elastomeric behavior" through the extrusion and cold drawing processes to induce the structural transformations and promote the

"elastomeric" behavior of s-PP was considered. To this aim a preliminary investigation of the "elastomeric" behavior of "plastically" deformed s-PP was performed to integrate the previous research performed by De Rosa's group.

2.4.1 Mechanical behavior of "plastically" strained s-PP

In this paragraph some results relevant to the mechanical behavior of the "plastically" deformed s-PP (not reported in the paper), are shown and discussed. Figure 6 (data from Figure 9b of the paper) shows the dependence of the strain recovered after unloading by virgin s-PP as function of the strain applied in tensile loading conditions.

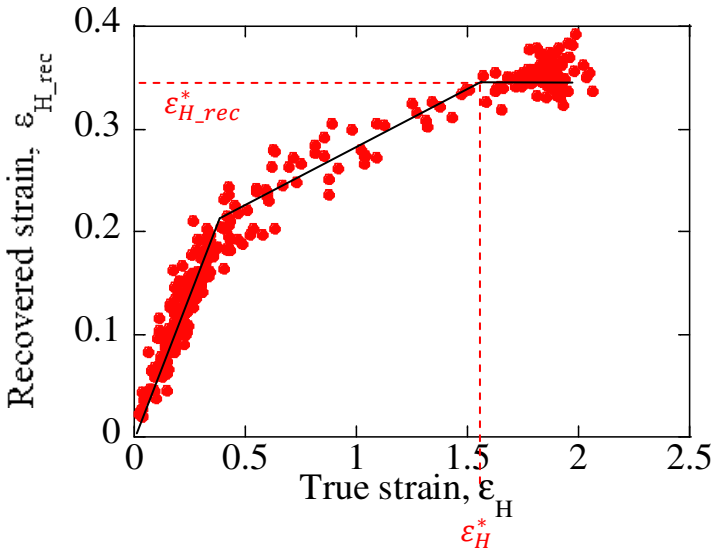

Figure 6. ***Dependence of the recovered true strain component at the end of unloading on the applied true strain for s-PP78 . Black lines are eyeguide***

Data are relevant to one of the studied materials having a [rrrr] pentad content of 78%. It has to be observed that the recovered strain at first increases and then it reaches a plateau level (here indicated as $\varepsilon^*_{H\_rec}$) in correspondence of the value of applied strain (here indicated as ε^*_H) which is

dependent of the material structure. For strain higher than ε_H^*, material deformation is fully plastic.

As stated in literature [1] and reported in paragraph 2.4 $\varepsilon_{H\_rec}^*$ is the strain range in which the "plastically" deformed s-PP will show an "elastomeric" behavior if re-loaded: this means that the virgin s-PP has to be "plastically" deformed up to ε_H^* (corresponding to the beginning of ε_{H_rec} plateau) to optimize its "elastomeric" behavior when subsequently strained.

To investigate preliminarily the "elastomeric" behavior of s-PP, multi-cycle loading-unloading uniaxial tensile tests were performed at a constant displacement rate on the "plastically" deformed s-PP78.

The following procedure was adopted:

1. virgin s-PP78 was stretched up to different nominal strain levels and unloaded (dumbbell specimens were tested at T_{room} and at a nominal strain rate of 0.15min^{-1})
2. rectangular shaped specimens of about 30 mm long were cut from the deformed dumbbell specimens
3. four subsequent loading–unloading cycles in tensile loading conditions were performed on each rectangular shaped specimens at T_{room} and at a nominal strain rate of 0.15min^{-1} after 0.5h, or 120h or 7200h. This time lag as referred to as $t_{recovery}$ in the following .
4. the residual strain component of the applied strain was measured at the end of unloading of each cycle (black marks placed on the rectangular specimen were used to measure the local strains)

As reported in the paper, necking propagation causes a not homogeneous deformation of the virgin s-PP specimen: rectangular specimens were cut where an almost homogeneous strain of 1.70 and 1.88 was applied.

The rectangular specimens will be referred to as $R_{1.7}$ and $R_{1.88}$ respectively.

In Figure 7 true stress-strain curves of the "plastically" deformed s-PP78 are reported: they are relevant to the first loading-unloading cycle performed on samples $R_{1.7}$. Solid line refers to a $t_{recovery}$= 0.5h and open symbols to $t_{recovery}$=7200h. The results indicate that the longer the recovery time the higher the rigidity of the material. This mechanical behavior can be not ascribed to the viscoelastic strain recovery since it was verified that it is almost completely exhausted 3 minutes after the unloading.

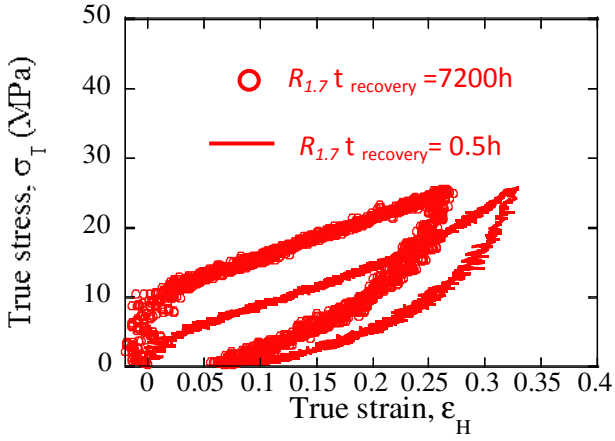

Figure 7. ***True stress-strain curves (1st cycle) relevant to samples $R_{1.7}$ $t_{recovery}$= 0.5h (solid line) and $R_{1.7}$ $t_{recovery}$=7200h (open symbols)***

In Figures 8a-c the true stress-strain curves of the four subsequent cycles performed on the "plastically" deformed s-PP78 are shown. They are relevant to: a) sample $R_{1.7}$, $t_{recovery}$= 0.5h, b) sample $R_{1.7}$, $t_{recovery}$= 7200h, c) sample $R_{1.88}$, $t_{recovery}$= 120h.

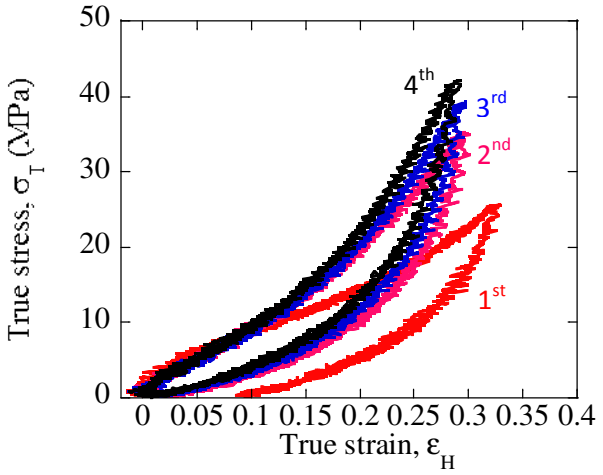

Figure 8a. ***True stress-strain curves of four subsequent cycles performed on $R_{1.7}$ $t_{recovery}$= 0.5h***

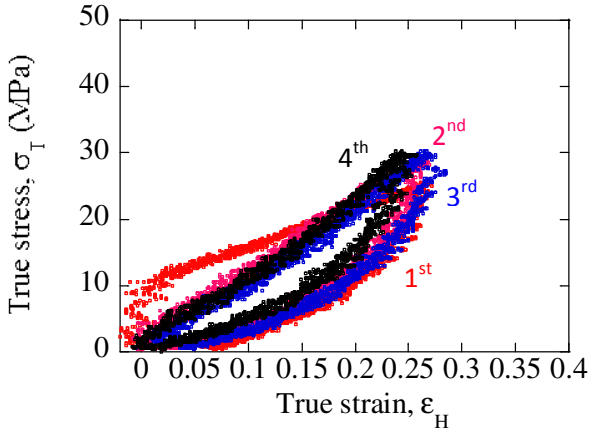

Figure 8b. ***True stress-strain curves of four subsequent cycles performed on $R_{1.7}$ $t_{recovery}$= 7200h***

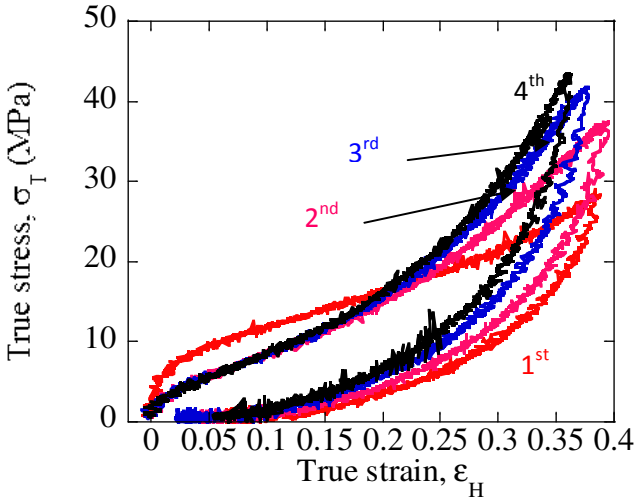

Figure 8c. ***True stress-strain curves of four subsequent cycles performed on $R_{1.88}$ $t_{recovery}$= 120h***

It can be observed that the behavior of the material in the first cycle is quite different from that of the following three which are more similar each other. All these results (Figures 7 and 8a-c) suggest that a change in s-PP78 structure affecting its mechanical behavior occurs within 0.5h (affecting the first cycle also for the lowest recovery time) but in a time range longer than the testing time (the following cycles are similar). The observed time-dependence of the "plastically" deformed s-PP mechanical response should be still investigated more deeply.

In Figure 9a the residual strain measured at the end of each cycle is reported as function of the applied strain for all the tested specimens. In Figure 9b the

percentage of the residual strain, determined as $\frac{\varepsilon_{H_{res},0}}{\varepsilon_H}$, as function of the applied strain for all the tested specimens is reported.

It can be observed that, even though residual strain after the first cycle is higher than that of the following cycles, it seems not to be affected by $t_{recovery}$ and by the value of the strain applied in each cycle. It has to be highlighted that the residual strains are lower than 0.1 (≈25% of the applied strain).

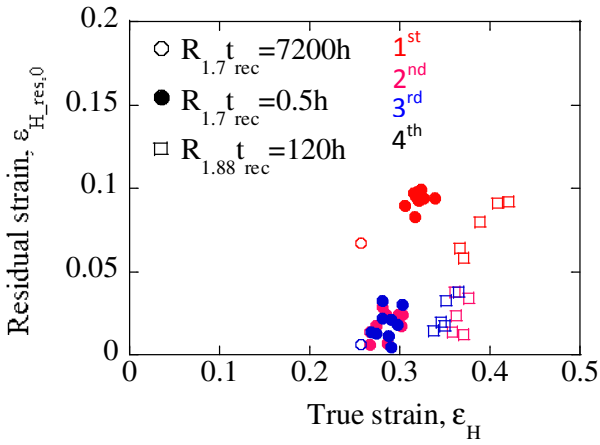

Figure 9a. ***Residual true strain component versus the applied true strain for all the tested specimens***

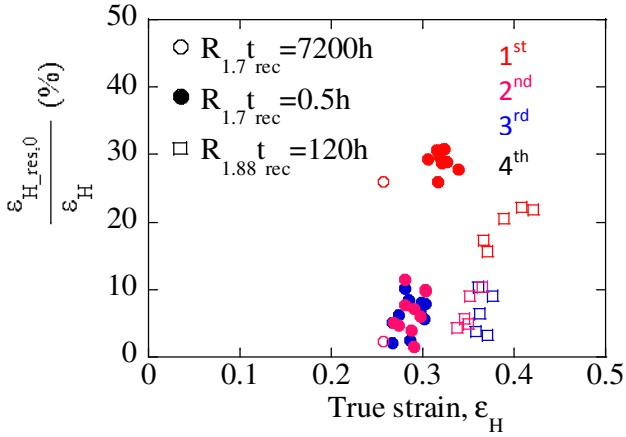

Figure 9b. ***Percentage of residual true strain component versus the applied true strain for all the tested specimens***

Even though this experimental activity was simply a preliminary study and a more deeply characterization of the material behavior is required, the capability of the "plastically" deformed s-PP78 to recover most of the applied strain suggests that s-PP could be suitable for the production of "elastic" fibers or films.

Bibliography

1. C. De Rosa, F. Auriemma, *Prog. Polym. Sci* **2006**, *31*, 145-237.
2. Y. Chatani, H. Maruyama, T. Asanuma, T. Shiomura, *J. Polym. Sci. Polym. Phys.* **1991,** *29,* 1649-1652.
3. C. De Rosa, P. Corradini, *Macromolecules* **1993**, *26*, 5711-5718.
4. C. De Rosa, F. Auriemma, V. Vinti, *Macromolecules* **1998,** *31***,** 7430-7435
5. C. De Rosa, F. Auriemma, V. Vinti, M. Galimberti, *Macromolecules* **1998,** *31***,** 6206-6210
6. F. Auriemma, O. Ruiz de Ballesteros, C. De Rosa, *Macromolecules* **2001,** *34***,** 4485-4491
7. C. De Rosa, F. Auriemma, O. Ruiz de Ballesteros, *Polymer* **2001,** *42***,** 9729-9734
8. C. De Rosa, M.C. Gargiulo, F. Auriemma, O. Ruiz de Ballesteros, A. Razavi, *Macromolecules* **2002,** *35***,** 9083-9095
9. C. De Rosa, F. Auriemma, O. Ruiz de Ballesteros, L. Resconi, A. Fait, E. Ciaccia, I. Camurati, *J. Am. Chem. Soc.* **2003,** *125***,** 10913-10920
10. F. Auriemma, C. De Rosa, *J. Am. Chem. Soc.* **2003,** *125***,** 13143-13147
11. C. De Rosa, O. Ruiz de Ballesteros, F. Auriemma, *Macromolecules* **2004,** *37***,** 7724-7735
12. C. De Rosa, O. Ruiz de Ballesteros, F. Auriemma, R. Savarese, *Macromolecules* **2005,** *38***,** 4791-4798
13. C. De Rosa, F. Auriemma, O. Ruiz de Ballesteros, *Chem. Mater.* **2006,** *18***,** 3523-3530
14. C. De Rosa, F. Auriemma, O. Ruiz de Ballesteros, *Phys. Rev. Let.* **2006,** *96***,** 1-4

15. O. Ruiz de Ballesteros, F. Auriemma, C. De Rosa, *Macromolecules* **2007,** *40***,** 611-622
16. F. Auriemma, C. De Rosa, S. Esposito, G.R. Mitchel, *Angew. Chem. Int. Ed.* **2007,** *46***,** 4352-432
17. L. Guadagno, C. Fontanella, V. Vittoria, P. Longo, *J. Polym. Sci: Part B* **1999**, *37,* 173-180
18. L. Guadagno, C. D'Aniello, C. Naddeo, V. Vittoria, S.V. Meille, *Macromolecules* **2002**, *35,* 3921-3927
19. L. Guadagno, C. Naddeo, C. D'Aniello, V. Vittoria, S.V. Meille, *Macromol. Symp.* **2004**, *218,* 125-135
20. L. Guadagno, C. Naddeo, C. D'Aniello, V. Vittoria, S.V. Meille, *Macromolecules* **2005**, *38,* 8755-8764
21. L. Guadagno, C. Naddeo, V. Vittoria, *Eur. Polym. J*. **2009**, *45,* 2192-2201

J_ID: z8q Customer A_ID: POLB23561 Cadmus Art: POLB23561 Ed. Ref. No.: 14-06-0279.R1 Date: 25-July-14 Stage: Page: 1

A Study of the Yield and Post-Yield Behavior of Syndiotactic Polypropylene

Claudia Marano, Nadia Perillo, Marta Rink

Dipartimento di Chimica, Materiali e Ingegneria Chimica "Giulio Natta", P.zza Leonardo da Vinci 32, 20133 Milano, Italia
Correspondence to: C. Marano (E-mail: claudia.marano@polimi.it)

Received 10 June 2014; revised 11 July 2014; accepted 11 July 2014; published online 00 Month 2014
DOI: 10.1002/polb.23561

ABSTRACT: The strain recovery of three syndiotactic polypropylenes (s-PPs) differing in the percentage of [rrrr] pentad is investigated. A suitable method based on loading–unloading tests at constant displacement rate in tensile loading conditions is adopted to measure the residual and recovered strain components of the applied strain. The method allows to obtain a large amount of data from few tests and to explore a wide strain range. The dependence of the material's strain recovery on the applied strain is analyzed in relation to s-PP strain-induced microstructural changes and crystalline form transitions, which are reported in literature. © 2014 Wiley Periodicals, Inc. J. Polym. Sci., Part B: Polym. Phys. **2014**, *00*, 000–000

KEYWORDS: crystal structures; poly(propylene) (PP); structure-property relations; syndiotactic; yielding

INTRODUCTION Syndiotactic polypropylene (s-PP) has been widely studied in the last fifty years mainly concerning its crystal polymorphism and morphology (see e.g., refs. 1–3) and the effects of drawing on material structure.[2–6] When slowly cooled from the melt state or when crystallized from solution, s-PP shows a crystalline phase consisting of an anti-chiral packing (right-handed and left-handed chains alternating along *a* and *b* axis of the unit cell) in which the macromolecular chains show a twofold helical conformation in an orthorhombic crystalline cell. This crystalline form, which is referred to as form I, transforms into the *trans*-planar conformation-arranged form III when material is strained. Form III is a metastable form of s-PP, characterized by an orthorhombic crystalline cell. The strain value at which the onset of the transformation of form I into form III occurs depends on the syndiotactic pentad [rrrr] content.[5] The appearance of a mesophase in place of form III or previous to form III formation is also controlled by the syndiotactic pentad [rrrr] content.[5]

When the material is annealed under stretching[2] or is unloaded,[5] form III transforms into the helical conformation-arranged form II, characterized by a C-center structure in which the macromolecular chains are packed with the same chirality. If the mesophase forms under stretching, the crystalline form I is present after unloading.

Several studies have been carried out also to analyze and interpret the peculiar "elastic" behavior of s-PP:[5,7–9] when s-PP is drawn beyond yield and then unloaded the applied strain partially recovers and, if reloaded within the recovered strain range and then again unloaded, it shows practically no residual strain. It thus behaves differently from the so-called "Hard elastic fibers" or "Springy polymers,"[10,11] whose elastic behavior is related to a particular material morphology which is induced during processing. The elastic behavior of s-PP has been related to the reversible crystal–crystal phase transition between the *trans* planar form III and the helical form II or I,[12] while other authors[7–9] report that molecules' conformational transitions from trans planar to helical conformation, both within and between crystals, are responsible for the observed elastic behavior.

A very significant advance in the study of yield and post-yield behavior of semicrystalline polymers has been achieved by Strobl and coworkers[6,13,14] performing cyclic tensile tests, using a video controlled tensile testing machine. The adopted experimental method allowed determining true stress–strain curves at constant strain rates, overcoming the problem of the neck formation. Moreover, the cyclic test allowed to measure the residual and recovered strain components of the applied strain and how they change as strain increases. Irrespective of the type of polymer, it was found that the material's "differential compliance," the strain dependence of the residual or recovered strain, and the material's crystalline microstructure simultaneously change at four strain values which are characteristic of the material, being affected neither by its crystallinity degree nor by the temperature. Further, different deformation processes, which are progressively activated at these strain levels, have been identified.

ID: srinivasanv Time: 19:42 I Path: N:/3b2/POLB/Vol00000/140093/APPFile/JW-POLB140093

J_ID: z8q Customer A_ID: POLB23561 Cadmus Art: POLB23561 Ed. Ref. No.: 14-06-0279.R1 Date: 25-July-14 Stage: Page: 2

TABLE 1 Characteristic Data of s-PPs

Material	M_w (10^3 g/mole)	[rrrr] (%)	T_g (°C)	T_m (°C)	χ^a (%)
s-PP91.5	766,000	91.5	0	160	37
s-PP78	193,000	78	0	125	26
s-PP54	1,300,000	54	0[b]	66[b]	11[b]

[a] $\chi = \frac{\Delta H_m}{\Delta H^0}$, where ΔH_m is the experimental melting enthalpy and $\Delta H^0 = 183 \frac{J}{g}$ is s-PP melting enthalpy for 100% of crystallinity.[6]
[b] Data measured four days after molding.

They have been described as isolated inter and intralamellae slip processes, collective slip processes, fragmentation of crystallites, and chain disentanglements, respectively. Further works[15–17] have examined the deformation mechanisms in semicrystalline polymers. In particular, the relative role of the amorphous phase and of the crystalline blocks are discussed[15,16] and the conversion of lamellar crystals into crystalline fibrils is described as a melting-recrystallization process.[15,17]

Furthermore according to the work by Men et al.[15] this process occurs when the stress transferred by the amorphous stretched phase to the crystallites reaches a critical value.

In the present work, loading–unloading tests were performed on three s-PPs, differing in syndiotactic pentad [rrrr] content. The residual and the recovered strain components of the overall strain were determined as a function of the applied strain for all the materials. A proper test method was set up to obtain true stress–strain curves using standard dumb-bell specimens also for materials which neck at yielding. This method reduced significantly the number of specimens to be tested, and allowed to explore a wide range of strains.

EXPERIMENTAL

Materials

Three commercial s-PPs, differing in syndiotactic pentad [rrrr] content, were studied in this work. The materials were kindly supplied by Atofina, who provided their structural characteristics, reported in Table 1. The material's code reflects its [rrrr] pentad content. Materials thermal properties (glass transition temperature, T_g, melting temperature, T_m, and crystallinity degree, χ), measured by differential scanning calorymetry tests performed at 10 °C/min heating rate, are also reported in Table 1. The data relevant to s-PP54 were measured 4 days after molding, when a constant value of crystallinity has been reached in the material, which crystallizes slowly at room temperature.

Test Specimens

s-PP plates 1 mm thick were obtained by compression molding (0.2 MPa and 180 °C, 165 °C, and 140 °C for s-PP91.5, s-PP78, and s-PP54, respectively). The plates were slowly cooled to room temperature. Dumb-bell specimens, with a gauge length of 33 mm, were obtained by die cutting. Black marks were placed along the specimen gauge length, as

FIGURE 1 Sample for tensile test: black marks were placed for strain measurement with video-extensometer.

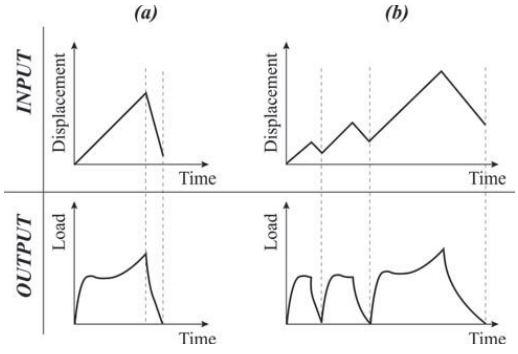

FIGURE 2 Sketch of a single-cycle (a) and multi-cycles (b) loading–unloading tensile tests.

ID: srinivasanv Time: 19:42 I Path: N:/3b2/POLB/Vol00000/140093/APPFile/JW-POLB140093

J_ID: z8q Customer A_ID: POLB23561 Cadmus Art: POLB23561 Ed. Ref. No.: 14-06-0279.R1 Date: 25-July-14 Stage: Page: 3

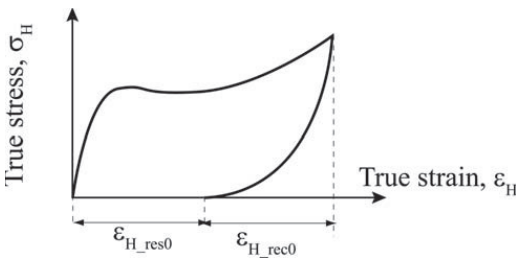

FIGURE 3 Definition of residual and recovered strain components of the overall true strain at the end of unloading.

F1 shown in Figure 1, to measure the local deformation using a video-extensometer.

Thus, measuring the distance between the marks delimiting the generic *i-Zone*, the local true strain, $\epsilon_{H_i} = \ln \lambda_i = \ln \frac{l_i}{l_{i_0}}$, was measured in every Zone of the specimen and the true stress, $\sigma_{T_i} = \frac{P}{A_{i_0}} \lambda_i$, determined ($P$ is the applied load, A_{i0} is the unstrained specimen cross-section, measured between two marks initially at a distance l_{i0} and l_i is their actual distance during the test).

Mechanical Tests

Uniaxial tensile loading–unloading tests were performed, at room temperature, on a displacement-controlled dynamometer (Instron 1121) at constant displacement rate. Both single-cycle and multi-cycles tests were carried out, as
F2 sketched in Figure 2.

Displacement rates of 5 and 50 mm/min were applied in both the loading and the unloading steps.

Residual ($\varepsilon_{H_{res}0}$) and recovered ($\varepsilon_{H_{rec}0}$) strain components of
F3 the overall true strain, ε_H, defined as in Figure 3, were measured for each value of the applied strain after unloading.

Testing Method

In this work, a simple test method was properly set up to analyze the material's strain recovery capability as a function of the applied strain. This method simplifies the experimental work by reducing significantly the number of specimens required. The method is sound when strain localization and necking take place. In this case, during a tensile test, the deformation is not homogeneous and different regions along the gauge length reach different strains at the same loading time. If the distance between two successive marks reported on a dumb-bell specimen (Fig. 1) is quite small, the specimen deformation within a "Zone" can be supposed to be homogeneous. Nevertheless, the different Zones will undergo different strain histories [see for e.g., Fig. 4(a) reporting the F4 true strain measured in two Zones of a s-PP78 specimen drawn at a displacement rate of 5 mm/min up to a nominal strain of 600%].

The different Zones can be considered as different test specimens provided the mechanical behavior is the same irrespective of the strain history. For example, this was verified for the two Zones in Figure 4(a), as shown by the good superposition of the two relevant stress–strain curves in Figure 4(b). As much as this hypothesis is valid, when a dumb-bell specimen is loaded up to a given overall strain and then unloaded the n_i Zones along the gauge length can be considered as n_i homogeneously deformed specimens drawn up to different strains and then unloaded.

RESULTS AND DISCUSSION

Some preliminary tests were performed to verify the applicability of the proposed test method for the three materials, that is the material's response is the same irrespective of the different strain histories applied in the different Zones of the specimen.

In Figure 5, the strain measured during a monotonic loading F5 tensile test at 5 mm/min in different Zones of a single specimen's gauge length is reported versus time for s-PP54 (a), s-PP78 (b), and s-PP91.5 (c) respectively. It can be observed that the deformation phenomenology is similar for s-PP78 and s-PP91.5: at first all the Zones are homogeneously drawn, then the strain mainly localizes in a single Zone, which rapidly deforms and reaches a plateau strain value

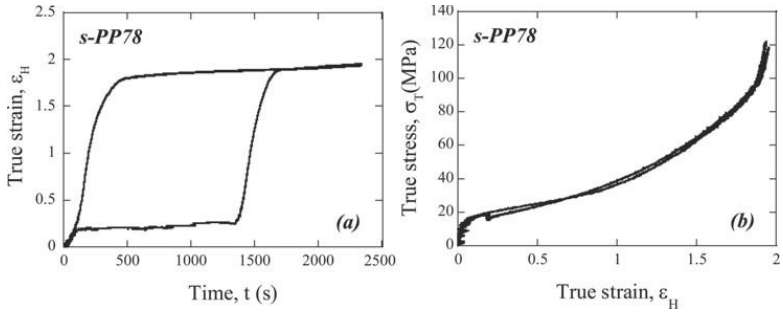

FIGURE 4 True strain vs. loading time measured in two different zones of a single s-PP78 dumb-bell specimen (a) and the relevant true stress–strain curves (b). Displacement rate 5 mm/min.

ID: srinivasanv Time: 19:43 I Path: N:/3b2/POLB/Vol00000/140093/APPFile/JW-POLB140093

J_ID: z8q Customer A_ID: POLB23561 Cadmus Art: POLB23561 Ed. Ref. No.: 14-06-0279.R1 Date: 25-July-14 Stage: Page: 4

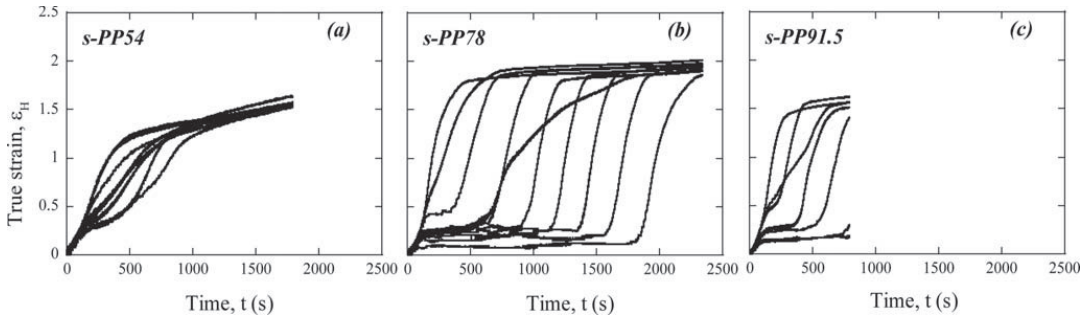

FIGURE 5 Time dependence of the true strain measured in different zones of a single specimen of s-PP54 (a), s-PP78 (b), and s-PP91.5 (c). Displacement rate 5 mm/min.

after which it is not further strained and another specimen's Zone starts to rapidly deform. For s-PP54, instead, the deformation results to be less localized: after an initial homogeneous strain of the whole gauge length, all the Zones are drawn but each at a different drawing rate, reaching a strain of about 1.4. Then the sample deforms almost homogeneF6 ously. In Figure 6, the true stress–strain curves relevant to the different Zones of a single specimen are reported for s-PP54 (a), s-PP78 (b), and s-PP91.5 (c), respectively: it can be observed that for the three materials the stress–strain response during loading is not affected by the applied drawing history.

To check that the deformation history does not affect the stress–strain response during unloading too, single cycle loading–unloading tests differing in the displacement rate of F7 the unloading step were performed. In Figure 7, the true stress–true strain curves of s-PP54 are reported as an example: it can be observed that the material behavior in the unloading step is not affected by the displacement rate. Similar results were obtained also for s-PP78 and s-PP91.5. The obtained results indicate that the testing method previously described can be applied for a single loading–unloading test for the three materials, that is different Zones of a single specimen can be considered as different specimens drawn up to different strain values. Figure 8 reports the true F8 stress–strain curves relevant to three Zones of a single specimen of s-PP54 (a), s-PP78 (b), and s-PP91.5 (c) under a multi-cycle loading–unloading tensile test performed at 5 mm/min. Curves relevant to monotonic loading up to failure are reported for comparison. For s-PP91.5 and s-PP78, the stress–strain curve of each loading step in the multicycles loading–unloading test overlaps with the stress–strain curve of the monotonic loading test for strain higher than the maximum strain reached in the previous cycle. Moreover it can be observed that material strain recovery in the unloading step and the subsequent loading curve result to be the same irrespective of the number of the applied loading–unloading cycles (see e.g., $\varepsilon_H = 0.85$ for s-PP78). Thus for s-PP91.5 and s-PP78, successive loading–unloading cycles on a single specimen give the same information as many single cycle tests.

For s-PP54, instead [Fig. 8(a)] it can be observed that in the multi-cycle loading history, when the sample is reloaded, the material shows a different behavior with respect to that of the monotonically loaded material. Therefore for s-PP54 only single cycle tests were performed.

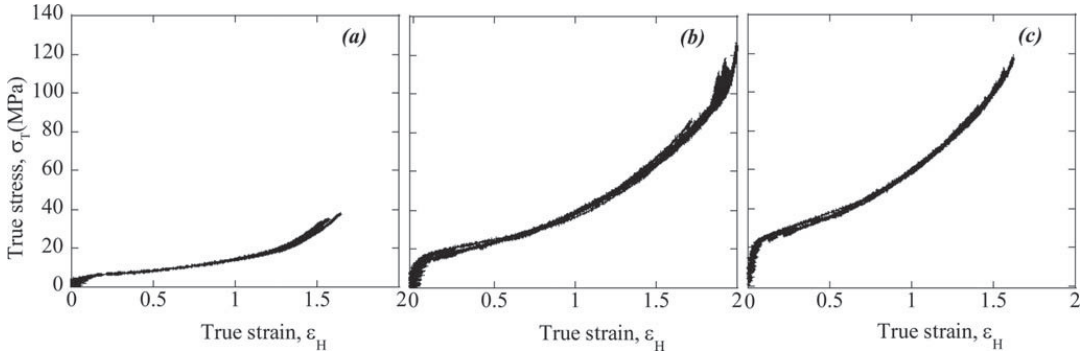

FIGURE 6 True stress–strain curves for s-PP54 (a), s-PP78 (b), and s-PP91.5 (c). Displacement rate 5 mm/min.

ID: srinivasanv Time: 19:43 I Path: N:/3b2/POLB/Vol00000/140093/APPFile/JW-POLB140093

J_ID: z8q Customer A_ID: POLB23561 Cadmus Art: POLB23561 Ed. Ref. No.: 14-06-0279.R1 Date: 25-July-14 Stage: Page: 5

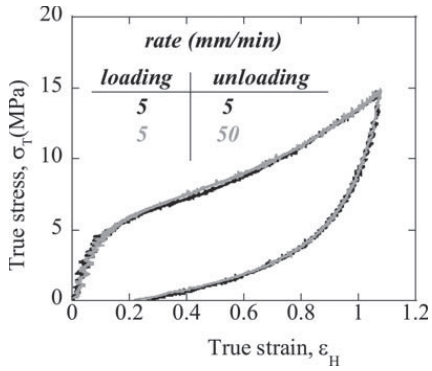

FIGURE 7 True stress–strain curves of s-PP54 in two single-cycle tests unloaded at different displacement rates.

From the multi-cycle tests performed on s-PP78 and s-PP91.5 and from the single-cycle tests performed on the three materials, the residual, $\varepsilon_{H_{res}0}$ and the recovered, $\varepsilon_{H_{rec}0}$, strain components of the applied strain, ε_H, at the end of the unloading (defined in Fig. 2) were measured. Figure 9 reports $\varepsilon_{H_{res}0}$ and $\varepsilon_{H_{rec}0}$ versus ε_H for s-PP54 (a), s-PP78 (b), and s-PP91.5 (c), respectively. F9

It can be observed that: (i) s-PP78 and s-PP91.5 behave similarly [Fig. 9(b,c)] and for both the materials $\varepsilon_{H_{res}0}$ is slightly lower than $\varepsilon_{H_{rec}0}$ up to an applied strain level of 0.4; at higher strains, the residual strain component is significantly higher than the recovered one; in s-PP54 [Fig. 9(a)], instead, $\varepsilon_{H_{rec}0}$ is higher than the residual strain component over the whole explored strain range; (ii) changes in the trend of both $\varepsilon_{H_{rec}0}$ and $\varepsilon_{H_{res}0}$ vs. applied strain can be observed for all the materials: for s-PP78 and s-PP91.5 [Fig. 9(b,c)] first $\varepsilon_{H_{res}0}$ increases fairly linearly with the applied strain up to $\varepsilon_H = 0.4$ after which it still increases but with a higher slope. At $\varepsilon_H = 1.8$ and $\varepsilon_H = 1.4$ for s-PP78 and s-PP91.5 respectively, $\varepsilon_{H_{rec}0}$ becomes constant and consequently the slope of the residual strain component vs. applied strain becomes unity, suggesting that the further deformation of the materials is completely plastic. This can be explained by the achievement at these strain levels of the maximum polymeric

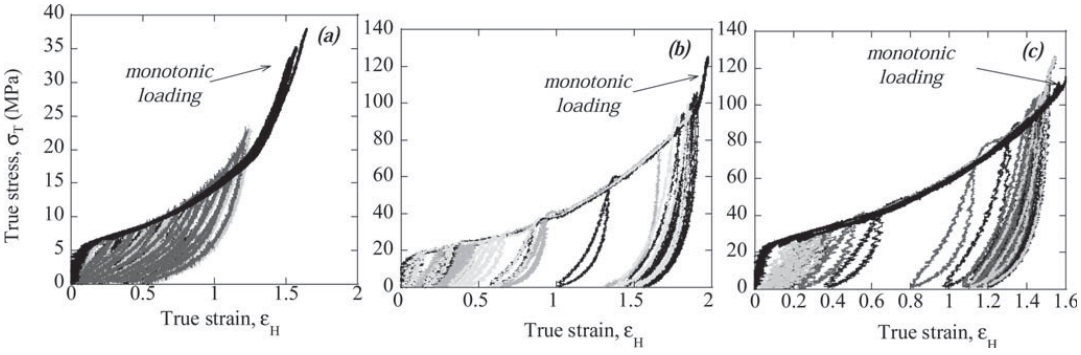

FIGURE 8 True stress–strain curves in monotonic loading and multi-cycles loading–unloading tests for s-PP54 (a), s-PP78 (b), and s-PP91.5 (c). Loading and unloading at 5 mm/min.

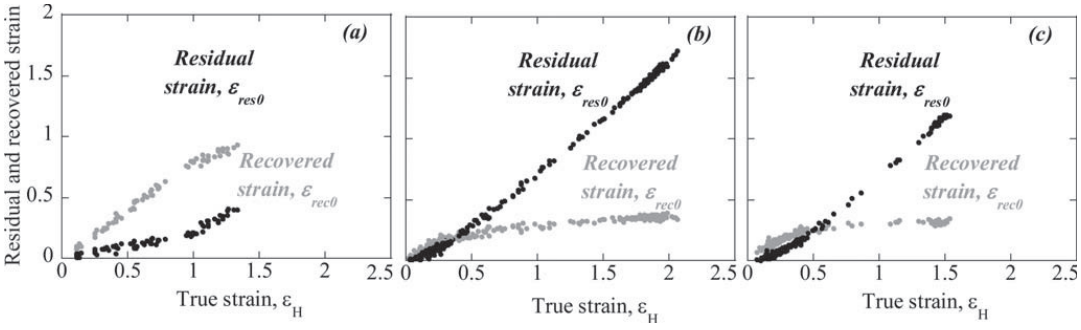

FIGURE 9 Dependence of the residual and recovered true strain components on the applied true strain for s-PP54 (a), s-PP78 (b), and s-PP91.5 (c).

ID: srinivasanv Time: 19:43 I Path: N:/3b2/POLB/Vol00000/140093/APPFile/JW-POLB140093

J_ID: z8q Customer A_ID: POLB23561 Cadmus Art: POLB23561 Ed. Ref. No.: 14-06-0279.R1 Date: 25-July-14 Stage: Page: 6

chains extension. In the case of s-PP54 [Fig. 9(a)] $\varepsilon_{H_{res}0}$ as function of applied strain shows a bilinear trend with a change in slope at about $\varepsilon_H = 1$.

An attempt was made to correlate the strains at which changes in the trends of recovered/residual strain components vs. applied strain occur with the strains at which microstructural or crystalline forms transitions take place.

For the three materials the first change in the trend of both $\varepsilon_{H_{res}0}$ and $\varepsilon_{H_{rec}0}$ occurs at a residual strain of ~0.2 as shown in F10 Figure 10. This strain value is in good agreement with the "critical plastic true strain" reported in literature[4] at which the conversion of lamellar crystals into crystalline fibrils occurs and a change in the slope of the residual strain vs. total applied F11 strain takes place. In Figure 11 the data by Deplace et al.[4] are shown together with the data from Men and Strobl[6] which again show a bilinear trend with a change in slope at a residual strain of 0.2. The total applied strain relevant to this residual strain is 0.4 for s-PP78 and s-PP91.5 and 1 for s-PP54. Such a shift in the overall strain at which fibrils start to form with crystallinity degree has been previously observed by Sun et al.[16] on two different ethylene-octene copolymers. The authors attribute the shift to a different structure of the crystalline phase in the two copolymers. In the more crystalline copolymer a macroscopic crystalline rigid network interpenetrated with an entangled amorphous network is present while, in the less crystalline one, crystalline lamellar stacks are only weakly coupled through the amorphous entangled phase which causes an inhomogeneous strain distribution during deformation. It can therefore be thought that for s-PP78 and s-PP91.5, an interpenetrated network structure is present while for s-PP54 lamellar blocks tend to constitute a dispersed phase in an amorphous entangled matrix.

Regarding the strain-induced crystalline form transitions, it may be observed that for s-PP54 the critical plastic strain of 0.2 occurs at $\varepsilon_H = 1$ at which the onset of the form I to mesoform transition takes place, as calculated from data reported by Auriemma and De Rosa[5] even if for s-PP78 no change in the trend of the residual strain component vs.

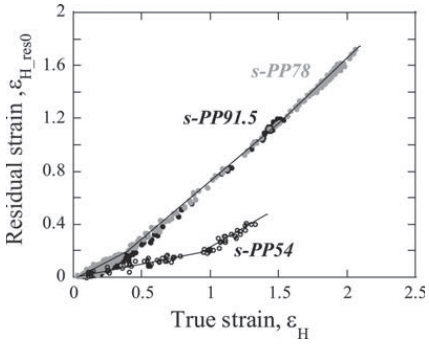

FIGURE 10 Dependence of the residual strain component on the applied true strain for s-PP54, s-PP78, and s-PP91.5.

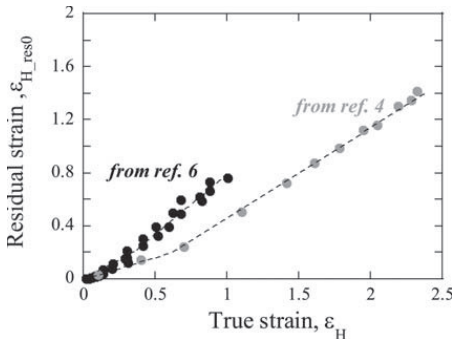

FIGURE 11 Dependence of the residual strain component on the applied true strain for a pure sPP (from ref. 6) and a sPP-EPR copolymer (from ref. 4).

applied overall strain occurs at $\varepsilon_H = 0.9$ at which the same crystalline form transition takes place. Furthermore, also for s-PP91.5 no change in the residual strain trend can be observed at $\varepsilon_H = 0.6$ at which the form I to form III transition sets in. The strains at which the recovered strain component relevant to s-PP78 and s-PP91.5 reaches a constant value result to be similar to the strains at which only the crystalline form III is present.[5]

CONCLUSIONS

Through a test method in which different Zones of a single specimen can be considered independently, the mechanical response of three s-PPs in terms of recovered/residual strain components was investigated up to large strains. Since during the test each Zone undergoes a different strain history, in order to apply the method it has to be verified that the mechanical response of the material is the same irrespective of loading history.

The main finding of this work is that at a critical residual strain value of about 0.2 there is a change in the overall strain dependence of the residual strain irrespective of the syndiotactic pentad [rrrr] content in pure s-PPs. Also in a thermoplastic elastomer in which s-PP hard blocks constitute the physical crosslinks the same critical residual strain was found.

This strain seems to be related to a microstructural change rather to a crystalline form transition.

ACKNOWLEDGMENT

Financial support by MIUR (PRIN 2008) is gratefully acknowledged.

REFERENCES AND NOTES

1 B. Lotz, J. C. Wittmann, A. J. Lovinger, *Polymer* **1996**, *37*, 4979–4992.

2 C. De Rosa, P. Corradini, *Macromolecules* **1993**, *26*, 5711–5718.

ID: srinivasanv Time: 19:43 I Path: N:/3b2/POLB/Vol00000/140093/APPFile/JW-POLB140093

J_ID: z8q Customer A_ID: POLB23561 Cadmus Art: POLB23561 Ed. Ref. No.: 14-06-0279.R1 Date: 25-July-14 Stage: Page: 7

3 J. Harasawa, H. Uehara, T. Yamanobe, T. Komoto, M. Terano, *J. Mol. Struct.* **2002**, *610*, 133–142.

4 F. Deplace, Z. Wang, N. A. Lynd, A. Hotta, J. M. Rose, P. D. Hustad, J. Tian, H. Ohtaki, G. W. Coates, F. Shimizu, K. Hirokane, F. Yamada, Y. Shin, L. Rong, J. Zhu, S. Toki, B. S. Hsiao, G. H. Fredrickson, E. J. Kramer, *J. Polym. Sci. Part B: Polym. Phys.* **2010**, *48*, 1428–1437.

5 F. Auriemma, C. De Rosa, *J. Am. Chem. Soc.* **2003**, *125*, 13143–13147.

6 Y. Men, G. Strobl, *J. Macromol. Sci. B Phys* **2001**, *40*, 775–796.

7 C. D'Aniello, L. Guadagno, C. Naddeo, V. Vittoria, *Macromol. Rapid Commun.* **2000**, *21*, 104–108.

8 L. Guadagno, C. D'Aniello, C. Naddeo, V. Vittoria, *Macromolecules* **2001**, *34*, 2512–2521.

9 L. Guadagno, C. D'Aniello, C. Naddeo, V. Vittoria, *Macromolecules* **2002**, *35*, 3921–3927.

10 B. S. Sprague, *J. Macromol. Sci. B Phys.* **1973**, *8*, 157–187.

11 S. L. Cannon, G. B. McKenna, W. O. Statton, *J. Polym. Sci. Macromol. Rev.* **1976**, *11*, 209–275.

12 F. Auriemma, O. Ruiz de Ballestreros, C. De Rosa, *Macromolecules* **2001**, *34*, 4485–4491.

13 R. Hiss, S. Hobeika, C. Lynn, G. Strobl, *Macromolecules* **1999**, *32*, 4390–4403.

14 S. Hobeika, Y. Men, G. Strobl, *Macromolecules* **2000**, *33*, 1827–1833.

15 Y. Men, J. Rieger, G. Strobl, *Phys. Rev. Lett.* **2003**, *91*, 1–4.

16 Y. Sun, L. Fu, Z. Wu, Y. Men, *Macromolecules* **2013**, *46*, 971–976.

17 Y. Wang, Z. Jaing, Z. Wu, Y. Men, *Macromolecules* **2013**, *46*, 518–522.

ID: srinivasanv Time: 19:44 I Path: N:/3b2/POLB/Vol00000/140093/APPFile/JW-POLB140093

Chapter 3

Material yielding in relation to the applicability of the Essential Work of Fracture method

3.1 Introduction

Nowadays thin polymeric films are widely adopted in industrial and food packaging. It is necessary for many applications to well characterize the failure of the films in order to avoid the damage or the degradation of packed products. There are several tests adopted in industry to characterize fracture of films (e.g. Tensile elongation and strength ISO527, tear strength ISO6383, Elmendorf Tear ASTM D1922). The data obtained by these tests are geometry dependent and therefore not material intrinsic properties.

The Essential Work of Fracture (EWF) method has been widely proposed in the literature. This method follows the fracture mechanics approach and should be appropriate for plane stress state which are characteristic of thin films.

Following the EWF method the specific fracture energy w_f, necessary to fracture a specimen containing a crack (or notch) can be expressed as: (Equation 1)

Equation 1.

$$w_f = w_e + \beta w_p L$$

where w_e is the essential work of fracture, the specific energy per unit area necessary to create the fracture surfaces in the *"fracture zone"* and $\beta w_p L$ is the non-essential work of fracture that is the energy per unit volume dissipated in the plastic deformation process in the region surrounding the fracture zone (p*rocess zone*) where β is a shape factor and L the uncracked cross-section length (ligament) [1-2].

To obtain w_e experimentally several specimens (e.g. DEN(T) Double Edge Notched Tension as shown in Figure 1) having different notch lengths are fractured under tensile loading.

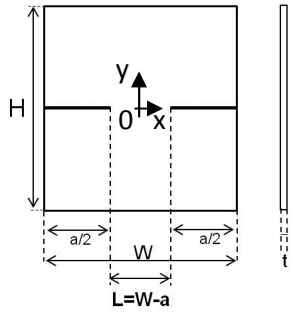

Figure 1. ***DEN(T) specimen geometry adopted for fracture tests***

The specific fracture energy w_f, calculated from the area under the load-displacement curves obtained from the fracture tests divided by the uncracked cross-section (L*t) is plotted as function of the ligament length. The essential work of fracture, w_e, is determined by linear extrapolation to zero ligament length of the specific fracture energy w_f while βw_p is the slope of this regression.

The essential work of fracture, w_e, related to the fracture toughness of the material and determined by the EWF method is an intrinsic characteristic of

the material but it is a function of the specimen thickness. A testing protocol, that is not yet a standard, based on this method was developed by ESIS Technical Committee TC4.

In order to apply EWF method three hypothesis have to be satisfied, as reported by Rink et. al.[3] :

- *"plane stress conditions must prevail: this limits the minimum acceptable ligament length (which should be larger than about 5 times the specimen thickness);*
- *non edge effect: this condition limits the minimum notch length (i.e. the maximum ligament length)*
- *the uncracked cross-section should be fully yielded before crack onset: this last requirement ensures that the fracture mechanism is the same irrespective of the ligament length (with self-similar load vs. displacement curves for different L) and W_p is proportional to L^2 , w_f thus being a linear function of L."*

Verifying that the ligament is completely yielded can be a difficult task. In many cases visual and therefore not objective methods (such as whitening or other signs of yielding) have been adopted.

Further in polymeric materials the yield onset is not easy to be determined as the onset of plastic strain. Due to the viscoelastic nature of polymers the residual strain after unloading could be made of a plastic and/or a viscoelastic component.

In this work a method was set up in order to verify the hypothesis that the *"uncracked cross-section is fully yielded before crack onset".* The strain in the

central zone of the ligament plane in a DEN(T) specimen at crack onset, $\varepsilon_{center}^{crack\ onset}$, was considered since if the central zone of the ligament plane, which is the less strained, has yielded, then the whole ligament has yielded too. The strain $\varepsilon_{center}^{crack\ onset}$ has to be higher than the strain at yield obtained, theoretically, in the same stress state that characterizes the DEN(T) specimen. This yield strain could be obtained by performing proper loading-unloading tests to find the strain at which the onset of permanent strain takes place on the DEN(T) test piece. Nevertheless, it would be easier to find the yield strain in a simple tensile test. Therefore it was verified if there is a significant dependence of the yield strain on the stress state. While the dependence of the yield stress on the stress state is reported in literature (see for example 4), the dependence of the yield strain on the stress state has not reported in the literature to the knowledge of the author of this thesis.

In this chapter:

- fracture tests on a HDPE thin film were performed on DEN(T) specimens to obtain the essential work of fracture, w_e.
- the strain state in the center of a DEN(T) specimen was analyzed in comparison with those determined in a uniaxial and in a plane-strain specimen during tensile deformation.
- The yield strain (strain at the onset of plastic deformation) was determined on DENT, dumbbell and plane-strain specimens.

The results obtained were used to assess the condition of fully yielded ligament before crack onset in the fracture tests.

3.2 Experimental

3.2.1 Materials

A commercial high-density polyethylene (HDPE) film obtained by blown-film-extrusion kindly supplied by Versalis-ENI was investigated in this work. It is characterized by a nominal thickness of 20 μm. The specimens used in tensile tests and in fracture tests were cut along the machine direction.

3.2.2 Test specimens

In this work different specimen geometries were adopted:

1. Dumbbell specimens, with a gauge length of 33 mm, were obtained by die cutting. Many black lines were placed along the specimen gauge length, as shown in Figure 2, to measure the local deformation using a video-extensometer. Measuring the initial distance $L_{0,i}$ and the actual distance $L_{t,i}$ between two lines during and after the test, local strains $\varepsilon_{i,loc} = \frac{L_{t,i}-L_{0,i}}{L_{0,i}}$ were calculated. An ink pattern was sprayed on the surface of some specimens using an aerograph in order to make a strain analysis through the digital image correlation (DIC) technique.

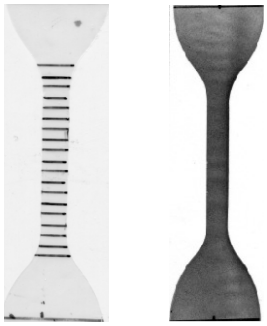

a b

Figure 2. ***Dumbbell specimens adopted in tensile tests: black lines (a) or an ink pattern (b) were placed on the specimens surface for strain measurement by a video-extensometer or by digital image correlation***

2. DEN(T) specimens having dimensions reported in Table 1, were obtained by die cutting. Several specimens were tested to determine the strain at yield onset. Four black markers were placed on the surface of these samples. Two markers just above and below the ligament plane in order to measure the local strain at crack onset close to the centre of specimen and equal to $\varepsilon_{center}^{crack\ onset} = \frac{L_{t,crack\ onset} - L_{0,i}}{L_{0,i}}$, using a video-extensometer (Figure 3a). Two markers at a distance $\pm\frac{L}{2}$ from the notch plane to measure the displacement in fracture tests to take into account only the process and the fracture zones (Figure 3a). [5] Other specimens, on whose surface an ink pattern was sprayed through an aerograph (Figure 3b), were tested to make the strain analysis through the digital image correlation (DIC) technique.

	length (mm)
H	35
W	35
L	from 5 to 15
a	from 15 to 10
t	0.020

Table 1. ***DEN(T) specimens dimensions adopted for fracture tests***

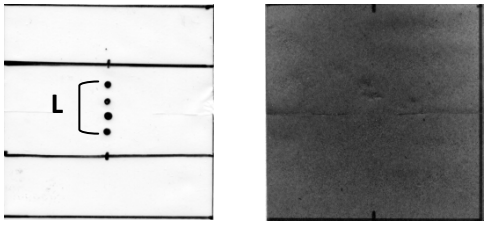

Figure 3. ***DEN(T) specimens for fracture tests: black markers (a) or an ink pattern (b) were placed on the specimens surface for strain measurement by a video-extensometer or by digital image correlation***

3. Plane-strain specimens (Figure 4), having dimensions reported in Table 2, should guarantee that the strain perpendicular to the loading direction is zero at each applied strain level. Specimens were sprayed with an ink pattern to make the strain analysis through the digital image correlation (DIC) technique.

	length (mm)
H	10
L	100
t	0.020

Table 2. ***Plane-strain specimens' dimensions adopted for tensile tests***

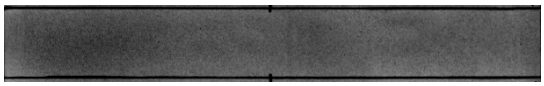

Figure 4. ***Plane-strain specimen: an ink pattern was sprayed on the specimens surface for strain measurement by digital image correlation technique***

3.2.3 Tests

All tests were performed at room temperature, on a displacement-controlled dynamometer (Instron 1121) at constant displacement rate such as to obtain approximately the same nominal strain rate of 0.3mm^{-1} in all tests. Each test was video-recorded in order to measure local strains.

The following tests were performed:

1. ***Fracture tests to obtain w_e and to determine $\varepsilon_{center}^{crack\ onset}$***. To obtain w_e experimentally several DEN(T) specimens, whose geometry is reported in Figure 1, having 5 different ligament lengths (5,7,9,13,15 mm), as reported in Table 1, are fractured under tensile loading condition. The displacement $\delta(mm)$ was determined, as previously

said, as the displacement of a couple of black markers drawn on the surface of specimens at an initial distance equal to the ligament length. The essential work of fracture, w_e, was determined by linear extrapolation to zero ligament length of the specific fracture energy w_f, obtained as the area under the loading-displacement curves divided by the uncracked cross-section (L*t), while βw_p was the slope of this regression.

From the fracture tests on DEN(T) specimens (Figure 3a) with the largest ligament length of 15mm the time at crack onset and the strain at crack onset in the central zone of the ligament plane were determined. The time at crack onset was detected by analyzing the video-recorded test. In correspondence of this time the strain at crack onset was determined from the markers placed just above and below the notch plane (Figure 3a).

2. ***Tests to determine the strain state in DEN(T) specimens.*** Digital image correlation technique was adopted using the commercial software VIC-2D to measure both the local strains along the loading direction and along the perpendicular one. Through an ink pattern, just described in paragraph 3.2.2 “Test specimens” for each specimen, sprayed on the specimens’ surface the displacement field, and then the strain field, between a reference image and each subsequent one was determined.
3. ***Loading-unloading tensile tests to determine the yield onset***. These tests were performed on DEN(T), uniaxial and plane-strain specimens and the local strains were measured for DEN(T) and uniaxial tensile specimens following the displacement of black markers and lines

respectively by means of a videoextensometer while for plane-strain specimens using the digital image correlation technique (DIC).

DEN(T) specimen with the largest ligament length equal to 15mm was chosen because longer the ligament more difficult the whole ligament yielding. During a fracture test, in fact, the stress and the strain distributions are not homogeneous along the ligament. The stresses and the strains assume the maximum values at tip notches and the minimum in the centre of ligament plane. This means that if the central zone of the ligament plane is yielded certainly the whole ligament is yielded.

Several specimens were tested in loading-unloading tests in tensile configuration at a constant displacement rate.

Residual strain component of the local applied strains, ε_{loc}, defined as in Figure 5, was measured for each value of the applied strain after unloading ($\varepsilon_{res,0}$) and in time ($\varepsilon_{res,t}$) until the viscoelastic strain component was completely recovered (ε_p). Therefore the plastic strain ε_p, as defined in Figure 5, was determined. Through the back extrapolation of the plastic strain component ε_p as function of the applied strain, the yield strain, ε_y, as the onset of plastic strain was determined.

Figure 5 reports a schematic true stress –strain curve and the definitions of recovered and residual strain components at the end of unloading and in time.

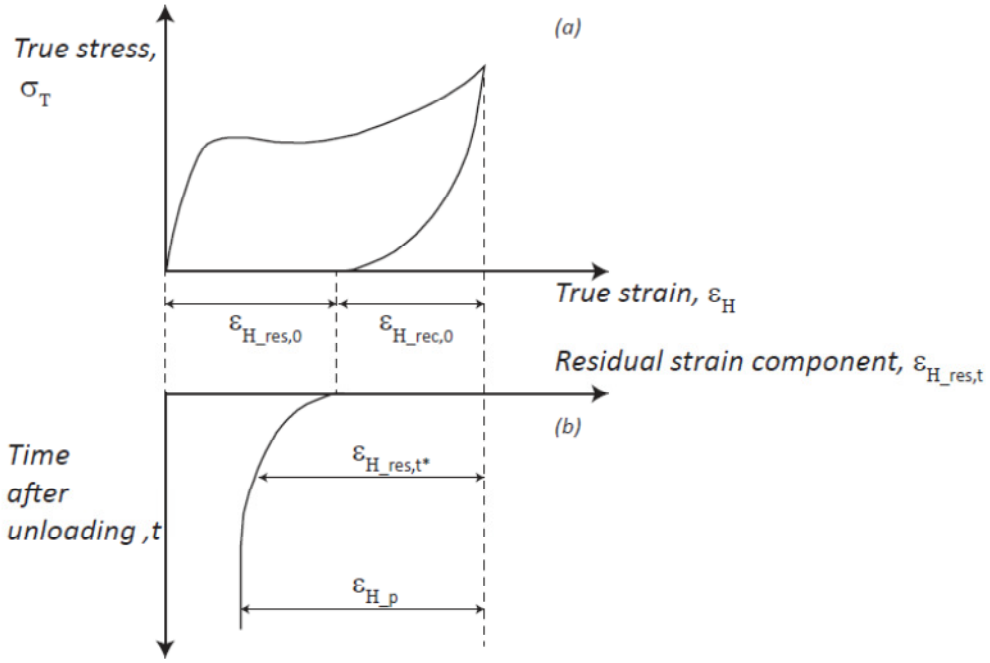

Figure 5. ***Definition of the residual and recovered strain components of the overall local strain at the end of unloading and in time***

3.3 Results and discussion

3.3.1 Fracture tests

In Figure 6 the loading-displacement curves at increasing ligament length are reported. They were obtained by fracture tests on DEN(T) specimens. It can be observed that these curves are self-similar.

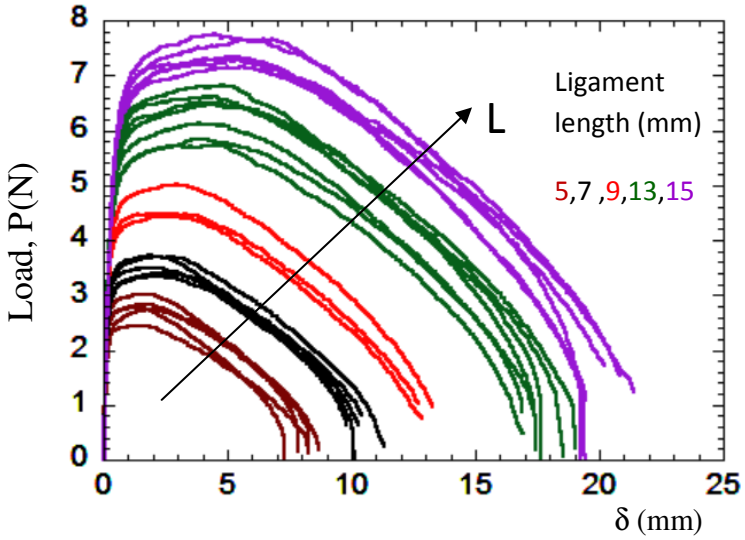

Figure 6. ***Loading-displacement curves up to specimens fracture of DEN(T) specimens having 5 different ligament lengths (5,7,9,13,15 mm)***

In Figure 7 the data of specific fracture energy w_f as function of ligament length with the relative linear regression are reported. It can be observed that R^2 is high (0.987).

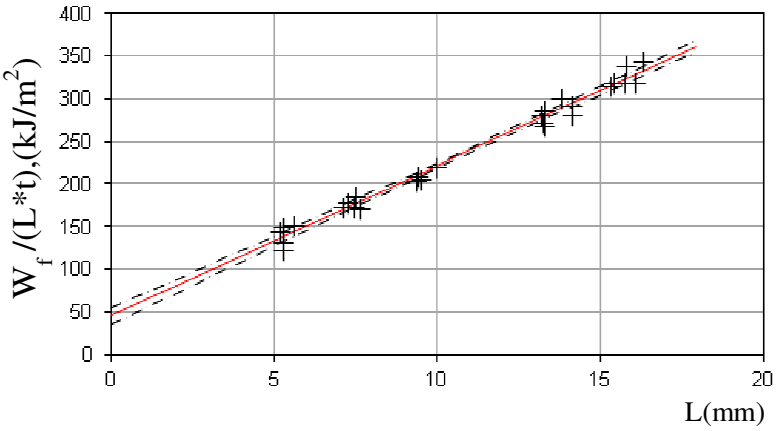

Figure 7. ***Specific fracture energy w_f (experimental data – black symbols) versus the ligament length for all the tested samples; Linear fit of the experimental data (red line) is also reported***

In Table 3 the value of w_e and βw_p obtained by the linear fit on experimental data reported in Figure 7 and the relative 95% confidence limit are reported. These data are in agreement with those reported in the literature. [3]

	Essential work of fracture, w_e	Non essential work of fracture, βw_p
	(kJ/m^2)	(MJ/m^3)
	45	17.7
95% confidence limit	± 9.6	± 0.84

Table 3. ***w_e and βw_p obtained using the EWF method on HDPE films***

Therefore these results cannot guarantee that the uncracked cross-section is fully yielded before crack onset.

An example of loading curve and local strain in the central zone of the ligament plane as function of time is reported in Figure 8. The mean value of the time at crack onset and of the strain at crack onset obtained from 5 different specimens are respectively (16±2)s and (6±1)(%).

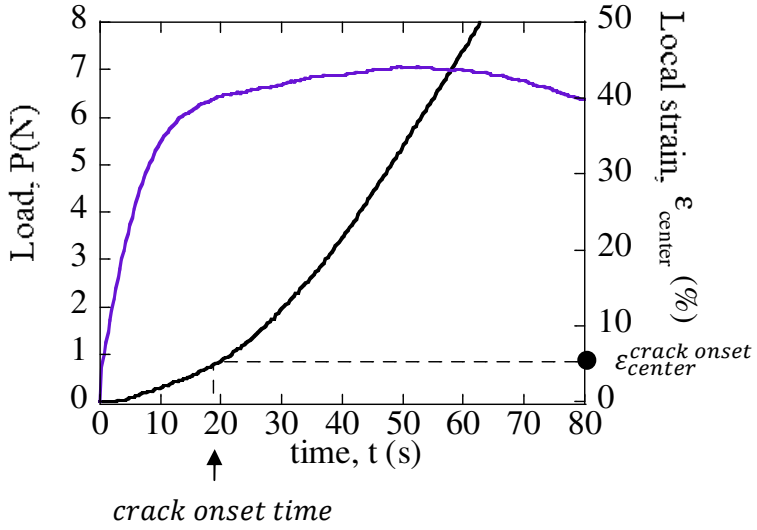

Figure 8. ***Load curve (purple line) and local strain in the central zone of the ligament plane (black line) as function of time; the time at crack onset and the strain at crack onset are also reported***

3.3.2 Strain state analysis

Figure 9 shows the local strains measured along (ε_{yy}) and perpendicularly to (ε_{xx}) the loading direction in the center and at distance of $\frac{L}{2}$ from the notch

plane in a DEN(T) specimen. In the same figure strain maps obtained by DIC analysis are also shown in correspondence of different applied strain levels.

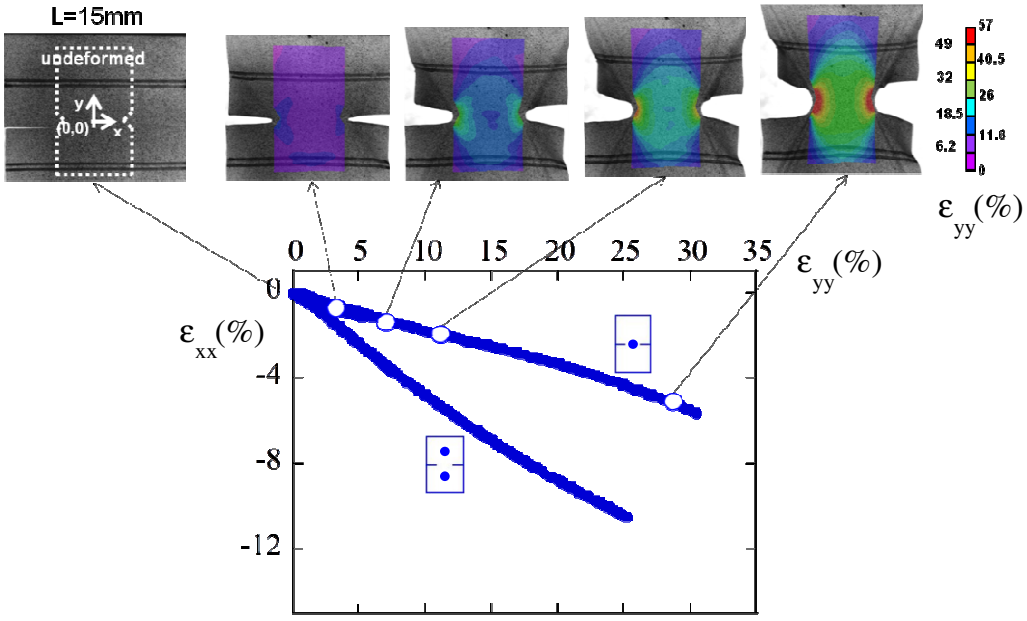

Figure 9. ***Local strains measured along (ε_{yy}) and perpendicularly to (ε_{xx}) the loading direction in the center and at distance of $\frac{L}{2}$ from the notch plane in a DEN(T) specimen. Strain maps obtained by DIC analysis are also shown in correspondence of different applied strain levels***

It can be observed that the lower value of ε_{xx} measured in the center of the notch plane with respect to the relevant strain far from the same plane at the same value of ε_{yy} indicates that a larger constraint is present in the center of the DEN(T) specimen.

In Figure 10 ε_{xx} and ε_{yy} measured along the gauge length of a uniaxial tensile specimen and in the center of a plane-strain specimen are reported together with the data presented in Figure 9.

It can be observed that the strains far from the notch plane in a DEN(T) specimen are similar to those of a uniaxial tensile specimen while the center of the DEN(T) specimen is characterized by a strain state more similar to a plane strain state.

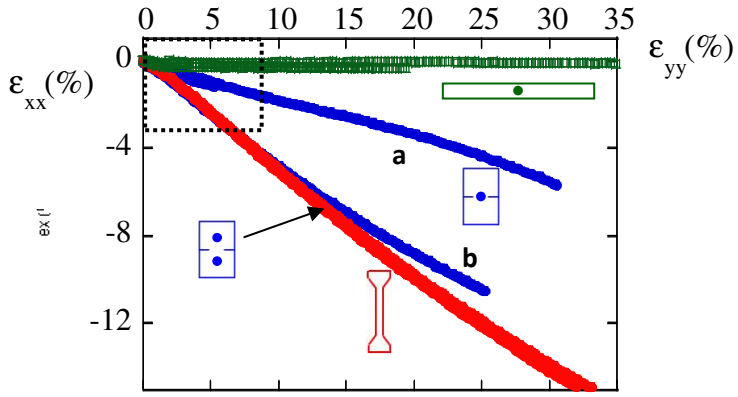

Figure 10. ***Local strains measured along (ε_{yy}) and perpendicularly to (ε_{xx}) the loading direction in the center and at distance of $\frac{L}{2}$ from the notch plane in a DEN(T) specimen (blue line), along the gauge length of a uniaxial tensile specimen (red line)*** **and in the center of a plane-strain specimen *(green line)***

In Figure 11 a detail of Figure 10 up to $\varepsilon_{yy} = 8\%$ that is a strain range comparable with $\varepsilon_{center}^{crack\ onset}$ determined in the center of the DEN(T) specimen is reported.

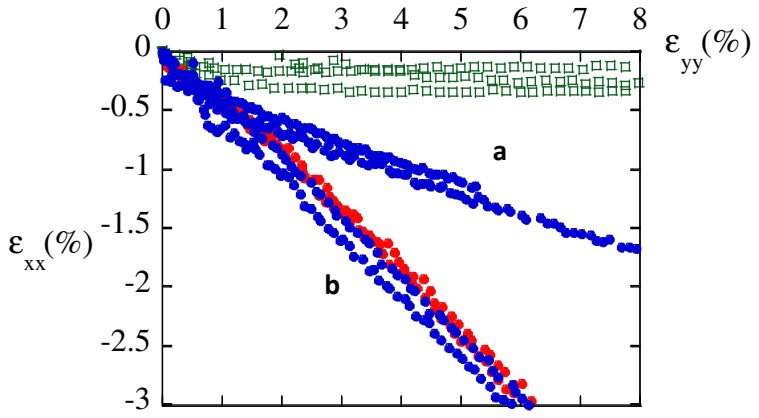

Figure 11. ***A detail of Figure 10 up to $\varepsilon_{yy} = 8\%$***

True stress-true strain curves both for uniaxial and plane-strain specimens are reported in Figure 12. It can be observed that the shape of the curves is the same but the stresses in plane-strain state are higher respect to the uniaxial stress state. It is not easy to quantify the true stress in the central zone of a DEN(T) specimen since the stress distribution is not uniform along the ligament. Therefore the true stress-true strain curve for a DEN(T) specimen in the central zone of ligament is not reported. The comparison of the mechanical response for uniaxial and plane-strain specimens in terms of deformation is reported in the next paragraph.

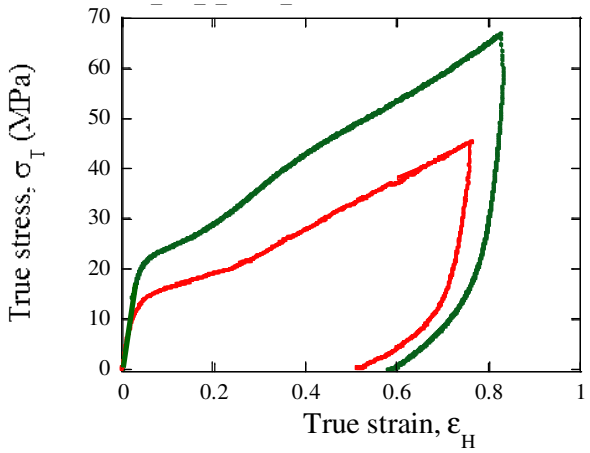

Figure12. ***True stress-true strain curves for uniaxial (red line) and plane-strain specimens (green line)***

3.3.3 Yield onset determination

The strain at yield onset was determined using the method set up by Quinson et al. [6] In Figure 13a,b the residual strains at the end of the unloading ($\varepsilon_{res,0}$) and in correspondence of the complete recovery of the viscoelastic strain component (ε_p) as function of the applied strain are reported. It can be observed that for HDPE the time range to reach the plateau value of the residual strain component was in the order of magnitude of 10^4 minutes after unloading. At longer recovery times no significant strain recovery can be measured.

Because of the data dispersion, it was not easy to perform the back-extrapolation of the plastic strain component, ε_p, as function of the applied strain to obtain the yield onset. Therefore the yield strain was determined as the mean value between that where the plastic strain oscillates around zero and that where it is definitely positive.

1% was found to be the half-amplitude of the strain range in which the plastic strain oscillates around zero and where it is definitely positive.

Adopting this criterion the yield strain resulted to be the same for all the specimens adopted and equal to 6.5±1(%), as shown in Figure 13b. More over it resulted to be fairly equal to the strain at crack onset determined in the center of a DEN(T) specimens $\varepsilon_{center}^{crack\ onset}$ = 6.0±1(%)(see paragraph 3.3.1).

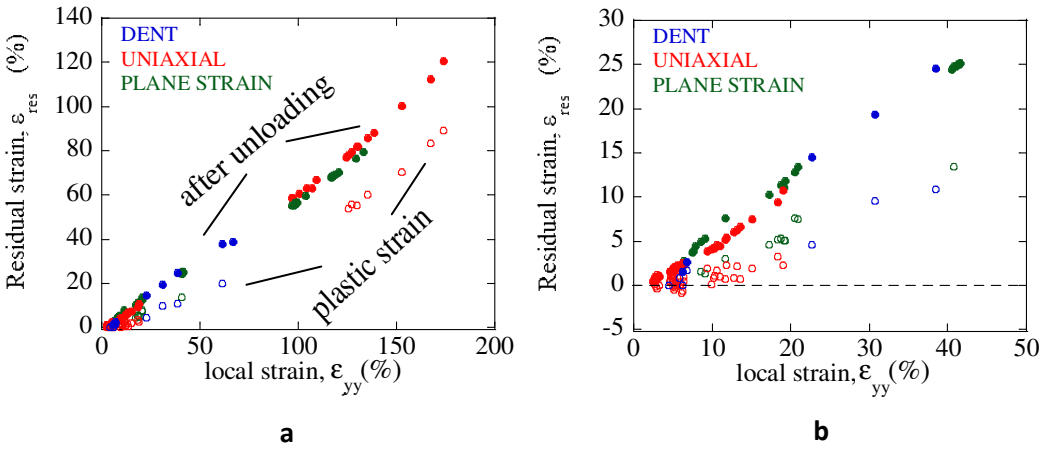

Figure 13. ***Residual strain component at the end of unloading $\varepsilon_{res,0}$ (fully symbols) and after the complete recovery of the viscoelastic strain component , ε_p ,(open symbols) versus the applied strain for uniaxial, DEN(T) and plane-strain specimens (a), detail of Figure 13a up to $\varepsilon_{yy} = 8\%$ (b)***

Although the local strain rate is different along the gauge length in uniaxial specimens and in the central zone of the ligament plane, it was verified that the time at which the yield onset occurs in uniaxial specimens and the time at which the crack initiates in DEN(T) specimens are fairly the same (15-18s).

In Figure 14 a detail of Figure 12 up to $\varepsilon_{yy} = 8\%$ that is a strain range comparable with the yield strain is reported. It can be observed that, even if the stresses for the plane-strain specimen are higher with respect to the uniaxial stress state, as previously observed, the strains seem to be the same in both the stress state.

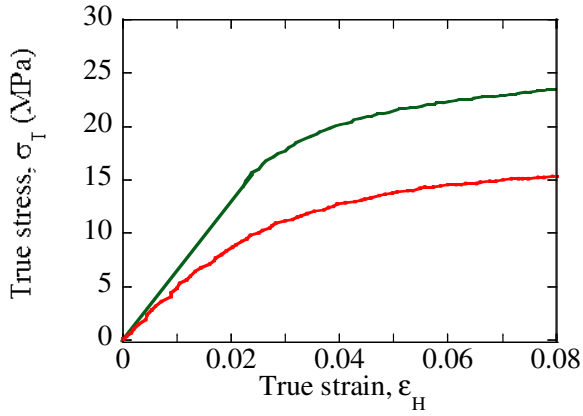

Figure 14. ***A detail of Figure 12 up to $\varepsilon_{yy} = 8\%$***

3.4 Conclusive remarks

From the point of view of the Essential Work of Fracture it seems possible, at least for the HDPE considered, to determine the yield strain from a tensile test and compare this value with the local strain in the center of the ligament plane in a DEN(T) specimen at crack onset. In addition the hypothesis of yielding of the whole cross-section was verified for the studied material.

From the point of view of the yield behavior it seems that the strain at yield onset does not significantly depend on the strain state.

In this thesis only two stress states and only one material have been considered. It would be necessary to extend and confirm these results to other strain states and examine other materials.

Bibliography

1. B. Cotterell, J.K. Reddel, *Int. J. Fracture* **1977**, *13*, 267-277
2. K.B. Broberg, *J. Mech. Phys. Solid* **1975**, *23*, 215-237
3. M. Rink, L. Andena, C. Marano, *Eng. Fract. Mech.* **2014**, *27*, 46-55
4. R. J. Young, *Introduction to Polymers* **1981,** *5*, 292-293.
5. J. Gamez-Perez, O. Santana, A.B. Martinez, ML. Maspoch, *Polym. Test.* **2008**, 27, 491-497
6. R. Quinson, J. Perez, M. Rink, A. Pavan, *J. Mater. Sci.* **1997**, *32*, 5,1371-1379

Chapter 4

Assessment of long-term performance of isotactic polypropylene using short-term tests

4.1 Introduction

The experimental activity described in this chapter was carried out in the laboratories at the Eindhoven University of Technology in the group of Prof. Govaert.

In the last decades polymers have been increasingly employed in the production of load-bearing component to be used also at relatively high temperature. Pipes for hot water and gas transportation are an example. For such applications it is necessary to predict the pipe lifetime; it is not a question of whether it will fail but only a question of on what timescale it will fail.

Pipes are commonly subjected to a fairly constant pressure in a large part of their service lives. This kind of loading history can be reproduced in laboratory as a creep test in which a specimen undergoes a constant applied load up to its failure. When a viscoelastic material like a polymer is subjected to a constant load as in a creep test, the deformation continues to increase in time up to the failure of the specimen.

The hoop stress versus failure time, schematically reported in Figure 1, providing the time at which the failure will occur for a pipe subjected to a certain stress level at a specific reference temperature, is commonly obtained by performing temperature accelerated creep tests (Figure 2)[1] on pipe sections (Figure 3).

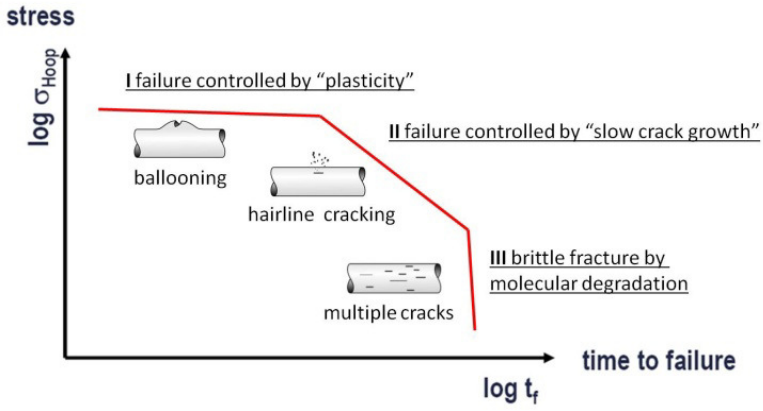

Figure 1. ***Schematic representation of a hoop stress vs. time-to-failure curve with the illustrations of failure mechanisms***

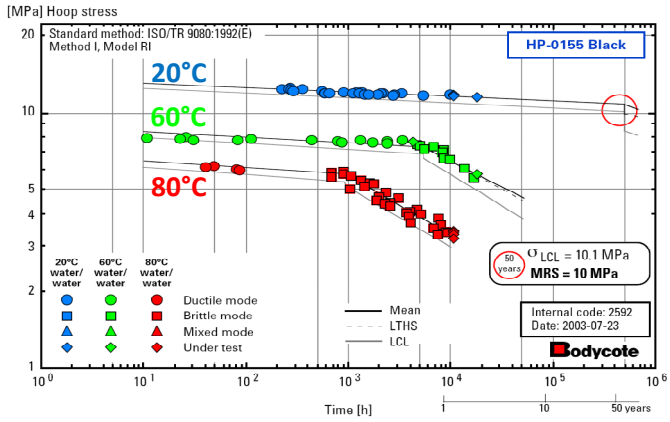

Figure 2. ***Hoop stress vs. time-to-failure curve built with experimental data of a PE100 at three temperatures (20°C, 60°C, 80°C). A standard method (ISO/TR 9080:1992(E)) was adopted to fit the data*** [1]

By extrapolation, it is possible to predict the pipe lifetime at service temperature using the experimental data at high temperatures (short time). Using a simple regression method, by data interpolation, it is possible to fit the data and to predict pipes time-to-failure in correspondence of the applied σ_{Hoop} as shown in Figure 2.[1]

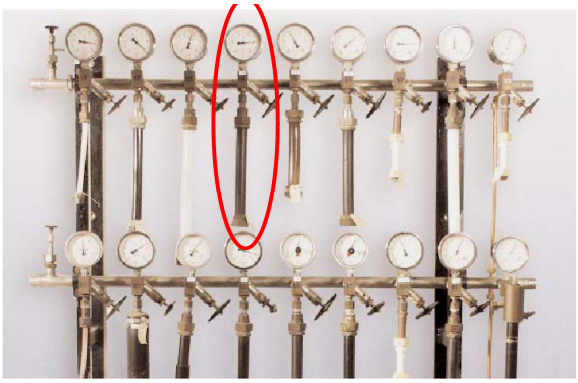

Figure 3. Hostalen GM 5010 pipes under constant pressure since 1956

The long-term creep data are normally used as certification data to ensure that a pipe will not break before 50 years at 20°C under a certain applied stress level.

Although this experimental method works the tests are expensive because time consuming with testing times exceeding 1.5 years. In conclusion this method is not a suitable tool for material selection.

As the scheme reported in Figure 1 shows, it is possible to recognize three different regions corresponding to different failure modes depending on the applied stress level. Region II is characterized by brittle fracture, caused by the stable growth of a hairline crack, that proceeds through the thickness of the pipe wall. It is usually investigated through fracture mechanic approach.

Instead, in the region I, the failure is ductile and it is preceded by large, local plastic deformations (ballooning). A fracture mechanic approach cannot be applied and there are not sound models for a quantitative prediction of this behavior. At even lower stress levels, the failure is largely due to chemical degradation of the polymer (region III), leading to a reduction of molar mass and causing, eventually , the formation of a multitude of cracks. The knee that marks the transition between region I and region II is termed "mechanical knee", while that between region II and region III is termed "chemical knee". Region III is not studied in this work since the thermal and chemical stability of polymers, especially of polyolefins, has been so enhanced in the last decades that this region has shifted to so long times that this kind of mechanism in service conditions for pipes failure is almost never observed.

There are several reasons to investigate and to develop a model for the plasticity-controlled failure region; firstly, it is crucial to determine the “mechanical knee”, as shown in Figure 1, that is influenced by the type of polymer as well as by the thermo-mechanical process that was applied on the material. Materials cooled with different cooling rates are characterized by a different behavior in region I causing a shift of the mechanical knee. [2-3] In addition, the improvement in the slow crack growth resistance of several HDPE pipes from the first to third generation has allowed to shift the region II towards very long times. Consequently this region could be not always critical. [2-3] Moreover it is crucial to understand how the modifications in the material properties affect the behavior in the two failure regions since they could have an opposite effect in the kinetics of slow crack growth and plasticity controlled phenomena. [2-3]

An approach to predict the ductile failure of amorphous polymers as PC[2-4], PVC[2-3],PMMA[5], PLLA[5], PS[5], , and of some polyolefins[4-8] by using short-term tensile tests was developed. The experimental work performed during the period spent at Eindhoven University of Technology was aimed at validating the approach in the case of other semicrystalline polymers, an isotactic polypropylene and one of its copolymer.

4.2 Methodology

The approach is based on the hypothesis that the plasticity-controlled failure in region I occurs when a certain amount of plastic strain is accumulated up to a critical strain value.[2-9]

From a creep test the strain as function of time schematically shown in Figure 4 can be obtained.

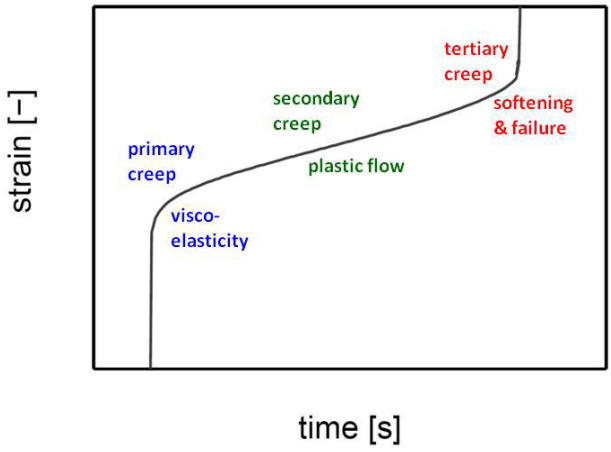

Figure 4. ***Schematic representation of a strain vs. time curve obtained by a creep test. Three regimes can be distinguished: primary, secondary and tertiary creep***

Strain rate first decreases during the primary creep and then becomes constant in the secondary creep. Eventually (tertiary creep) it increases up to specimen failure. The time corresponding to the sudden strain rate increase in tertiary creep is defined "time to failure" (the time at which the failure initiates).

In Figure 5 data from Crissman and McKenna [10] are reported as an example. They show that the higher the applied load is the shorter the failure, the faster the plastic flow. The strain at failure is constant.

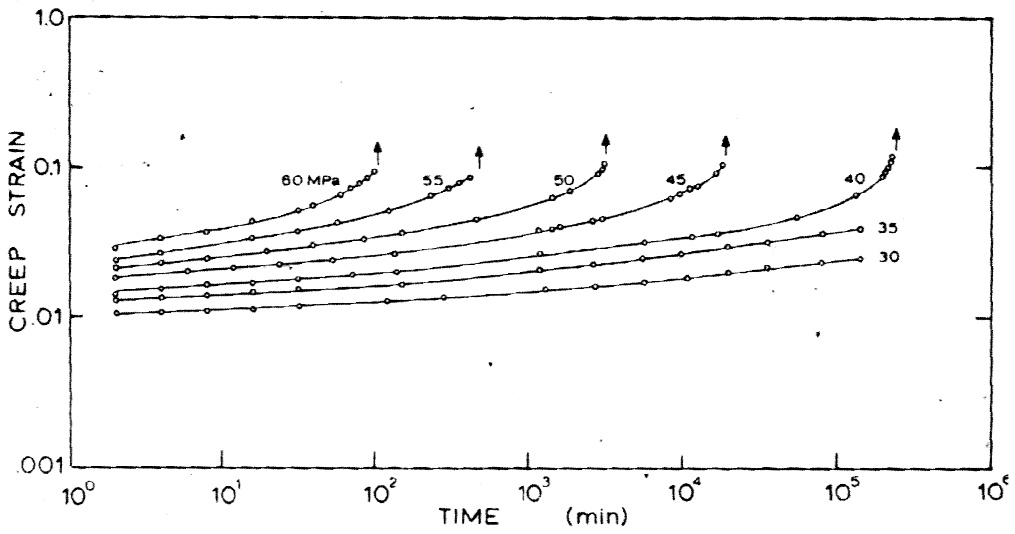

Figure 5. ***Creep strain versus time for PMMA aged at T_{room} for over 5 years at different applied engineering stresses (T=22.5°C)*** [10]

It was reported [10,11] that the product between the strain rate at failure $\dot{\varepsilon}_f$ and the time to failure t_f is a constant independently of the level of the applied

stress (Equation 1) as the trend of $\dot{\varepsilon}_f$ versus t_f data obtained from creep tests on polycarbonate [4], reported as an example in Figure 6, show.

Equation 1.

$$\dot{\varepsilon}_f(\sigma) t_f(\sigma) = constant \qquad \forall \sigma$$

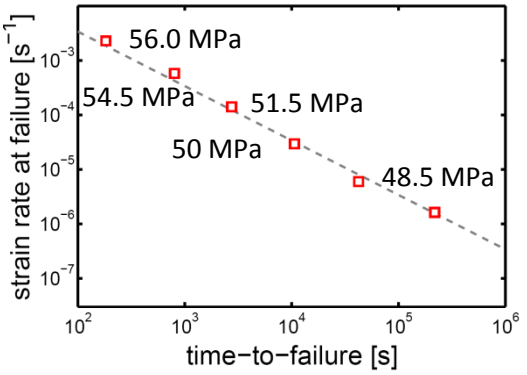

Figure 6. ***Strain rate at failure versus the time-to-failure from creep tests on a polycarbonate [4]***

In Figure 7a the slope of the strain versus time curves relevant to a polycarbonate[4] as an example is plotted as a function of the applied strain (Sherby-Dorn plots) [12-13]. In Figure 7a experimental data[4] are reported as an example.

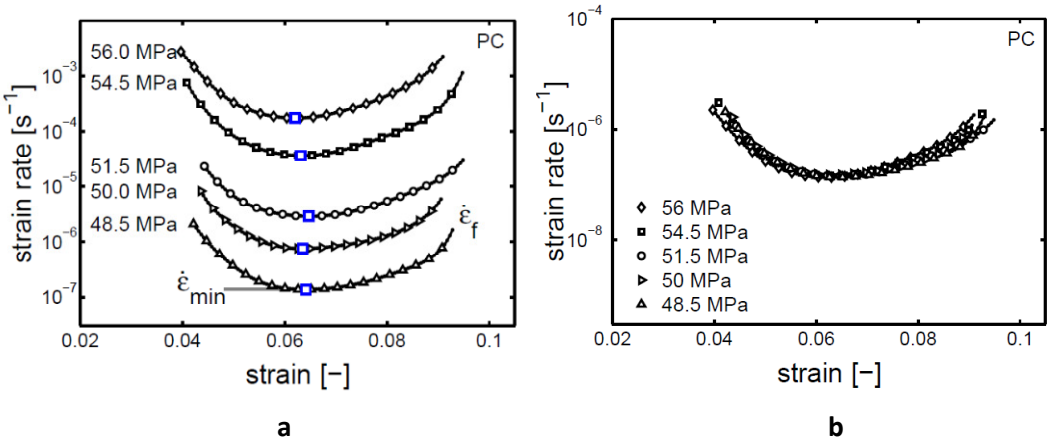

Figure 7. ***a)Strain rate versus strain by creep tests performed on a polycarbonate at different applied stress levels (Sherby-Dorn plots).[4] b) Sherby-Dorn curves shifted to the curve from 48.5 MPa to illustrate the similarity of the curves [4]***

Generally speaking, initially the strain rate decreases then it becomes constant and then it increases again up to failure. The strain range over which the strain rate keeps its maximum value depends on the type of polymer. For PC it resulted to be quite small while for PE a wider strain range was observed.[2-3] From the literature[4] it is known that a strain rate versus strain master curve can be obtained as shown in Figure 7b. From the results shown in Figure 7b it comes out that the ratio between the strain rate at failure for two creep tests at different applied stresses is equal to the ratio between the corresponding minimum strain rates, that is (Equation 2) [12-13]:

Equation 2.

$$\frac{\dot{\varepsilon}_f\,(\sigma_1)}{\dot{\varepsilon}_f\,(\sigma_2)} = \frac{\dot{\varepsilon}_{min}\,(\sigma_1)}{\dot{\varepsilon}_{min}\,(\sigma_2)}$$

The superposition of Sherby-Dorn plots is verified if these hypothesis reported in literature [10] are satisfied: (i) the creep curves are superposable irrespective of the applied load level; (ii) the strain at failure is constant; (iii) the vertical

shift factor of the creep curves for the obtaining of a master curve is equal to the ratio between the applied stress and the reference stress.

From Equations 1 and 2, it is possible to write the Equation 3:

Equation 3.

$$\dot{\varepsilon}_{min}(\sigma)\, t_f(\sigma) = \varepsilon_{cr} \quad \forall\sigma$$

where the right-hand term, named "critical strain", ε_{cr} , is independent of the applied stress; it can be regarded as the amount of plastic strain that would be accumulated if the material would display plastic flow at the constant strain rate in secondary creep ($\dot{\varepsilon}_{min}$) for the entire lifetime. Actually the critical strain is smaller than the real plastic strain at failure since in the tertiary creep the strain rate gradually increases[2-4]. Even if the value of ε_{cr} is underestimated a quantitative prediction of the time to failure is possible.[4]

The failure occurs when the accumulated plastic strain is equal to the critical strain (Equation 4).

Equation 4.

$$t_f(\sigma) = \frac{\varepsilon_{cr}}{\dot{\varepsilon}_{min}(\sigma)}$$

So using this relationship the time to failure can be predicted without conducting creep tests until fracture; in fact it is sufficient from creep tests deriving the critical strain and the secondary creep rates for each level of stress.

Furthermore the steady state reached in creep tests (applied constant load condition) in correspondence of the minimum strain rate (secondary creep rate) is identical to the state reached in correspondence of the yield point during a constant strain rate experiment; it results in $\dot{\varepsilon}_{min} = \dot{\varepsilon}_{pl}$.

Therefore after obtaining by short-term tensile tests the strain rate dependence of the yield stress, it is possible to linearly extrapolate in a semilogarithmic plot at lower strain rates the correspondent stresses[4]. The data that describe the dependence of the yield stress on the strain rate, obtained from tensile tests at applied constant strain rate, are on the same curve of the data that describe the stress dependency of the plastic strain rate, obtained from creep tests under a constant static load,[10] as presented in Figure 8. This indicates the equivalence between the steady state reached in constant load experiments and the steady state reached in constant strain rate experiments; the deformation kinetics under an applied load can be described using the kinetics of an applied strain rate experiment.

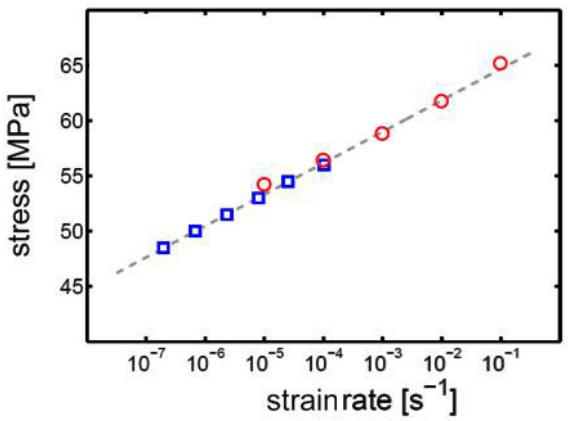

Figure 8. ***Relation between the stresses and the applied strain rates in constant strain rate tests (red symbols) and between the applied stresses and the secondary creep strain rates in creep tests (blue symbols)*** [4]

To model the dependence on stress and temperature of the plastic strain rate in tensile tests in constant strain rate experiments Eyring flow equation can be used (Equation 5).

Equation 5.

$$\dot{\varepsilon}_{pl}(T,\sigma) = \dot{\varepsilon}_0(S)\exp\left(-\frac{\Delta U}{RT}\right)\sinh\left(\frac{\sigma V^*}{kT}\right)$$

The right-hand side of this equation consists of a pre-exponential factor depending on the thermodynamic state of the material and an exponential term for the temperature dependence of the plastic stain rate related to the activation energy ΔU and a term for the stress activation related to the activation volume V^*.

A pressure-modified Eyring flow relation should be used to take into account the influence of the hydrostatic pressure on plastic deformation: this would allow to describe the plastic deformation kinetics under loading conditions more complex than the uniaxial loading.

Using the parameters of Eyring flow equation ($\dot{\varepsilon}_0$, ΔU, V^*) obtained by fitting the data that describe the dependence of the yield stress on the strain rate and the data obtained by performing creep tests at 20°C at different applied stress levels, thanks to this equivalency, - $\dot{\varepsilon}_{min} = \dot{\varepsilon}_{pl}$ - the value of critical strain can be determined by Equation 6.

Equation 6.

$$\dot{\varepsilon}_{pl}(\sigma)\, t_f(\sigma) = \varepsilon_{cr} \quad \forall\sigma$$

Once that the critical strain has been determined, time to failure predictions at other temperatures can be made, as shown in equation 7, performing tensile tests at constant strain rate instead of creep tests that are time consuming and experimentally complex.

Equation 7.

$$t_f(\sigma) = \frac{\varepsilon_{cr}}{\dot{\varepsilon}_{pl}(\sigma)} \quad \forall\sigma$$

4.3 Experimental

A preliminary characterization of the materials was performed to evaluate the effect of different cooling temperatures and of ageing performing uniaxial tensile tests. Then uniaxial tensile test at different applied strain rates and at different temperatures were performed on both materials to evaluate their deformation kinetics. Using the parameters of Eyring flow equation ($\dot{\varepsilon}_0$, ΔU, V^*) obtained by fitting the data that describe the dependence of the yield stress on the strain rate and the value of the critical strain kept by literature, [7] time to failure predictions were made at each temperature. Successively creep tests at different applied stress levels and at the same temperatures previously investigated were performed to validate the prediction. Eventually long term creep data kindly supplied by Sabic were included to validate the method to predict long term performance in the plasticity-controlled region.

4.3.1 Materials

Two isotactic polypropilenes, a homopolymer (i-PP_1) and a copolymer (i-PP_2) with a percentage of ethylene units equal to 3.3 randomly dispersed were studied in this work. The materials were kindly supplied by Sabic, who provided the polymers molecular weight and molecular weight distribution, Mw/Mn, which are reported in table 1. Melting temperature, T_m, and crystallinity degree, χ, were measured by DSC tests performed at 10°C/min heating rate and are reported in table 1 as well.

Material	Mw	Mw/Mn	T_m	χ	Ethylene units
	(10^3 g/mole)	----	(°C)	(%)	(%)
i-PP_1	740	4.4	168	53.8	---
i-PP_2	710	4.4	144	49.7	3.3

[a] $\chi=\frac{\Delta H_m}{\Delta H^0}$, where ΔH_m is the experimental melting enthalpy and $\Delta H^0 = 207.1\, J/g$ [14] is α-form i-PP melting enthalpy for 100% of crystallinity;

Table 1. ***Characteristic data of i-PPs***

4.3.2 Samples preparation

For the preliminary characterization of both the materials (i-PP_1, i-PP_2) dumbbell specimens with a gauge length of 20 mm were obtained by die cutting from 1.5mm thick plates compression molded at 220°C and cooled down to different cooling temperatures (T_{cool} = 20°C, 40°C, 60°C, 80°C, 100°C). After the cooling step in the "cooling" press, each plate was cooled down to T_{room} leaving it in air. In both steps the cooling rate was not controlled. Only one plate of i-PP1 was obtained by compression molding at 220°C and was cooled down to T_{room} really slowly (turning off the heating elements of the heating plates). In Figure 9 a schematic graph describing the cooling process is reported. The different cooling temperatures and consequently the different cooling rates have an evident effect on the microstructure: faster the cooling process, lower the crystallinity degree, less ordered or smaller the crystals. Data relevant to these specimens will be referred to as "TU/e" data.

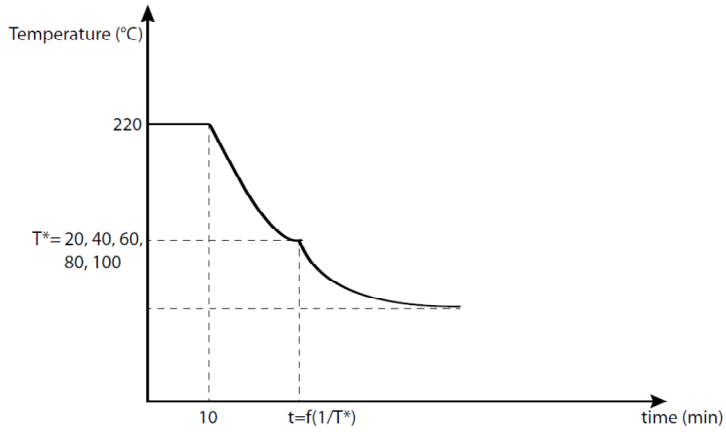

Figure 9. ***Schematic graph reporting the conditions (time, temperature) of the cooling process adopted in the compression molding process for i-PP_1 and i-PP_2 at TU/e***

For both materials (i-PP_1, i-PP_2) Sabic provided plates that had been compression molded and cooled down to T_{room} at a cooling rate of 15°C/min replicating the material thermal history during pipe manufacturing process. Dumbbell samples with a gauge length of 20 mm were obtained from Sabic plates. Data relevant to Sabic specimens will be referred to as "Sabic" data.

4.3.3 Uniaxial tensile tests for preliminary testing

Uniaxial tensile tests were performed with a dynamometer Zwick/Roell at T_{room} at a constant strain rate of $10^{-3}s^{-1}$ after a maximum time loss of 5 h after molding on specimens of both materials (i-PP_1 and i-PP_2) cooled down to different cooling temperature. Nominal stress-strain curves are reported in Figure 10a(i-PP_1) – b (i-PP_2). The yield stress was determined as the maximum of the stress-strain curve. In Figure 11a,b the yield stress is reported

as function of $T_{cooling}$ for both materials. It can be observed that both for i-PP_1 and i-PP_2 the yield stress reaches a constant value for $T_{cooling}$ between 80°C and 100°C while the mechanical behavior of i-PP_1 slowly cooled is less ductile.

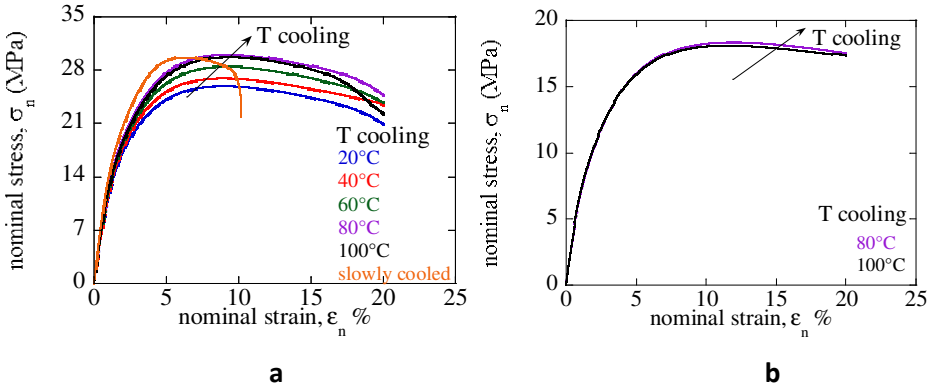

Figure 10. ***Nominal stress-strain curves of i-PP_1 (a) and i-PP_2 (b) cooled down to different temperatures; tests performed at $\dot{\varepsilon} = 10^{-3}s^{-1}$ and at T_{room}.***

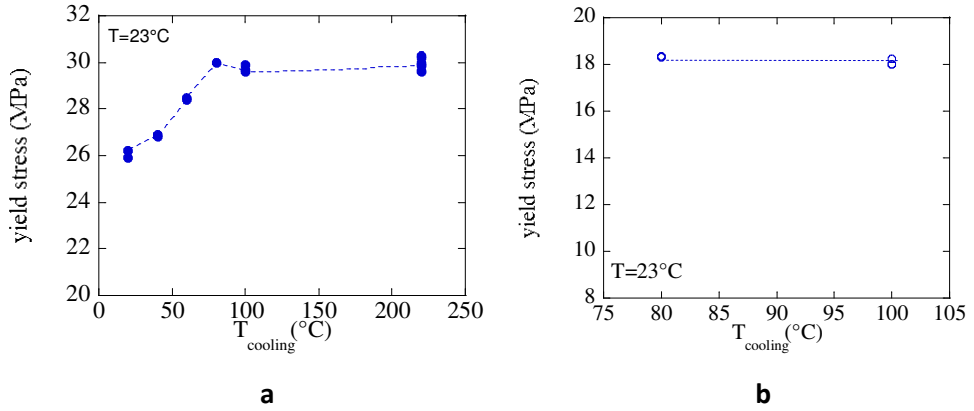

Figure 11. ***Yield stress versus $T_{cooling}$ for i-PP_1 (a) and i-PP_2 (b) cooled down to different temperatures. Data are relevant to uniaxial tensile tests performed on i-PP_1 and i-PP_2 at $\dot{\varepsilon} = 10^{-3}s^{-1}$ and at T_{room}***

The results reported in Figure 10 gave an important indication concerning the degree of crystallinity of both the materials. Since the yield stress reached a constant value for $T_{cooling} \geq 80°C$, the degree of crystallinity obtained for $T_{cooling} \geq 80°C$ is as higher as possible regarding the adopted compression molding conditions. No further increase in crystallinity degree is expected with time.

Figure 12a shows the nominal stress-strain curves as results of tensile tests performed on i-PP_1 TU/e dumbbell specimens at T_{room} at a constant applied strain rate of $10^{-3}s^{-1}$ both after molding and cooling down to 100°C and after 1 week after molding. Figure 12b shows the nominal stress-strain curves as results of tensile tests performed using the same conditions regarding the temperature and the strain rate reported before on i-PP_1 Sabic dumbbell specimens tested after 1 day and 1 week after molding at TU/e laboratory. Figure 12c shows a comparison between the mechanical response of Sabic and TU/e samples after 1 week after molding. It can be observed that the nominal stress-strain curves are perfectly superimposable.

Figure 13a shows the nominal stress-strain curves as results of tensile tests performed on i-PP_2 TU/e dumbbell specimens at T_{room} at a constant applied strain rate of $10^{-3}s^{-1}$ both after molding and cooling down to 80°C and after 1 week after molding. Figure 13b shows the nominal stress-strain curves as results of tensile tests performed using the same conditions regarding the temperature and the strain rate reported before on i-PP_2 Sabic dumbbell specimens tested after 1 day and 1 week after molding at TU/e laboratory. Figure 13c shows a comparison between the mechanical response of Sabic and

TU/e samples after 1 week after molding. It can be observed that the nominal stress-strain curves are perfectly superimposable.

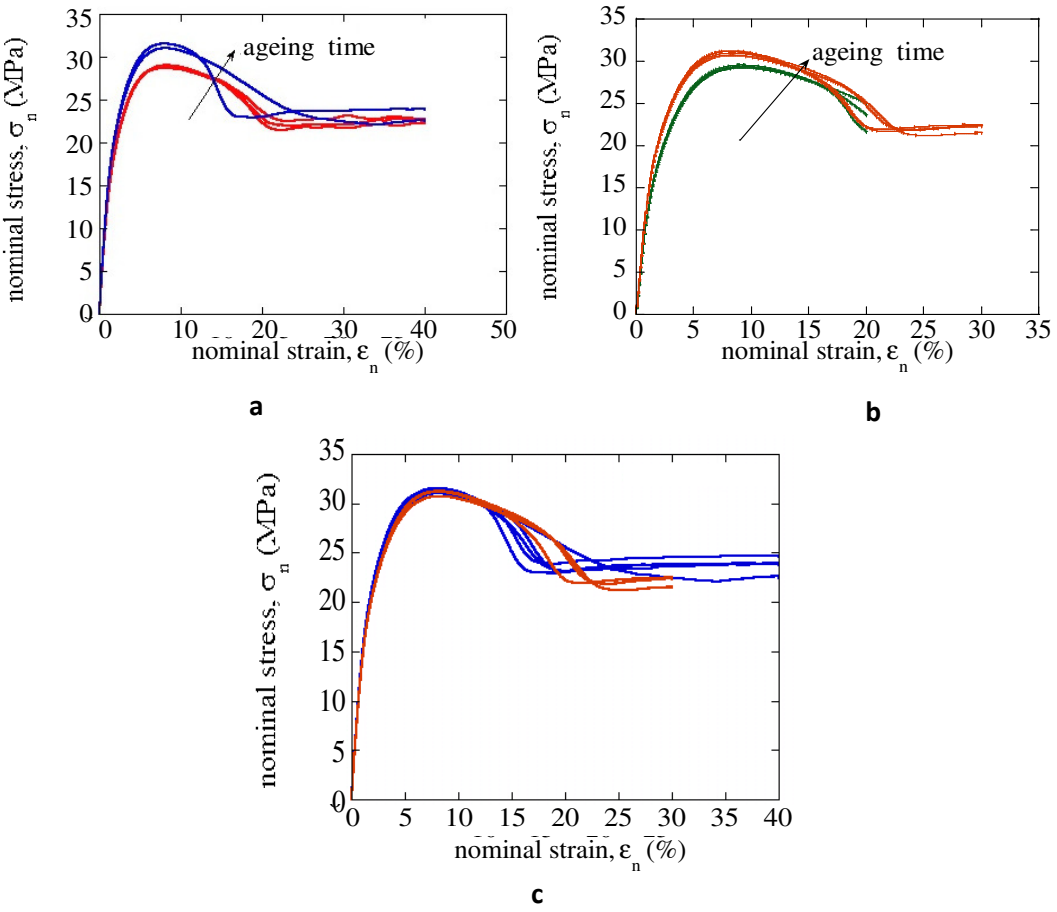

Figure 12. ***a) Nominal stress-strain curves of i-PP_1 compression molded at TU/e and cooled down to 100°C . Tests performed both after molding and 1 week after molding at $\dot{\varepsilon} = 10^{-3}s^{-1}$ and at T_{room} . b) Nominal stress-strain curves of i-PP_1 compression molded at Sabic. Tests performed both after 1day and 1 week after molding at $\dot{\varepsilon} = 10^{-3}s^{-1}$ and at T_{room} . c) Comparison of the mechanical response of i-PP_1 compression molded at TU/e and in Sabic after 1 week ageing.***

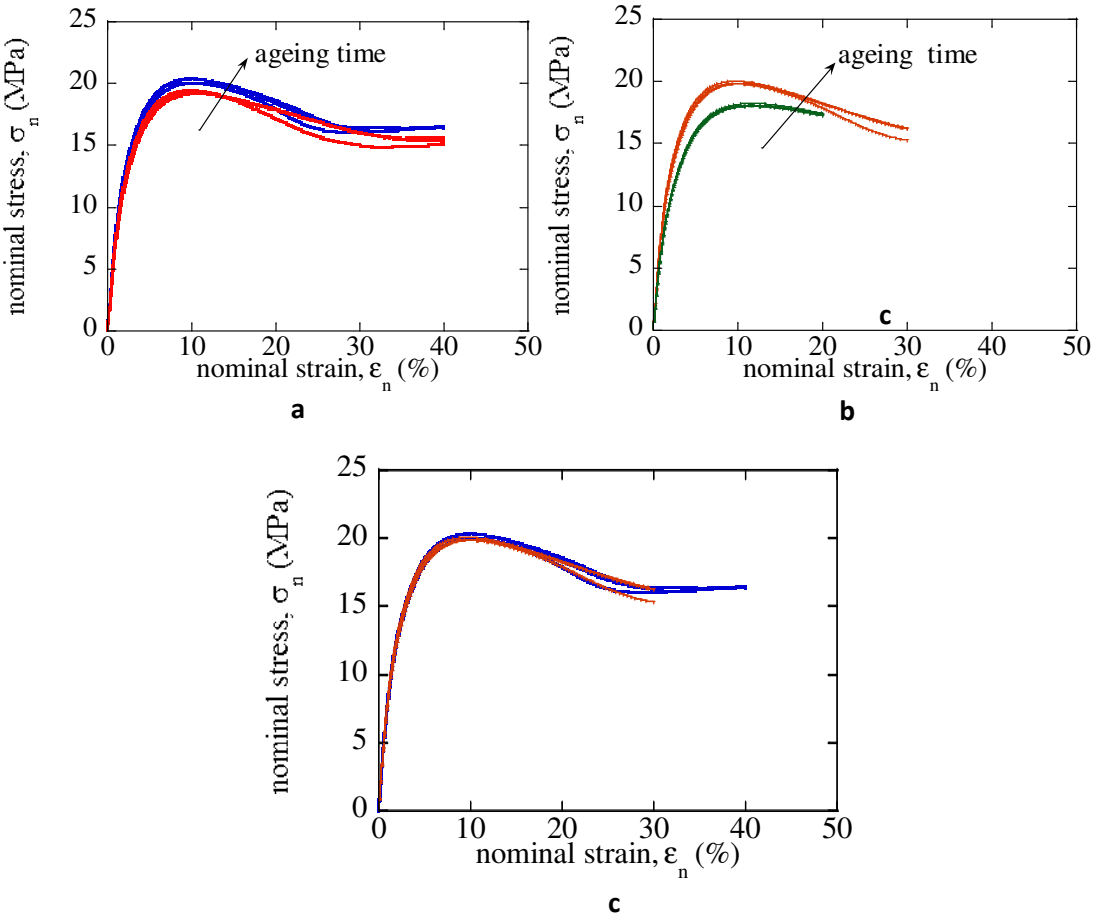

Figure 13. ***a) Nominal stress-strain curves of i-PP_2 compression molded at TU/e and cooled down to 80°C . Tests performed both after molding and 1 week after molding at $\dot{\varepsilon} = 10^{-3}s^{-1}$ and at T_{room} . b) Nominal stress-strain curves of i-PP_2 compression molded at Sabic. Tests performed both after 1day and 1 week after molding at $\dot{\varepsilon} = 10^{-3}s^{-1}$ and at T_{room} . c) Comparison of the mechanical response of i-PP_2 compression molded at TU/e and in Sabic after 1 week ageing.***

Generally speaking, the amorphous glassy polymers and the amorphous phase of semicrystalline polymers under T_g , which are out of their equilibrium state, show a variation also in their mechanical response due to the physical ageing that causes a densification of the material, a reduction of the free volume to gain the equilibrium state.

Glass transition temperature of the i-PP amorphous fraction is lower than T_{room} therefore the amorphous phase should behave as a rubber at this temperature. Therefore no physical ageing effect should be occur in the amorphous phase of i-PP. In semicrystalline polymers e over T_g with the amorphous pha the amorphous phase closer to the crystalline domains (see paragraph 1.1) is more rigid than the amorphous phase far from these domains with relaxation times longer than the rubberlike amorphous and the molecular mobility more difficult because of the presence of crystalline phase. The T_g of RAP is higher than the previous one and physical ageing of this amorphous fraction can occur (Figure 14).

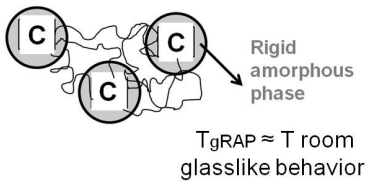

Figure 14. ***Schematic representation of the rigid amorphous phase***

This theoretical background can help to explain the experimental results reported in Figures 11a,b and 12a,b; both the materials i-PP_1 and i-PP_2

show an increase in the yield stress with ageing time that can be explained with the physical ageing of the rigid amorphous phase closer to the crystalline

domains. Even if the thermal history applied on TU/e i-PP_1 and on Sabic i-PP_1 plates were different their mechanical response after 1 week ageing were the same. The same consideration can be made for TU/e i-PP_2 and Sabic i-PP_2 plates.

By the preliminary characterization of i-PP_1 and i-PP_2 regarding the effect of different cooling temperatures and of ageing time the optimized "process" conditions to obtain the same mechanical response of plates prepared in Sabic both for i-PP_1 and i-PP_2 prepared at TU/e were determined and were reported in Table 2

Material	$T_{compression\ molding}$	$T_{cooling}$	Ageing time
	(°C)	(°C)	
i-PP_1	220	100	1 week
i-PP_2	220	80	1 week

Table 2. ***Optimized "process" conditions for i-PP_1 and i-PP-2 compression molded at TU/e***

4.3.4 Deformation kinetics

Dumbbell specimens of both the materials with a gauge length of 20 mm were obtained by die cutting from 1.5mm thick plates prepared at TU/e using the optimized process conditions reported in table 2 in paragraph 4.3.3.

Uniaxial tensile tests at a constant applied strain rate were performed with a dynamometer Zwick/Roell at different applied strain rates and at different temperatures.

In Figure 15 a,b yield stresses as function of strain rate applied in constant strain rate tests at different temperatures are reported for i-PP_1 and 1-PP_2 respectively. Data fitting according to Ree-Eyring equation were reported as well.

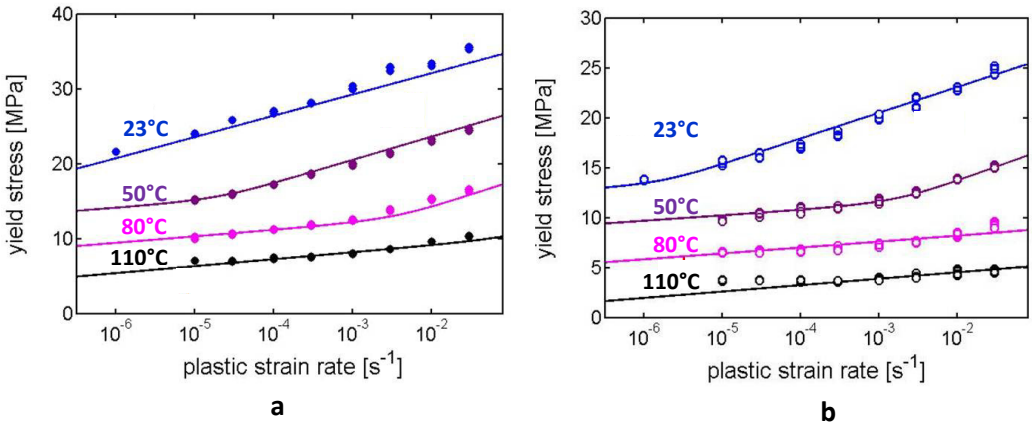

Figure 15. ***Yield stresses as function of the applied strain rates for i-PP_1 (a) and for i-PP_2 (b). The lines are data fitting according to Ree-Eyring equation.***

For each material activation volumes, V^*,activation energies ΔH and the pre-exponential factors (rate constants) $\dot{\varepsilon}_0$ were determined for both processes. All the parameters determined were reported in Table 3.

Material	Process I			Process II		
	V^*_1	ΔH_1	$\dot{\varepsilon}_{0,1}$	V^*_2	ΔH_2	$\dot{\varepsilon}_{0,2}$
	nm^3	$kJmol^{-1}$	s^{-1}	nm^3	$kJmol^{-1}$	s^{-1}
i-PP_1	10	360	$1*10^{39.5}$	4.5	222	$5*10^{31}$
i-PP_2	10	360	$2*10^{44}$	5.6	222	$6*10^{33}$

Table 3. ***Ree-Eyring parameters for i-PP_1 and i-PP_2***

For both materials i-PP_1 and i-PP_2 it can be observed a bilinear trend of experimental data. Generally speaking, for thermoreologically complex polymers as some amorphous polymers, heterogeneous blends and semicrystalline polymers, the yielding, that is a thermally activated process , is influenced by different molecular deformation processes that are characterized by their own characteristic kinetics.[7] In these case two processes can be recognized:

- Process I that dominates at high temperature and/or low strain rates with a flat slope and weak temperature dependence.
- Process II that dominates at low temperature and/or high strain rate with a steeper slope and a stronger temperature dependence.

By a molecular point of view, considering the microstructure of a semicrystalline polymer the process I is linked to intra-lamellar deformations in the crystalline phase (crystal slip mechanisms) while the process II is linked to the chain diffusion through the crystal that initiates the mobility within the rigid amorphous phase surrounding the crystal as schematically reported in Figure 16. As suggested by Séguéla et. al. [15,16] the crystal slip mechanisms are facilitate by dislocations that nucleate and propagate along the easiest crystals

slip systems. In process II the deformation takes place in the amorphous phase so that this process is linked to the α-relaxation processes that can be regarded as to pulling chains out of the crystals.[15,16]

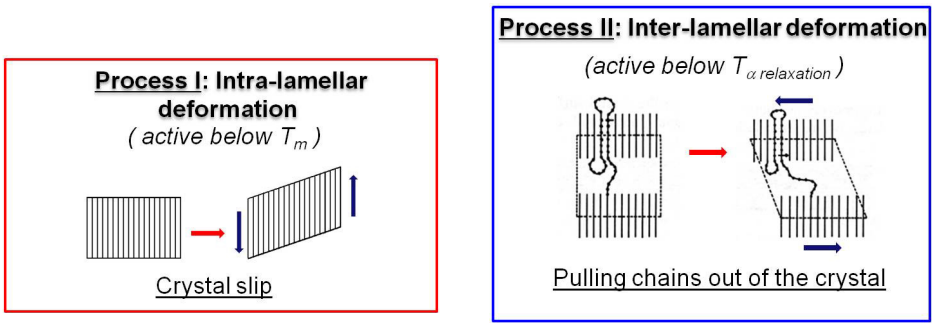

Figure 16. ***Schematic representation of the molecular mechanisms involved in processes I and II*** [4]

In these cases it is possible to use the Ree-Eyring modification of the Eyring flow equation which assumes that the two relaxation processes previously described act independently and their stress contributions are additive as reported in Equation 8.

Equation 8.

$$\sigma_{total} = \sigma_1 + \sigma_2 = \frac{kT}{V_I^*} sinh^{-1}\left(\frac{\dot{\varepsilon}}{\dot{\varepsilon}_{0,I} exp(-\frac{\Delta U_I}{kT})}\right) + \frac{kT}{V_{II}^*} sinh^{-1}\left(\frac{\dot{\varepsilon}}{\dot{\varepsilon}_{0,II} exp(-\frac{\Delta U_{II}}{kT})}\right)$$

In Figure 15 it can be observed that for i-PP_1 at 80°C both processes I and II are distinguishable while for i-PP_2 at the same temperature the process I is still dominant. Moreover it can be noticed that for i-PP_2 the data at 110°C

deviate from the fitting line because of the annealing effect (see paragraph 4.3.5).

4.3.5 Creep tests

Once that the Ree-Eyring flow equation (Equation 8) parameters were obtained by the data fitting presented in paragraph 4.3.4, creep tests at 20°C should be performed as previously described in the paragraph reporting the methodology and, eventually, the critical strain ε_{cr} can be obtained by Equation 6. After determining the value of ε_{cr} time to failure predictions for other temperatures can be determined adopting Equation 7. In this work the critical strain for both the materials was not directly calculated but kept by literature [7] and reported in Table 4.

Material	critical strain ε_{cr}
i-PP_1	0.065
i-PP-2	0.12

Table 4. ***Critical strain values for i-PP_1 and i-PP_2***

Adopting these values of critical strain for both i-PP_1 and i-PP_2 time to failure prediction was obtained through Equation 7 (continuous lines in Figure 17a,b).

Dumbbell specimens of both the materials with a gauge length of 20 mm were obtained by die cutting from 1.5mm thick plates prepared at TU/e using the optimized process conditions reported in table 2 in paragraph 4.3.3.

Creep tests on dumbbell specimens were performed using a dynamometer Zwick/Roell in uniaxial tensile configuration applying for each test a loading ramp of 10 s in order to reach a certain load that was applied for the whole test up to the specimen failure (necking formation). The duration of the adopted loading ramp was at least 2 orders of magnitude shorter that the minimum time to failure measured.

Figure 17a,b reports data relevant to short term creep tests which validate the prediction (continuous lines).

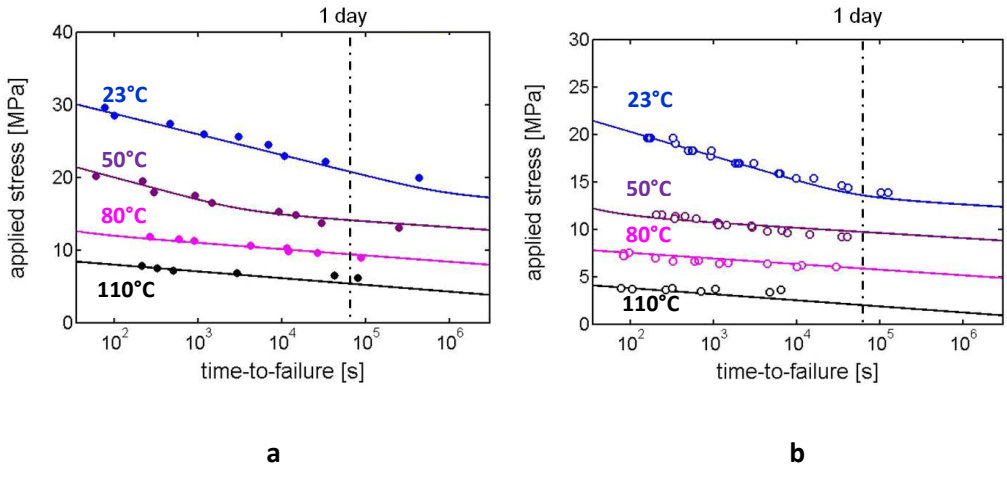

Figure 17. Time to failure prediction (continuous lines) and short term creep experimental data for i-PP_1 (a) and for i-PP_2 (b)

Long-term creep data at several temperatures were provided by Sabic for i-PP_2. To validate the lifetime prediction they are reported in Figure 18 together with the prediction continuous lines.

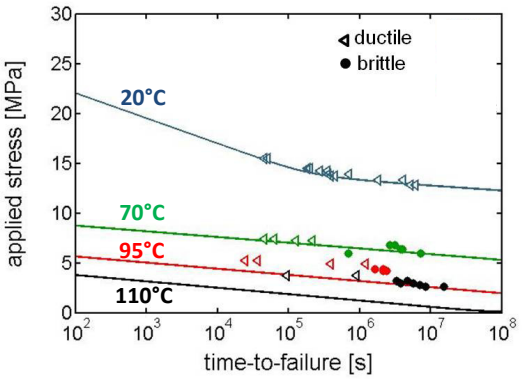

Figure 18. ***Time to failure prediction (continuous lines) and long- term creep experimental data (data by Sabic) for i-PP_2***

By the plot in Figure 18, it can be observed that the adopted model works really well but a deviation at long times from the predictive lines at 110°C and 95°C is present.

4.3.6 Annealing effect

To investigate the cause of the observed deviation dumbbell specimens of i-PP_2 were kept at 110°C for different thermal treatment times (t = 30 min, 1h, 3h, 10h, 30h, 100h, 300h, 1000h) before testing with tensile tests at the same temperature (T_{test}= 110°C) at an applied strain rate equal to $10^{-3}s^{-1}$ because in this conditions only process I mainly acts as shown in Figures 15,17b and no deviation from the prediction can be observed.

In Figure 19 an almost linear dependence of the yield stress on annealing time in a semilogarithmic plot can be observed. It is the result of a microstructure modification during the thermal process: lamellar thickness growth. [8,15-16]

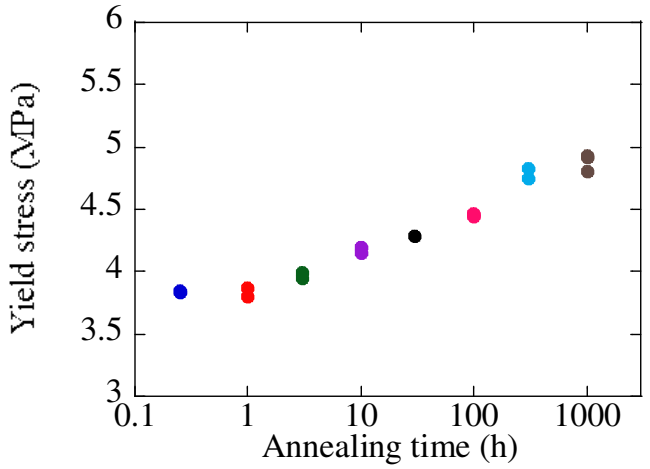

Figure 19. ***Yield stresses as function of annealing times (h) on a semilogarithmic scale for i-PP_2. Data relevant to uniaxial tensile tests performed at $\dot{\varepsilon} = 10^{-3}s^{-1}$ and at T=110°C.***

The annealing effect should be taken into account in the model. It is known that the pre-exponential factor in Eyring equation is dependent on prior thermal history and progressive ageing, therefore it is possible to express it with this equation (Equation 9)[17]

Equation 9[17]

$$\dot{\varepsilon}_{pl}(T,\sigma) = \dot{\varepsilon}_0(S)\exp\left(-\frac{\Delta U}{RT}\right)\sinh\left(\frac{\sigma V^*}{kT}\right)$$

$$\dot{\varepsilon}_0(S) = \dot{\varepsilon}_{0,r}\exp\left(-S_A(t)\right)$$

$$S_A = C_0 + C_1\ln\left(\frac{t}{t_0} + C_2\right) \qquad C_2 = \exp\left(-\frac{C_0}{C_1}\right)$$

in which S_a is dependent not only on the annealing time (thermal treatment) but also on initial annealing time (time at which the thermal treatment begins to show its effect) [17].

Considering also the annealing effect in the predictive model only for process I a better fitting of the experimental data was obtained as shown in Figure 20.

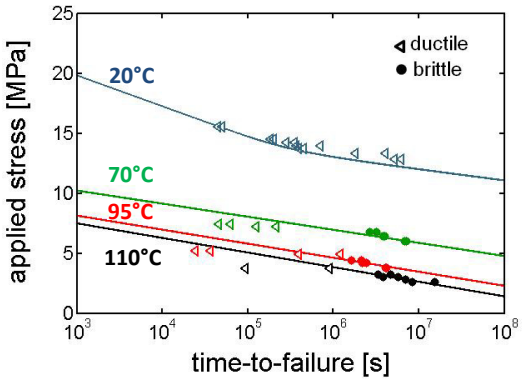

Figure 20. ***Time to failure prediction (continuous lines) and long-term creep experimental data (data by Sabic) for i-PP_2 including the annealing effect***

4.4 Conclusions

The good agreement between the prediction and the long-term creep data of the i-PP_2 is promising for describing the long term performances of semicystalline polymers.

Also the annealing effect is included in the model in order to take into account some microstructural modifications that occur during really long tests.

Bibliography

1. www.bodycotepolymer.com
2. H. A. Visser, T. C. Bor, M. Wolters, T. A. P. Engels , L. E. Govaert, *Macromol. Mater. Eng.* **2010**, *295*, 637-651
3. R. Visser, *Residual lifetime assessment of uPVC pipes* **2010** (PhD thesis)
4. M.J.W Kanters, *Assessment of long-term performance of solid polymers using short-term testing* **2011**
5. L. C. A. van Breemen, T. A. P. Engels, E. T. J. Klompen, D. J. A. Senden, L. E. Govaert, *J. Pol. Sci. Part B* **2012** ,*50*, 1757-1771
6. A. Sedighiamiri , D.J.A. Senden , D. Tranchida , L.E. Govaert , J.A.W. van Dommelen, *Comp. Mater. Sci.* **2014**, *82*, 415–426
7. T. B. Van Erp, C. T. Reynolds, T. Peijs, J. A. W. Van Dommelen, L. E. Govaert, *J. Pol. Sci. Part B* **2009**, *47*, 2026–2035
8. T. B. van Erp, D. Cavallo, G. W. M. Peters, L. E. Govaert, *J. Pol. Sci. Part B* **2012** ,*50*, 1438-1451
9. C. Bauwens-Crowet, J-M. Ots, J-C Bauwens, *Mater. Sci. Let.* **1974**, *9*, 1197-1201.
10. J.M. Crissman, G.B. McKenna, *J. Polym. Sci. Part B: Polym. Phy.* **1987**, *25*, 1667-1677.
11. E.J. Kramer, E.W. Hart, Polymer **1984**, *25*, 1667-1678.
12. O.D. Sherby, J.E. Dorn, *J. Mech. Phys. Solids* **1957**, *6*, 145-162.
13. M.J. Mindel, N. Brown, *J. Mater. Sci.* **1973**, *8*, 863-870.
14. B. Wundelich, *Macromolecular physics, Academic press* **1980**

15. R. Séguéla, V. Gaucher-Miri, S.Elkoun, *J. Mater. Sci.* **1998**, *33*, 1273-1279
16. R. Séguéla, S.Elkoun,V. Gaucher-Miri, *J. Mater. Sci.* **1998**, *33*, 1801-1807
17. R. Séguéla, E. Staniek, B. Escaig, B. Fillon, *J. Appl. Polym Sci.***1999***, 71,*1873-1885
18. L. E. Govaert, T. A. P. Engels, E. T. J. Klompen, G. W. M. Peters, H.E.H. Meijer , *Intern. Polymer Processing XX.* **2005** ,2, 170-177

Publications

2011 "*CO_2 as a blowing agent for PCL: thermodynamic and mass transport properties of molten polymer/gas solutions as measured by a newly developed experimental technique*" – (long abstract) **Biofoams 2011** – Capri (IT)

2012 "*A study of the mechanical behaviour of sPP adopting cyclic tensile tests*" (long abstract and poster) – **Deformation, Yield and Fracture of Polymers 2012** – Kerkrade (NL)

2012 "*A study of the time dependence of the post yield behavior of syndiotactic polypropylene*" (long abstract and poster) – **Times of polymers and composites 2012** – Ischia (IT)

2014 *"Assessment of long-term performance of iPP pipe grade using only short-term testing***"** (poster) – **Dutch Polymer Days 2014** Lunteren (NL)

2014 *"Verification of the whole ligament yielding before fracture in EWF tests***"** (long abstract and poster) – **7th International Conference on Fracture of Polymers, Composites and Adhesives -** Les Diablerets (CH)

2015 *"Yield onset determination for polyethylenes in two different stress states"* (long abstract) – **Deformation, Yield and Fracture of Polymers 2015** – Kerkrade (NL)

CO_2 as a blowing agents for PCL: thermodynamic and mass transport properties of molten polymer/gas solutions as measured by a newly developed experimental technique

Maria Giovanna Pastore Carbone[1], Ernesto Di Maio[1], Nadia Perillo[x], Giuseppe Mensitieri[1] and Salvatore Iannace[2]

[1]*Department of Materials and Production Engineering, Faculty of Engineering, University of Naples Federico II, P.le Tecchio 80, 80125 Naples, Italy*
[2]*Institute of Composite and Biomedical Materials, National Research Council, P.le Tecchio 80, 80125 Naples, Italy*

Abstract
The foaming process of poly(ε-caprolactone) (PCL) with carbon dioxide (CO_2) was recently investigated, both theoretically and experimentally. As foaming agent for PCL, CO_2 was found to lead to a peculiar morphology of the final foam. This is due to the typical transport, chemical and physical properties of the observed polymer/gas mixture. By adopting a new experimental technique, we have investigated the thermodynamic and mass transport properties of molten PCL/ CO_2 solutions, by measuring solubility, diffusivity, specific volume and interfacial tension of the molten polymer-gas solution. This approach is based on the coupling of the gravimetric measurement with the Axysimmetric Drop Shape Analysis and provides all of the aforementioned properties in a single experiment, without relying on any theoretical assumption or equation of state at any stage of the properties evaluation. The simultaneous measurements on PCL/CO_2 solutions have been performed at three different temperatures (80, 90 and 100° C) and at gas pressures up to 4.2 MPa.

Keywords: solubility, diffusivity, interfacial tension, specific volume, axysimmetric drop shape analysis, poly(ε-caprolactone), carbon dioxide

INTRODUCTION

Gas foaming technologies have been drawing increased attention in the last decades since the extremely wide range of application of polymeric foams in several fields such as packaging, acoustic and thermal insulation, tissue engineering and separation [1]. The density and the morphology of a foam play the most important role in the final properties of the foam itself. In fact, a foam with a high density and good mechanical properties (i.e. high Young modulus and tensile strength) can be adopted for the design of structural parts, while a foam characterized by a low density are generally used in insulation or packaging. The development of supercritical fluid foaming technique paved the way to the production of microcellular foams, which are characterized by improved mechanical and impact properties as compared to standard foams, since the very small dimension of pore diameter (smaller than 10 μm) and a population density that is larger than 10^9 cells per cm^3 [2]. The fine tuning of processing conditions and the selection of the blowing agent allows for the tailoring of the structure of a foam and, consequently, of its final properties. Hence, a careful selection of the proper combination of polymer/foaming agent system and the proper coordination of the individual steps in the process are required in

the manufacturing of foamed products. The fluidodynamic behavior of macromolecular viscoelastic materials containing a dissolved gas at high concentration and at thermodynamic conditions able to promote the formation of gas bubbles in the melt is the driving force of the foaming process. Nucleation and growth rates, which determine the final morphology of the foam, are related to the chemical, physical and transport properties of the polymer-foaming agent system: interfacial and rheological properties of the polymer/gas solution, solubility and diffusivity of the gas into the melt.

Several pieces of literature provide a qualitative frame for the investigation of the effect of working conditions (e.g. temperature and gas pressure) and thermodynamic and mass transport properties of polymer/gas solutions of interest in this process on the kinetic of foam formation and on final pore structure of the foam [3-7]. For instance, a very detailed experimental and theoretical analysis of the effect of the processing conditions on the final morphology of poly(ε-caprolactone) (PCL) foams has been carried out by Di Maio et al. [8], showing that the peculiar interaction of the gas adopted as foaming agent (in that case, CO_2 or N_2) with the polymer melt led to different morphology, in terms of foam density, cell number density, and cell size.

In particular, the properties which play a role in the homogeneous bubble nucleation in polymeric thermoplastic foaming are: solubility, mutual diffusivity, interface tension and specific volume of the polymer/gas solution [3,8]. In a previous paper, we have presented a purely experimental approach allowing the direct and concurrent determination of all of these aforementioned properties of interest, without relying on any theoretical assumption or equation of state at any stage of the properties evaluation [9]. The proposed approach is based on the coupling of gas sorption and Axysimmetric Drop Shape Analysis (ADSA) measurements, allowing for the simultaneous measure of those properties in a single experiment. The new experimental set-up consists of a magnetic suspension balance equipped with a high pressure and temperature view cell where both gravimetric and interfacial tension measurements are performed synchronously. The pendant drop method (a molten polymer drop hanging from a rod) has been coupled with the classical gravimetric measurement performed on samples placed in a cylindrical crucible. In this experimental configuration, while the magnetic suspension balance is measuring the weight change during sorption of the sample placed in the crucible, the profile of the pendant drop, at the same temperature and pressure, is monitored with a high resolution camera, giving information about volumetric and shape changes.

Here we illustrate the results of our investigation performed with this new, fully experimental methodology on molten PCL/CO_2 solutions, a promising binary system in the field of the 'eco-friendly' foaming processes. Simultaneous measurements of solubility, diffusivity, interfacial tension and specific volume of PCL/CO_2 solutions have been performed at three different temperatures (80, 90 and 100 °C) and at CO_2 pressures up to 4.2 MPa.

EXPERIMENTAL

Coupled measurement methodology and experimental setup

Simultaneous measurement is based on the coupling of ADSA and gas sorption experiment performed into a custom-designed apparatus. Sorption experiment was carried out by continuously weighing the polymer contained in a crucible placed in a high temperature-high pressure view cell of a magnetic suspension balance (Rubotherm Prazisionsmesstechnik GmbH, Germany). Concurrently, the optical monitoring of a pendant drop placed in the same view cell was performed, allowing the acquisition of drop shape and size to be used to monitor the swelling of the molten polymer/gas solution and for the determination of interfacial tension by ADSA. By properly combining the information collected in these two measurements, it is possible to obtain a fully experimental and reliable measure of solubility, diffusivity, specific volume and interfacial tension of the polymer/gas solution. Details of the methodology and of the whole data treatment chain are well described in a previous work [9].

A custom-designed sample holder, consisting of a rod to which the polymer-gas solution drop is stuck (for ADSA) and a crucible containing a few grams of polymer-gas solution (for weight monitoring), was placed in the high temperature-high pressure view cell. The crucible hangs from the hook of the balance weight measuring unit while the rod is fixed inside the cell in such a way as to avoid any interference with the gravimetric measurement and to allow the reliable continuous acquisition of the drop shape. Drop monitoring is made possible through two optical quality windows, mounted perpendicular to the axis of the cell, by using an adjustable high resolution CCD camera, equipped with a modular zoom lens system. The optimal threshold for digitizing the drop image is achieved by a uniform bright background, that is provided by light emitting diodes.

The CCD camera is connected to a computer, and commercial software is used to analyze drop profile. Details of the equipment and the description of the preliminary experimental phases (i.e. drop preparation, optimization of CCD parameters and image calibration) are reported elsewhere [9].

Sorption and ADSA experiments were carried out by isothermal step-change pressure increments up to 4.2 MPa, at 80 °C, then 90 and 100 °C. Step-wise increments of the gas pressure (about 0.5 MPa steps) were performed with pre-heated gas, after the attainment of equilibrium sorption in the previous step. Concurrently, during each pressure step, image acquisition of the pendant drop was performed every 10 min.

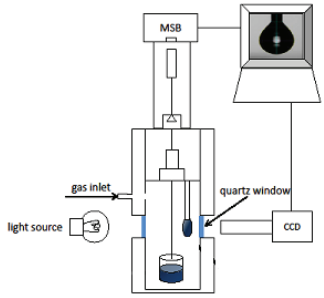

FIGURE 1. Schematic illustration of experimental equipment used in the simultaneous measurement.

Materials

Poly(ε-caprolactone), a biodegradable polymer with a melting point of ca. 60 °C, was supplied by Solvay Interox Ltd. (PCL CAPA 6800) and used as received. High purity grade carbon dioxide and nitrogen were supplied by SOL (Italy).

RESULTS AND DISCUSSION

The sequence of data flow necessary to calculate solubility, diffusivity, specific volume and interfacial tension of the polymer/gas solution is summarized in the following.

First, from the sorption experiment, apparent solubility (i.e. not yet corrected to account for the effect of change of sample buoyancy due to sorption and compressive action of gas) was measured as a function of gas pressure. Concurrently, from ADSA, the volume of the pendant polymer/gas drop was computed. Having assumed that, at equilibrium, drop curvature has negligible effects on specific volume and local gas concentration [24-26] and, consequently, that the drop and the sample in the crucible reach the same volume per unit mass of starting polymer, it was possible to calculate the volume of the polymer/gas solution contained in the crucible, thus allowing for the correction of sorption data with the proper buoyancy force and, consequently, for the calculation of actual solubility and diffusivity of the polymer/gas solution. Gas sorption amount and solution volume per unit mass of polymer were then used to calculate the specific volume of the polymer/gas solution. As a final step, this value was fed to the ADSA software to calculate the actual interfacial tension. The whole detailed description of data treatment can be found in Ref. 9.

CO_2 sorption isotherm in molten PCL

Figure 2 shows the actual sorption isotherms of CO_2 in PCL at the three temperatures. As expected, ω_{ACT} increases with the pressure and decreases with the temperature. It is important to highlight the importance of the effect of the swelling of the gas saturated polymer during sorption for the proper buoyancy correction and the evaluation of actual sorption data: in the whole temperature and pressure range, ω_{ACT} remains ca. 2% higher than ω_{APP} for each MPa of increase of CO_2 pressure (data not shown) [9], this error summing up to 10% ca. at the highest pressure investigated in this work.

CO_2 as a blowing agents for PCL: thermodynamic and mass transport properties of molten polymer/gas solutions

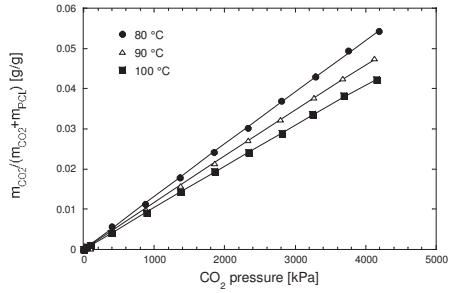

FIGURE 2. Actual sorption isotherms for the PCL/CO_2 systems.

Evaluation of CO_2 mutual diffusivity

The values of $\overline{D}$ of carbon dioxide in PCL, as obtained from eq. 6, are reported in Figure 3, as a function of CO_2 mass fraction. Within the investigated pressure range, it was found that $\overline{D}$ exhibits a slight dependence on CO_2 concentration, showing a maximum value at a CO_2 mass fraction equal to 0.02.

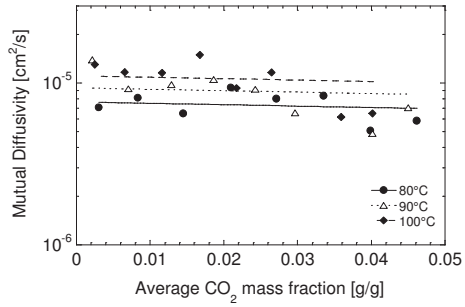

FIGURE 3. Mutual Diffusivity for the PCL/CO_2 solution as a function of CO_2 concentration.

Specific volume of PCL/CO_2 solutions

In Figure 4, the specific volume of the PCL/CO_2 solutions is reported as a function of CO_2 mass fraction. This experimental technique has highlighted a peculiar trend for V_s: initially, it is found to decrease with gas concentration; then, for a CO_2 mass fraction approximately higher than 0.025, it starts increasing. In order to understand this behavior, it is important to consider that, when a molten polymer is exposed to a high-pressure gas, two mechanisms compete in affecting the specific volume: on one hand, the external gas exerts a mechanical action leading to the compression of the gas saturated polymer melt, on the other hand, gas solubilization is responsible to mass and volume increases. Finally, the overall variation of the specific volume of the solution is the result of the combination of both the mass increase and the volume changes. The final balance of mass and volume contributions giving the non monotonic profile of the effect of gas pressure on the specific volume.

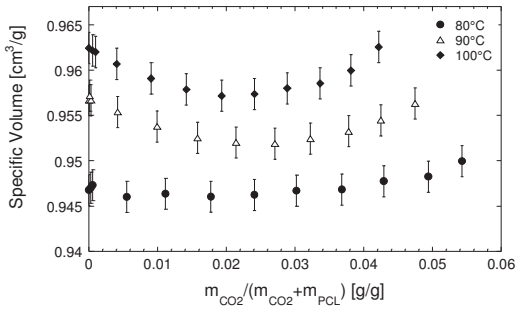

FIGURE 4. Specific volume of the solution PCL/CO_2 as a function of CO_2 mass fraction. Error bars evaluated by accounting for the error propagation in the whole measurement chain.

Interfacial tension

The interfacial tension of the polymer/gas solution, as evaluated on the basis of the described procedure, are shown in Figure 5 as a function of CO_2 concentration. In the selected experimental range, interfacial tension of the solution is found to be a nearly linear decreasing function of the CO_2 pressure. This trend of the interfacial tension with the gas concentration has already been reported elsewhere [10, 11] and is generally attributed to the plasticizing action of carbon dioxide on molten polymer. Also temperature drives the interfacial tension down: it was also estimated that, for the pure PCL, the interfacial tension decreases with a temperature coefficient of -0.059 mNm/°C as compared to -0.073 mNm/°C for the mixture (see inset of the Figure 5).

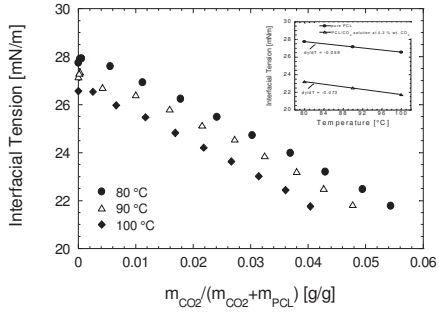

FIGURE 5. Effect of CO_2 concentration on the interfacial tension of PCL in CO_2. Inset: Effect of temperature on the interfacial tension of the solution PCL/CO_2 as a function of CO_2 mass fraction.

CONCLUSIONS

The simultaneous measurement of solubility, diffusivity, specific volume and interfacial tension of molten PCL/CO_2 solutions has been performed at three different temperatures and at CO_2 pressures up to 4.2 MPa. The coupling of the gravimetric measurement (performed using a magnetic suspension microbalance equipped with a pressurizable view cell) with the ADSA-based monitoring of a polymer pendant drop allows for a fully-experimental determination of the aforementioned properties, without resorting to any predictive modeling. The effect of temperature on CO_2 sorption isotherm and on interfacial tension was studied. Mutual diffusivity coefficients have been found to have a weak dependence on CO_2 concentration and to increase with temperature. Specific volume of the PCL/CO_2 solution was found to show a non monotonic profile than can be ascribed to the final balance of the two contribution of the effect of gas pressure (volume and mass changes). Interfacial tension of the solution was found to decrease with a nearly linear trend with gas concentration and with temperature.

ACKNOWLEDGMENTS

REFERENCES

1. D. Klemppner, K.C.Frisch (Eds.), *Handbook of Polymeric Foams and Foam Technology*; Munich: Hanser, 1991.
2. D.F. Baldwin, C.B. Park, N.P. Suh, Polym Eng Sci **36,** 1437-45 (1996).
3. M.A. Shafi, R.W. Flumerfelt, Chem Eng Sci **52**, 627—633 (1997).
4. K. Taki, Chem Eng Sci **63**, 3643 - 3653 (2008).
5. J.S. Colton, N.P. Suh, Pol Eng Sci **27**, 500-503 (1987).
6. S.K. Goel, E.J. Beckman, Polym. Eng. Sci. **34** 1137-1147 (1994b).
7. J.H. Han, C.D. Han, J Pol Sci B **28** 711(1990).
8. E. Di Maio, G. Mensitieri, S. Iannace, L. Nicolais, W. Li, R.W. Flumerfelt, Polym Eng Sci **45**, 432–441, (2005).
9. M.G. Pastore Carbone, E. Di Maio, S. Iannace, G. Mensitieri, Pol Testing **30**, 303–309 (2011).
40. D. Liu, D.L. Tomasko, J. Supercrit. Fluids **39**, 416(2007).
51. H. Li, L.J. Lee, D.L. Tomasko, Ind. Eng. Chem. Res. **43:2**, 509 (2004).

A study of the mechanical behaviour of sPP adopting cyclic tensile tests

N. Perillo, C. Marano, M. Rink

Dipartimento di Chimica, Materiali e Ingegneria Chimica "Giulio Natta"
P.zza Leonardo da Vinci 32, 20133 Milano- Italia
nadia.perillo@mail.polimi.it, claudia.marano@polimi.it, marta.rink@polimi.it

Summary: The post-yield behavior of a syndiotactic polypropylene was studied performing tensile loading-unloading tests at constant displacement rate. A correlation between the recovered and residual strains measured at different applied strains and the strain-induced structure modifications reported in literature was attempted.

Introduction

The yield and post-yield behaviour of semicrystalline polymers have been widely studied as concerns the structure modification induced by deformation. In particular, syndiotactic polypropylene has been extensively investigated by Strobl et al. [1] and Auriemma et al. [2] as concerns the correlation between mechanical behaviour and microstructural changes and the strain-induced crystal form transitions respectively. The interest for s-PP is related to the significant material strain recovery even when strained up to high strain ($\lambda = 6 \div 7$).

Figure1 schematically shows the strain-induced structure modifications for a general semicrystalline polyolephine. Up to point A, the material has a spherulitic morphology of the crystalline phase and shows a linear-elastic behaviour. B identifies the yield point at which the spherulites are disrupted while at the point C the lamellar crystals transform in fibrils, oriented in the stretching direction. At the point D chain disentanglements with the orientation of the amorphous phase, occurs [3]. Strobl [1,4] has shown that these phenomena take place at critical values of deformation which are characteristic of the specific polyolephines.

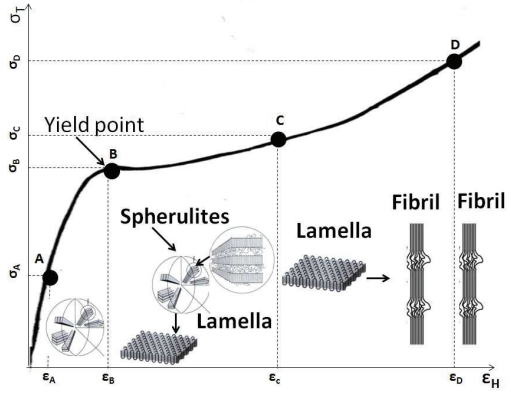

Figure 1: True stress-true strain curve for a semicrystalline polyolephine with microstructural changes occurring during the tensile test [4]

Strobl determined the strain values at points A, B, and C for s-PP and they are 0.04, 0.12 and 0.4 respectively [1]. In his experimental set-up, he was not able to explore strains above 1.

Auriemma et al. [2] have focused their attention on the different crystal-crystal transitions occurring during a tensile test up to final rupture on s-PP. A transformation from the thermodynamically stable crystal form I (orthorhombic crystalline cell with polymeric chains in helical conformation arranged with opposite chirality (left-handed and right-handed)) to the metastable crystal form III (orthorhombic crystalline cell with polymeric chains in trans-planar conformation) occurs. The strain at which the onset of form I-form III transformation occurs ($\varepsilon_{I->III}$), depends on the stereoregularity degree of s-PP (% rrrr pentad). This parameter affects also the strain at which the transformation completes (ε_{III}) and if the mesoform III appears in place or before the formation of form III ($\varepsilon_{I->mIII}$). When the material is unloaded the crystal transformation form III-form II occurs (form II: body-centered orthorhombic crystalline cell with polymeric chains in helical conformation arranged with the same chirality). In this work the s-PP (% [rrrr]=78%) was considered and table 1 summarizes the information reported in literature on it.

Table 1: Summary of literature results on s-PP

Characteristic strains	Nominal strains (%)	True strains	Microstructure [1]	Crystalline forms[2]
ε_A	/	0.04 [1]	spherulite	form I [1,2]
ε_B	/	0.12 [1]	spherulite -> lamella	
ε_C	/	0.40 [1]		
$\varepsilon_{I->mIII}$	160 [2]	(0.96)*	lamella -> fibril	form I + meso form III[2]
$\varepsilon_{I->III}$	400 [2]	(1.61)*		form I + form III[2]
ε_{III}	600 [2]	(1.95)*		
			fibril	form III[2]

* true strain corresponding to the nominal strain values reported in [2]

In this work, a simple experimental method, based on tensile loading-unloading tests, was properly adopted to characterize the post-yield behavior of a commercial s-PP and to correlate the recovered and residual strains measured at different applied strains with the strain-induced structure modifications reported in literature.

Materials and Methods

The material studied was a commercial syndiotactic polypropylene (Fina 3) kindly supplied by Atofina, characterized by a concentration of *rrrr* pentad equal to 78%. From DSC measurements, performed at 10°C/min, the glass transition and melting temperatures were found to be 0°C and 125°C respectively and the crystallinity degree 26%, (ΔH_o = 183 J/g [1]). Plates of 1 mm thick were compression moulded at 180°C, 2 bar for 20 min and then slowly cooled to room temperature. Tensile tests have been performed with a Instron 1121 dynamometer at a constant displacement rate of 5mm/min using dumb-bell specimens with a 33 mm gauge length. Since, after yielding, the deformation along the gauge length is not homogeneous but localized, giving rise to necking, several black marks have been placed on the specimen and their relative displacements measured using a video-extensometer. For each zone of the specimen between two marks, it was possible to calculate the true stress (σ_T), and the true strain (ε_H) as follows:

$$\sigma_{T_i} = \frac{P}{A_{i_0}} \lambda_i \qquad \varepsilon_{H_i} = \ln \lambda_i = \ln \frac{l_i}{l_{i_0}}$$

in which P is the applied load, A_{i_0} the mean value of the cross-section measured between two marks initially distant l_{i_0} in the unstrained specimen, l_i the actual value of the distance between the marks.
On each specimen different loading-unloading cycles were performed at increasing strain up to specimen's rupture. A displacement rate of 5 mm/min for both the loading and the unloading steps, were adopted. As proposed by Strobl [1], the residual, ε_{Hres}, and the recovered, ε_{Hrec}, strain-components of the applied strain ε_H were determined for each cycle at the end of the unloading (fig. 2).

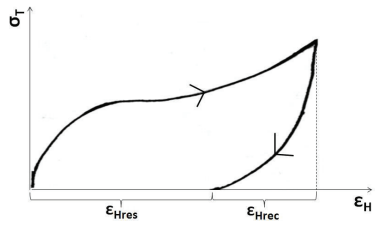

Figure 2: Definition of recovered strain(ε_{Hrec}) and residual strain (ε_{Hres}) components

After unloading some strain recovery could still occur but it is not included in the ε_{Hrec} defined above.

Results and discussion
In figure 3 the true strain/time curves for three different zones of a single specimen relevant to a monotonic tensile test are reported. In figure 4 the corresponding true stress/true strain curves are shown.

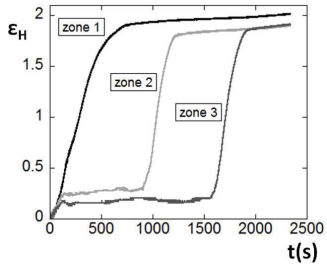

Figure 3: Hencky strain/time curves for three zones of a single s-PP specimen, in a monotonic tensile test.

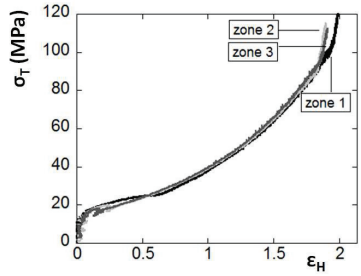

Figure 4: True stress/true strain curves of s- PP

From these curves it can be observed that, despite the three zones of the same specimen, identified as 1, 2 and 3 in fig. 3, have undergone a quite different deformation history, their true stress-true strain curves overlap perfectly: this means that the difference in the deformation history has no significant influence on the mechanical response of the material. This result is also supported by the curves in fig. 5: the black curve relevant to a monotonic loading history up to failure overlaps with the grey one relevant to cyclic loading-unloading tensile test at increasing strains. Starting from this result, the different zones of one specimen simultaneously strained up to different strain levels can be considered as single specimens differently strained. A lot of data were thus obtained from very few specimens.

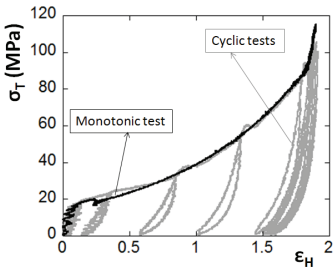

Figure 5: True stress/true strain curves for multi-cycles test (grey line) compared to those related to monotonic test (black line)

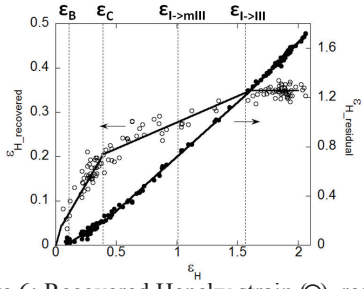

Figure 6: Recovered Hencky strain (○), residual Hencky strain (●) at the end of the unloading vs the applied Hencky strain. The characteristic strains reported in tab.1 are indicated.

From the cyclic tests, the residual, ε_{Hres}, and the recovered, ε_{Hrec}, strain-components were determined for each value of applied strains ε_H and fig. 6 reports the data obtained. It has to be underlined that all the data reported in fig. 6 are relevant to only three specimens. Referring to the characteristic strain values reported in tab. 1 it can be observed that:

(i) ε_{Hrec} increases as ε_H increases up to $\varepsilon_{I->III}$ after which it becomes constant.

(ii) The experimental data in the strain range $0 < \varepsilon_H < \varepsilon_B$ are very few and it is not possible to observe any trend nor in ε_{Hrec} or in ε_{Hres}.

(iii) At ε_C a decrease in the slope of ε_{Hrec} vs ε_H is observed. This result disagrees with that reported by Strobl in [1] where a constant value of ε_{Hrec} is found for strains above ε_C where lamella-fibril transformation occurs.

(iv) The transition from crystal form I to crystal mesoform III does not affect the dependence of the residual and recovered strain components of ε_H.

(v) As for ε_{Hres} it increases with ε_H over the range of strains explored and from the data obtained no evident changes in the trend are observed. Nevertheless, after $\varepsilon_{I->III}$, where ε_{Hrec} becomes constant, the ε_{Hres} vs ε_H displays unit slope indicating that the deformation of the fibrillar crystals into form III is entirely permanent.

Conclusions

A simple experimental method was set up to characterize the yield and the post-yield behaviour of a commercial syndiotactic polypropylene The dependence of the residual and recovered strains on the applied strain was analyzed in terms of the strain-induced structure modifications. The experimental method allowed to explore a wider range strain than that considered in [1]. The experimental method developed is now to being applied to other polypropylenes with different degrees of crystallinity and stereoregularity.

Acknowledgment

Financial support by MIUR (PRIN 2008) is gratefully acknowledged.

References

[1] Men, Y.; Strobl, G., *J. Macromol. Sci-Physics* **2001**, *B40(5)*, 775-796

[2] De Rosa, C.; Auriemma F., *Prog. Polym. Sci* **2006**, *31*, 145-237

[3] Young, R. J., *Introduction to Polymers*, 1st ed.; Chapman and Hall: New York, 1981; p 293-294.

[4] Hong, K.; Rastogi, A.; Strobl, G., *Macromolecules* **2004**, *37*, 10165-10173

A study of the mechanical behaviour of s-PP adopting cyclic tensile tests

N. Perillo, C. Marano, M. RinK
Dipartimento di Chimica, Materiali e Ingegneria Chimica " Giulio Natta" - Politecnico di Milano- Italia

Introduction

Deformation mechanisms and crystalline forms of syndiotactic poypropylene (s-PP) have been widely studied [1, 2, 3].

General stress-strain curve of a semicrystalline polymer [1]

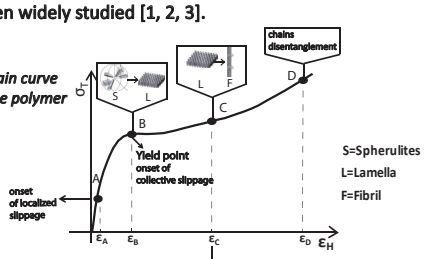

[2]

The onset of deformation mechanisms is strain-controlled.

For s-PP [rrrr]=78% :
ε_{HA} = 0.04
ε_{HB} = 0.12
ε_{HC} = 0.4
ε_{HD} = not determined

[3]

Crystal-crystal transformations occur during deformation.

For s-PP [rrrr]=78% the characteristic strains are:

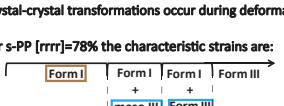

Form I — Helicoidal

Form III Mesoform III — Transplanar

Aim

Separate the applied strain in a tensile test into its components and analyze their dependence on strain-induced structural modifications.

Experimental details

Material

provided by Atofina

s-PP (FINA 3)

[rrrr]=78% Tg = 0°C

χ= 26% Tm = 125°C

Equipment

- Instron 1121 Dynamometer
- Videoextensometer (VE) (local strains measurements)

Black markers to measure relative displacement with VE

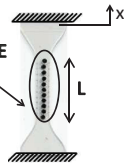

Specimen geometry

Dumb-bell
L = 33 mm (gauge lenght)
$A_0 \approx 6mm^2$
1 mm thick

Tests

Monotonic tensile test

Loading-unloading tensile test

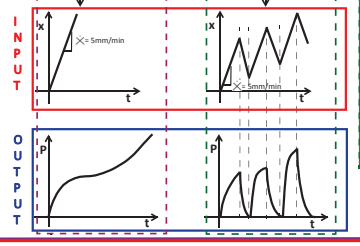

Data elaboration

Hencky strain $\varepsilon_{H_i} = \ln\lambda_i = \ln\frac{l_i}{l_{i_0}}$

True stress $\sigma_{T_i} = \frac{P}{A_0}\lambda_i$

- recovered strain ε_{rec}
- residual strain ε_{res}

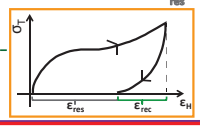

Results and discussions

Monotonic tensile test

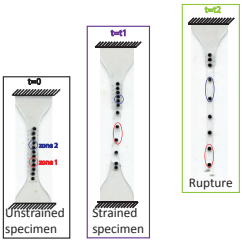

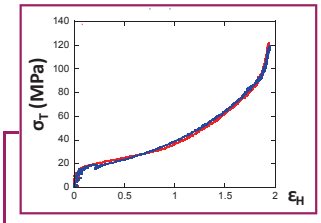

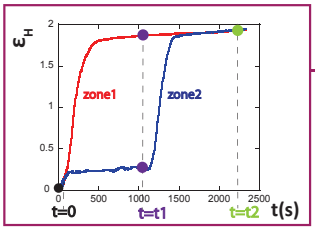

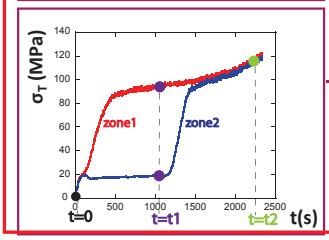

Stress-strain behavior is indipendent of the loading hisrory: the different zones of a single specimen can be considered as different single specimens

Loading-unloading tensile test

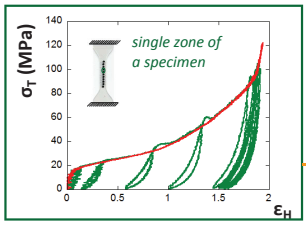

Results obtained from the different zones of only three specimens

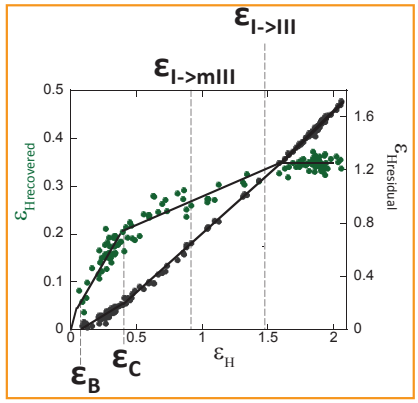

(i) ε_{Hrec} increases as ε_H increases up to $\varepsilon_{I->III}$ after which it becomes constant.
(ii) From the data obtained ε_B cannot be identified.
(iii) At ε_C, where lamella-fibril transformation occurs [2], a decrease in the slope of ε_{Hrec} vs ε_H is observed.
(iv) At $\varepsilon_{I->mIII}$ no change in the trend of ε_{Hrec} and ε_{Hres} vs ε_H is observed.
(v) At about $\varepsilon_{I->III}$ where ε_{Hrec} becomes constant the ε_{Hres} vs ε_H displays, as expected, unit slope .

Conclusions

- A simple experimental method was set up to characterize the yield and the post-yield behaviour of a commercial syndiotactic polypropylene.

- From changes in the trend of ε_{Hrec} vs ε_H two characteristic strains at about 0.4 and 1.6 could be well identified and associated with a morphological [2] and a crystal-crystal transformation [3] respectively.

Acknowlegment

Financial support by MIUR (PRIN 2008) is gratefully acknowledged.

References

[1] Young, R. J., Introduction to Polymers, 1st ed.; Chapman and Hall: New York, 1981; p 293-294.
[2] Men, Y.; Strobl, G., J. Macromol. Sci-Physics 2001, B40(5), 775-796
[3] De Rosa, C.; Auriemma F., Prog. Polym. Sci 2006, 31, 145-237.

A Study of the Time Dependence of the Post Yield Behavior of a Syndiotactic Polypropilene

C. Marano, N. Perillo, M. Rink

Dipartimento di Chimca, Materiali e Ingegneria Chimica "Giulio Natta", P.zza Leonardo da Vinci 32, 20133 Milano- Italia

Abstract. Cyclic tensile tests at constant displacement rate have been performed on a syndiotactic polypropylene to study the effect of the loading history on its mechanical behavior. A test procedure was, at first, properly set up to take into account the inhomogeneous deformation occurring in the adopted dumb-bell specimen. A dependence of the material behavior on the loading history was observed up to yielding, as expected. No effect of the loading history was, instead, observed, neither in the post-yield behavior nor in the strain recovery during and after unloading.

Keywords: Syndiotactic polypropylene, yielding, strain recovery
PACS: 8105Lg

INTRODUCTION

The interest for syndiotactic polypropylene has recently increased as concerns the "elastic" behaviour that oriented sPP samples show, provided that a proper crystallinity degree of the material is present. The non-conventional elasticity of the oriented sPP has been interpreted referring to strain induced crystal-crystal transition of the polymorphic sPP [1] or in the light of typical models of crystalline polymer deformation [2]. In [3] the dependence of the "elastic" behaviour of solid state-drawn sPP samples was investigated as a function of the applied draw ratio, governing the material structural modification. This work is aimed at investigating the time dependence of the post-yield behaviour of sPP.

MATERIALS AND METHODS

A commercial syndiotactic polypropylene (Fina 3), kindly supplied by Atofina, having a concentration of *rrrr* pentad equal to 78%, was studied in this work. Glass transition and melting temperatures of 0 and 125°C respectively and a crystallinity degree of X = 26%, (ΔH_o = 183 J/g [4]) were determined by DSC measurement performed at 10°C/min. The material was compression moulded at 180°C and then let to slowly cool down to room temperature: dumb-bell specimens with a 33 mm gauge length were prepared from the obtained 1 mm thick sheets. Tensile tests were performed at constant displacement rate ($\dot{x}$ = 5 or 50 mm/min) for a preliminary material characterization. Moreover, a series of cyclic tensile tests at displacement rate of 5 or 50 mm/min for the loading and the unloading steps ($\dot{x}_{up}$ and $\dot{x}_{down}$ respectively) were carried out progressively increasing the displacement up to specimen's rupture. Since necking occurred during loading, strain was not homogenous along the specimen gauge length and thus it was locally measured using a video-extensometer. By placing several marks along the gauge length, from a single specimen, in each each test, several true stress (σ_T) - true strain (ε_H) curves were thus obtained as follows:

$$\sigma_{T_i} = \frac{P}{A_{i_0}}\lambda_i \qquad\qquad \varepsilon_{H_i} = \ln\lambda_i = \ln\frac{l_i}{l_{i_0}}$$

where: P is the applied load, A_{i_0} is the unstrained specimen cross-section, measured between two marks placed on the specimen at the initial distance l_{i_0} , l_i is the actual value of the distance between the marks.

The residual strain, $\varepsilon_{H,res}$, was measured as a function of time, after the unloading for at least 10 minutes.

RESULTS AND DISCUSSION

In figure 1 the true stress/true strain curves of sPP in monotonic tensile tests at displacement rate of 5 and 50 mm/min are reported. It can be observed that the yield stress increases as the loading rate increases, as expected, while the post-yield behaviour after a true strain of about 0.7 seems not to be affected by the loading rate.

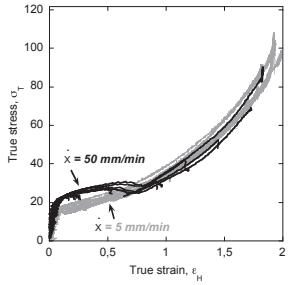

FIGURE 1 Stress/strain curves of sPP

As for the multi-cycles test, the load versus time curve recorded for a single specimen when $\dot{x}_{up} = \dot{x}_{down} = 5$ mm/min is reported in figure 2a as an example. In figure 2b and 2c the strains and the stresses measured simultaneously in two distinct parts of the specimen along the gauge length (indicated as specimen-part A and part B) are respectively reported. It can be observed that, as previously said, the material deformaion is not homogenuos along the specimen, which thus experiments different loading histories in its different parts.

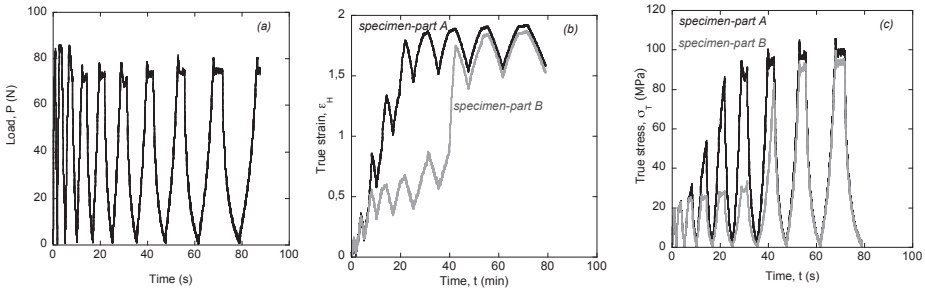

FIGURE 2 (a) Load (b) true strain and (c) true stress versus time for a single specimen in a multi-cycles tensile test (see text).

The true stress/true strain curves relevant to data reported in figure 2 are shown in figure 3a. In figure 3b, the curves of figure 3a are compared to those of the monotonically loaded material (fig. 1) for the same value of the displacement rate (grey line). It can be observed that: (i) the loading curve of the monotonic test well overlaps with those of the multi-cycles test; (ii) the material strain recovery in the unloading step and the subsequent loading curve are the same irrespective of the loading history (see for example in fig. 3a tests at which $\varepsilon_H = 0.8$ was applied). In figure 3c the loading curves relevant to multi cycles tests performed at 5 mm/min in the loading steps and at 5 (gray lines) or 50 (black lines) mm/min in the unloading steps, are compared. It seems that, for each strain level, the unloading displacement rate has no effect on both the material strain recovery and the subsequent loading curve. All these results suggest that the material behaviour is not significantly dependent on the applied loading history, indicating that viscoelastic behaviour cannot be evidenced from the test performed. Nevertheless a time dependent strain recovery after unloading was observed and is reported I figure 4. In figure 4, the residual strains, $\varepsilon_{H,res}$

measured at 0 and 10 minutes after the unloading (no significant change of $\varepsilon_{H_i res}$ was measured at time higher than 10 min) are plotted versus the applied strain for tensile tests differing in unloading displacement rate. As expected from the results of fig. 3, the residual strain seems to be not affected by the unloading displacement rate, at least for the rates examined in this work.

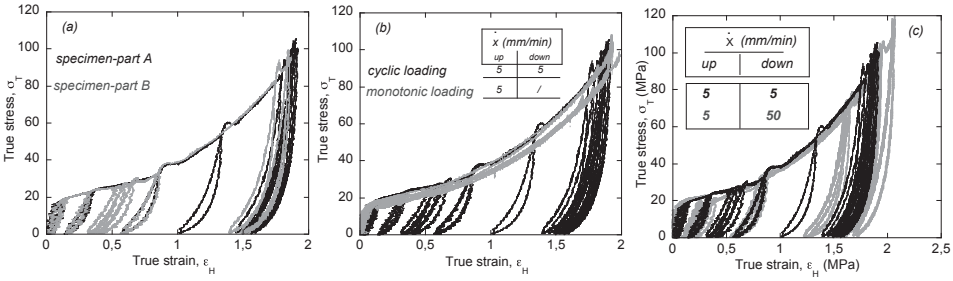

FIGURE 3 True stress/true strain curves for multi-cycles test (a) compared to those related to monotonic test (b) (displacement rate of 5 mm/min for the loading and unloading steps), (c) multi cycles tests at different unloading displacement rates.

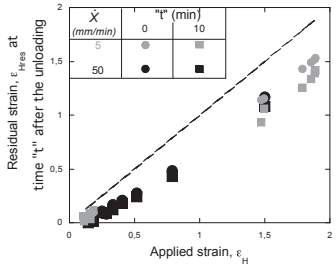

FIGURE 4 Residual strain after the unloading as a function of the applied strain.

CONCLUSIONS

From the loading histories examined viscoelastic effects were observed, as expected, on the yield stress, while in the post-yield regime there were no evident effects of the loading history. A time-dependency was observed on the strain recovery after unloading. During and after unloading strain recovery can be thought being related to: (i) the crystal-crystal transition which takes place during unloading but this has been quantified [2] to be much less than the strain recoveries of about 30% observed in this work; (ii) the recovery of the amorphous phase of the sPP. Being the glass transition temperature below the testing temperature one could expect that the relevant relaxation times are much shorter the time involved in the tests. Nevertheless, some molecules are bound to the crystalline phase and their relaxation times can be much shorter and thus responsible for the viscoelastic effect observed. Tests at other strain rates and tests on sPP with different degree of crystallinity could give support to the present interpretation.

ACKNOWLEDGMENTS

Financial support of the MIUR (PRIN 2008) is gratefully acknowledged.

REFERENCES

1. F. Auriemma, O. Ruiz de Ballesteros, C. De Rosa, *Macromolecules* **34**, 4485-4491 (2001).
2. L. Guadagno, C. Naddeo, V. Vittoria. *European Polymer Journal* **45**, 2192-2201 (2009).
3. N. Perillo, C. Marano, M. Rink to be presented at the *15th International Conference on Deformation, Yield and Fracture, DYFP2012*, April 1-5 2012, Kerkrade, NL.
4. Y. Men, G. Strobl, *J. Macromol. Sci. Physics* **B40(5)**, 775-796 (2001).

A study of the time dependence of the post yield behavior of syndiotactic polypropylene

C. Marano, N. Perillo, M. Rink
Dipartimento di Chimica, Materiali e Ingegneria Chimica " Giulio Natta" - Politecnico di Milano - Italia

Introduction

Deformational behavior of s-PP up to large strains and the relevant strain-recovery have been widely studied [1,2,3] and results interpreted in terms of:

[1] Strain-induced crystal-crystal transitions between two crystalline forms

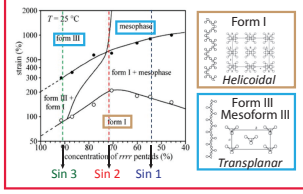

[2-3] Typical model of plastic deformation of semicrystalline polymers

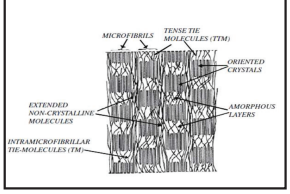

Aim

Investigation of the time-dependence in the s-PP yield and post-yield behavior.

Tests

Equipment

- Instron 1121 Dynamometer
- Videoextensometer (VE) (local strains measurements)

Loading conditions

Loading (↑) unloading (↓) displacement rate

↑ ẋ = 5 or 50 mm/min | ↑ ẋ = 5mm/min
↓ ẋ = 5 or 50 mm/min | ↓ ẋ = 5 or 50 mm/min!

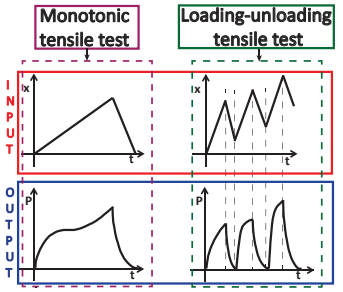

Experimental details

Materials

Syndiotactic Polypropylene provided by Atofina

Material	[rrrr] %	Tg(°C)*	Tm(°C)*	χ(%)*
Sin 1	54	0**	66**	11**
Sin 2	78	0	125	26
Sin 3	91.5	0	160	37

(*) Data obtained from DSC tests (10°C/min)
(**) Data obtained 2 days after molding

Specimen geometry

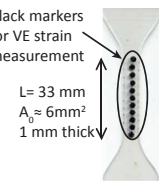

Data elaboration[4]

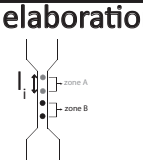

$$\varepsilon_{H_i} = \ln \lambda_i = \ln \frac{l_i}{l_0} \qquad \sigma_{T_i} = \frac{P}{A_0}\lambda_i$$

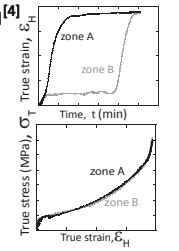

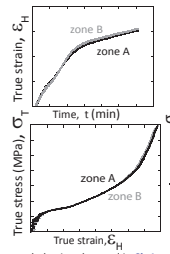

Definition of
- **recovered strain**
- **residual strain**

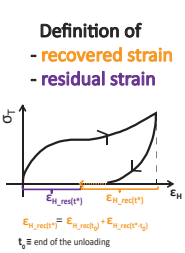

Results and discussions

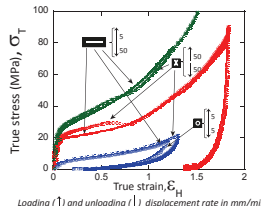

Loading (↑) and unloading (↓) displacement rate in mm/min

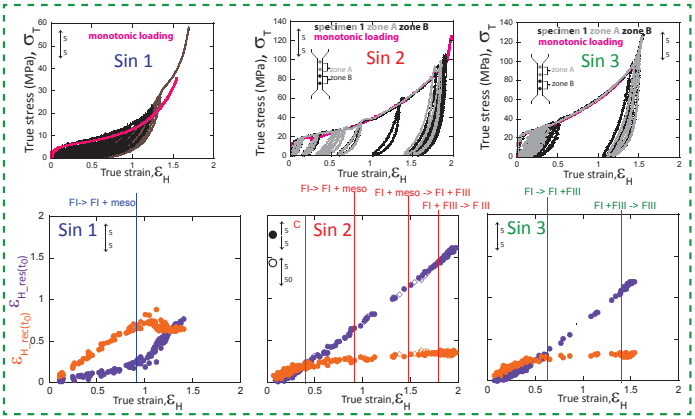

Is the material behavior dependent on	the loading rate?	the unloading rate?
Sin1:	slightly	NO
Sin2:	YES, but only up to yield	NO
Sin3:	slightly	(not yet investigated)

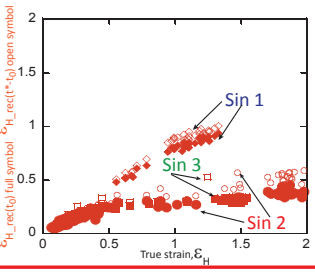

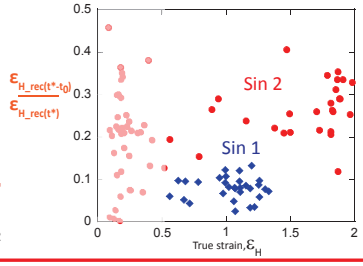

- A strain recovery after the unloading has been observed for all the materials

- The strain recovered after the unloading is about 10% and 25% of the whole strain recovered for ***Sin 1*** and ***Sin 2*** respectively.

Strain localization

Sin 1: No | ***Sin 2, Sin 3:*** Yes

Not all strain values are investigated in the loading-unloading tests

Loading history affecting the mechanical behavior?

Sin 2, Sin 3: No | ***Sin 1:*** Yes

Different zones of a single specimen, differently strained due to strain localization, can be considered as distinct specimens

Strain recovery analysis 1: _recovery during the unloading

Sin 1
- $\varepsilon_{H\_rec} > \varepsilon_{H\_res}$ over almost the whole ε_H range explored
- ε_{H_rec} increases with ε_H up to rupture only in case of monotonic loading

Sin 2, ***Sin 3***
- the two materials show a similar behavior
- $\varepsilon_{H\_rec} > \varepsilon_{H\_res}$ only at the lower strains ($\varepsilon_H < 0.5$)
- for $\varepsilon_H > 0.5$, ε_{H_rec} is fairly constant,
- the unloading strain-rate seems not to affect the strain recovery (see ***Sin 2***)

Sin 1 shows a higher strain recovery than ***Sin2*** and ***Sin3***.

Conclusions

- Not significant strain-rate depedence was observed for the studied materials in the strain-rate range explored.
- A difference between the monotonic loading conditions and the loading-unloading conditions can be observe only in Sin 1 (is it related to structural change?).
- A time-dependency of the residual strain after the unloading was observed, relatable to higher relaxation times of the amorphous phase molecules bound to the crystalline phase.
- Tests at other strain rates could give support to the present interpretation.

Acknowledgment

Financial support by MIUR (PRIN 2008) is gratefully acknowledged.

References

[1] De Rosa, C.; Auriemma F., Prog. Polym. Sci 2006, 31, 145-237.
[2] L. Guadagno, C. Naddeo, V. Vittoria. European Polymer Journal (2009) 45, 2192-2201.
[3] Men, Y.; Strobl, G., J. Macromol. Sci-Physics 2001, B40(5), 775-796
[4] N. Perillo, C. Marano, M. Rink 15th International Conference of Deformation, Yield and Fracture, DYFP2012, April 1-5 2012, Kerkrade, NL., 198-201

Assessment of long-term performance of iPP pipe grade using short-term testing

N. Perillo, H.J.M. Caelers, M.J.W. Kanters, L.E.Govaert

Technische Universiteit Eindhoven University of Technology

POLITECNICO DI MILANO

Introduction

Polymers are increasingly employed in engineering applications most of them load bearing sometimes at elevated temperature. One of these applications is *pressurized pipes*.

For these artifacts, which are subjected to a constant load at a certain temperature during their life, it is really useful to determine and predict their *life-time*.

State of art

Long-term hydrostatic tests (ISO/TR 9080:1992(E)), perfomed on a pipe under a constant hoop stress and at a certain temperature, are actually used to determine pipes life-time but they are expensive and time consuming with testing time exceeding 1.5 years.

certification data trend

Region	Failure mode
I	plasticity controlled
II	crack growth controlled
III	degradation controlled

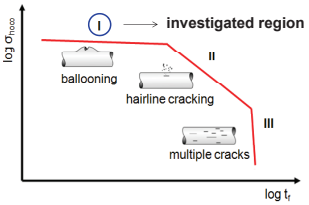

Aim

Test methodology to predict pipes life time using ONLY short term testing → Validation using certification data

Method (based on phenomenological observations)

1 stress dependence — constant strain rate — stress dependence

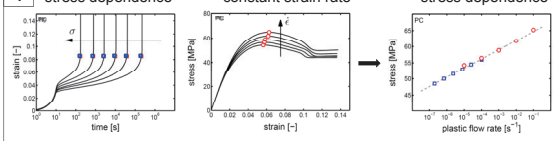

steady state reached in constant strain rate is identical to that reached in constant stress

2 Ree- Eyring equation

$$\sigma_{total} = \sigma_I + \sigma_{II}$$

$$= \frac{kT}{V_I^*}\sinh^{-1}\left(\frac{\dot{\varepsilon}}{\dot{\varepsilon}_{0,I}\cdot\exp(-\Delta U_I/kT)}\right) + \frac{kT}{V_{II}^*}\sinh^{-1}\left(\frac{\dot{\varepsilon}}{\dot{\varepsilon}_{0,I}\cdot\exp(-\Delta U_{II}/kT)}\right)$$

- Two processes that act indipendently
- Stress contributions are additive

Process I: Intra-lamellar deformation

Crystal slip

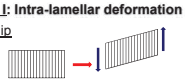

Process II: Inter-lamellar deformation

Pulling chains out of the crystal

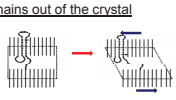

3 concept of critical strain

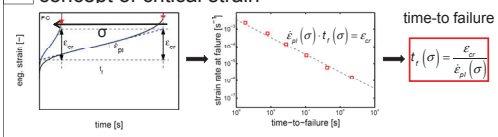

- critical strain is the critical plastic strain for failure
- critical strain is stress-indipendent
- time-to-failure is equal to the ratio between ε_{cr} and $\dot{\varepsilon}_{pl}$ in secondary creep.
- Because of 1 $\dot{\varepsilon}_{pl}$ can be substituted by $\dot{\varepsilon}_{pl}$ in constant strain rate tests. Therefore time-to-failure can be determined ONLY with constant strain rate tests (once known ε_{cr})

Materials

Name	Material	Tm (°C)(*)	χ(%) (*)	Ethylene units (%wt)
iPP_1(**)	iPP-homopolymer	168	54	
iPP_2(**)	iPP-copolymer	144	50	3.3%

(**)Samples have been supplied by Sabic

(*) DSC tests at 10°C/min (TU/e)
(*) χ(%) → X ray data (TU/e)

Results & discussion

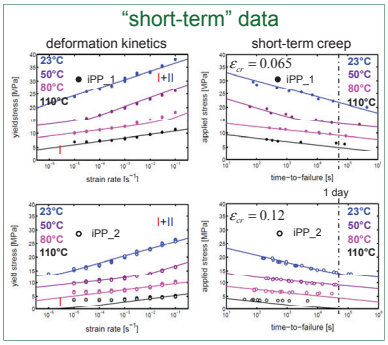

Eyring parameters (eq. 2)

iPP_1

Activation volume	Activation energy
$V_I^* = 10nm^3$	$\Delta U_I = 360kJmol^{-1}$
$V_{II}^* = 4.5nm^3$	$\Delta U_{II} = 222.2kJmol^{-1}$

Rate constants: $\dot{\varepsilon}_{0,I} = 1*10^{39.5}s^{-1}$ | $\dot{\varepsilon}_{0,II} = 3*10^{31}s^{-1}$

iPP_2

Activation volume	Activation energy
$V_I^* = 10nm^3$	$\Delta U_I = 360kJmol^{-1}$
$V_{II}^* = 5.6nm^3$	$\Delta U_{II} = 215kJmol^{-1}$

Rate constants: $\dot{\varepsilon}_{0,I} = 1.44*10^{44}s^{-1}$ | $\dot{\varepsilon}_{0,II} = 3*10^{32}s^{-1}$

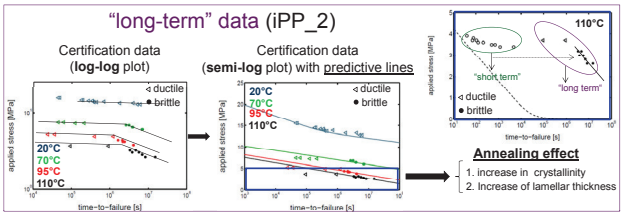

Annealing effect

1. increase in crystallinity
2. Increase of lamellar thickness

Conclusions

- Good description at low temperatures (T_{room})
- **Annealing** (thermal treatment for long time) induces an increase in yield stress → deviation from predictive lines
- **Long term kinetics** at higher temperatures resembles **plasticity**

Acknowledgment

The authors acknowledge the support provided by Rieky Steenbakkers and Klaas Remerie. Long-term data have been determined in Sabic.

Title:

Verification of the whole ligament yielding before fracture in EWF tests

Authors & affiliations:

Nadia Perillo, Claudia Marano, Marta Rink
Politecnico di Milano - Dipartimento di Chimica, Materiali e Ingegneria Chimica "Giulio Natta"
P.zza Leonardo da Vinci 32, I-20133 Milano - Italia

Abstract:

The essential work of fracture (EWF) method is a useful test to characterize fracture toughness of thin films. DENT (Double Edge Notch Tension) specimens are often adopted. Fracture tests in tension are performed on specimens having different 'ligament' lengths: a linear trend in specific energy vs. ligament length plot is expected. The EWF is obtained from the linear extrapolation of this line to zero ligament.
To apply EWF test method three hypothesis have to be satisfied:

- self similar load-displacement curves ,
- plane stress state,
- yielding of the whole ligament before crack onset.

In this work a method to verify the satisfaction of the third hypothesis has been set-up considering an HDPE film.
Loading-unloading tests up to different strain levels were performed on dumbbell specimens and on DENT specimens having the largest ligament length considered for which complete yielding is more critical. After the test, specimens were kept at room temperature until the viscoelastic component of the residual strain is recovered. Strains were measured both during the tests and after unloading from the distance between two marks placed just above and below the ligament plane and along the gauge length in the case of the DENT and dumbbell specimens respectively. From the 'plastic' strain vs. applied strain plot the onset of yield was found by extrapolation. It resulted that the strain at yield onset was the same for the two test configurations. This result is not straight forward since the strain state is different as was verified from digital image correlation analysis.
The yielding of the whole ligament before crack onset can thus be verified by comparing the strains at the center of the ligament at crack onset in the fracture tests with the strain at yield onset determined from tensile tests. The applicability of this procedure for other materials is in due course.

Verification of the whole ligament yielding before fracture in EWF tests

N. Perillo, C. Marano, M. Rink
Dipartimento di Chimica, Materiali e Ingegneria Chimica "Giulio Natta" - Politecnico di Milano - Italia

Introduction and Aim

The essential work of fracture (EWF) test method is used to characterize fracture toughness of thin films.

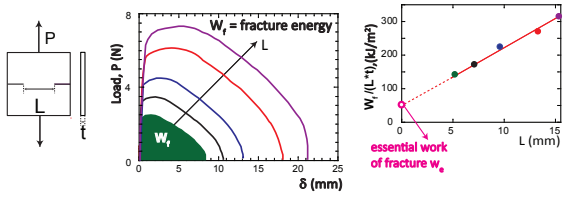

w_e is determined performing:

fracture tests in tensile loading condition on Double Edge Notched Tension (DENT) with different ligament (L) lengths

w_e is valid if:

1. load-displacement curves are self-similar
2. specimens are in plane stress state
3. yielding of the whole ligament occurs before crack onset

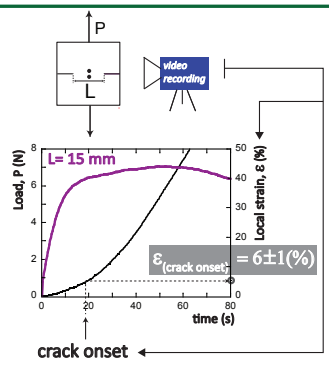

How can the whole ligament yielding be verified?

Experimental details

- *material: HDPE*
- *test specimens adopted*

dumbbell DENT wide specimen

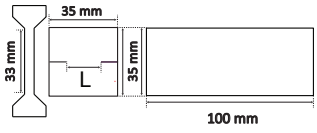

thickness: 20 μm

- *displacement rate = 10 mm/min*
- *strain measurement :*
  - *Videorecording*
  - *DIC (Digital Image Correlation)*

How can the yield onset be determined on viscoelastic materials ?

yield: onset of plastic strain

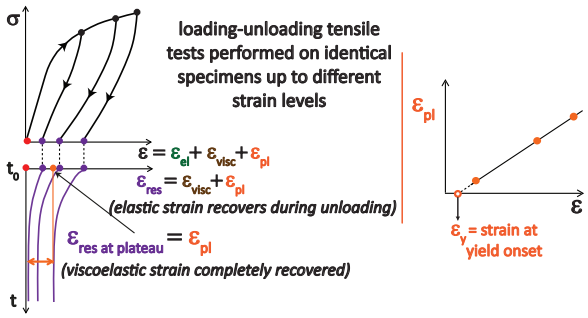

Application of the method on DENT and dumbbell specimens

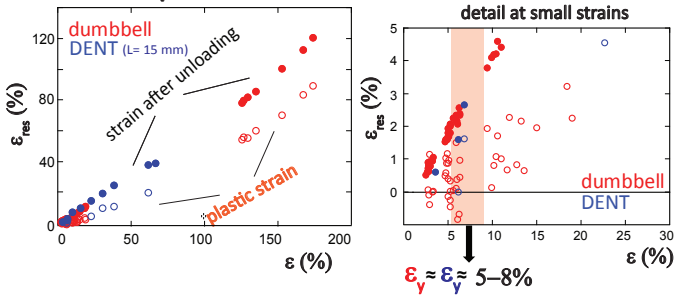

1. strain at yield onset does not depend on specimen geometry
2. yielding of the whole ligament occurs before crack onset

Is the stress state in the two specimens the same?

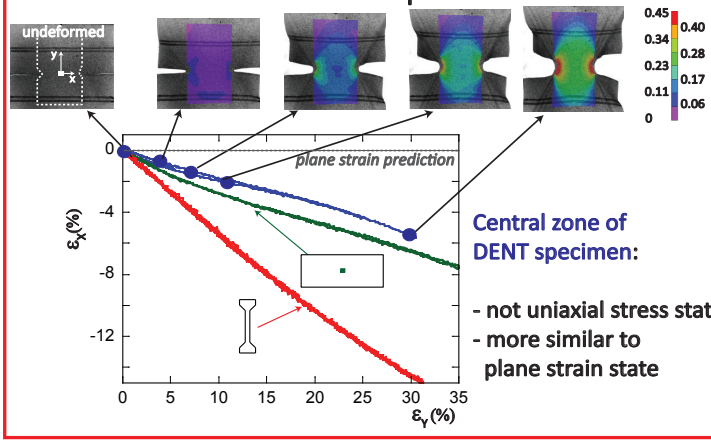

Central zone of DENT specimen:

- not uniaxial stress state
- more similar to plane strain state

Conclusive observations

- For this material to verify yielding of the whole ligament before crack onset

strain at crack onset in fracture tests on DENT specimens **can be compared with** strain at yield onset in (easy) tensile tests on dumbbell specimens

References

T. Bárány, T. Czigány, J. Karger-Kocsis, *Prog. Polym. Sci. 2010, 35, 1257–1287*
M. Rink, L. Andena, C. Marano, *Eng. Fract. Mech.* 2014, *127*, 46-55
R. Quinson, J. Perez, M. Rink, A. Pavan, *J. Mater. Sci.* 1997, *32*, 5,1371-1379

Yield onset determination for polyethylenes in two different stress states

Nadia Perillo, Claudia Marano, Marta Rink

Dipartimento di Chimica, Materiali e Ingegneria Chimica "Giulio Natta"- Politecnico di Milano
P.zza Leonardo da Vinci 32, 20133 Milano - Italia
nadia.perillo@polimi.it , claudia.marano@polimi.it , marta.rink@polimi.it

Summary: The yield onset of two polyethylenes was determined under tensile uniaxial and plane strain loading. The strain at yield onset resulted to be the same irrespective of material and stress state.

Introduction

Yield criteria, as the modified Tresca or the modified Von Mises criteria, have been generally adopted to describe the yield behavior of amorphous and semicrystalline polymeric materials in different stress states [1-3] and to take into account the effect of the hydrostatic pressure on the yield stress. Yield occurs when the maximum shear stress (in the modified Tresca criterion) or the distortional strain energy density (in the modified Von Mises criterion) reaches a critical value.
Referring to literature, yielding of polyolefins occurs at strains which are characteristics of the material, irrespective of the crystallinity degree, temperature and strain rate [4-7]. Bartczak [8] has found that for polyethylene under plane strain compression the yield point occurs at the same strain as that determined by Strobl et al. [4-7] under uniaxial tensile loading conditions.
The aim of this work is to determine the yield strain through the back extrapolation of the plastic strain component following the method proposed in literature [1], in tensile tests both in uniaxial and in plane strain conditions. The experimental activity was performed on two polyethyelenes differing in their crystallinity degree.

Materials and Methods

The materials studied are two commercial polyethyelenes (HDPE and LDPE) kindly supplied by Versalis ENI. Films, obtained by blown-film-extrusion, with a thickness of 0.2 mm and 0.02 mm were used for HDPE and LDPE respectively. Loading-unloading tensile tests at room temperature were performed on a Instron 1121 dynamometer at constant displacement rates (nominal strain rates of $5*10^{-3}s^{-1}$ for HDPE and $10^{-2}s^{-1}$ for LDPE). Dumbbell specimens with a 33 mm gauge length and rectangular shaped specimens with L=100mm and h=10mm were die cut from the films and used for the tensile tests in uniaxial and plane strain conditions respectively. Deformation fields were measured for both the specimens geometries through the digital image correlation (DIC) technique using the commercial software VIC-2D. Each tested specimen was properly sprayed on its surface to obtain a speckles pattern. For both the specimen geometries true stress (σ_T) – strain (ε_H) curves were obtained according to the following relations in the hypothesis of volume constancy:

$$\varepsilon_H = \ln(\lambda) \qquad \sigma_T = \frac{P}{A_0}\lambda$$

in which P is the applied load, A_0 is the sample cross-section and λ is the draw ratio.

The residual, ε_{H_res}, and the recovered, ε_{H_rec}, strain components of the applied strain ε_H were measured both at the end of the unloading (zero time after unloading) (Figure 1a) and after the recovery of the viscoelastic strain component has occurred. In this work the residual strain

after the recovery of the viscoelastic strain component will be referred as plastic strain, ε_{H_p} , (Figure 1b).

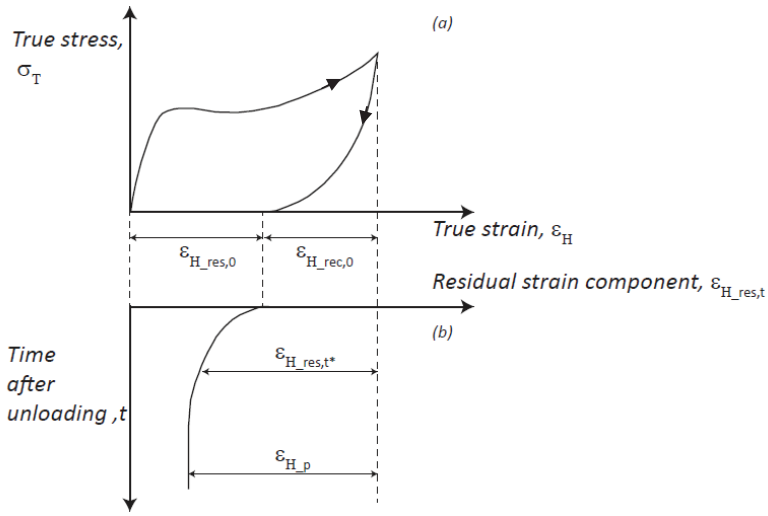

Figure 1: Definition of recovered strain ($\varepsilon_{H\_rec,0}$) and residual strain ($\varepsilon_{H\_res,0}$) components at the end of unloading (a). The plastic strain component (ε_{H_p}) is also defined (b).

Plotting the plastic strain component, ε_{H_p} , versus the applied strain, ε_H ,the yield strain for both the loading conditions was determined.

Results and discussion

In Figure 2a-b some of true stress-strain curves relevant to loading-unloading tensile tests performed up to different strains performed in uniaxial and plane strain loading conditions are reported for HDPE (a) and LDPE (b). The strains were measured along the gauge length of dumbbell specimens and in the centre of the rectangular shaped specimens in uniaxial and plane strain loading conditions respectively. For the tensile tests, both materials show diffuse neck.

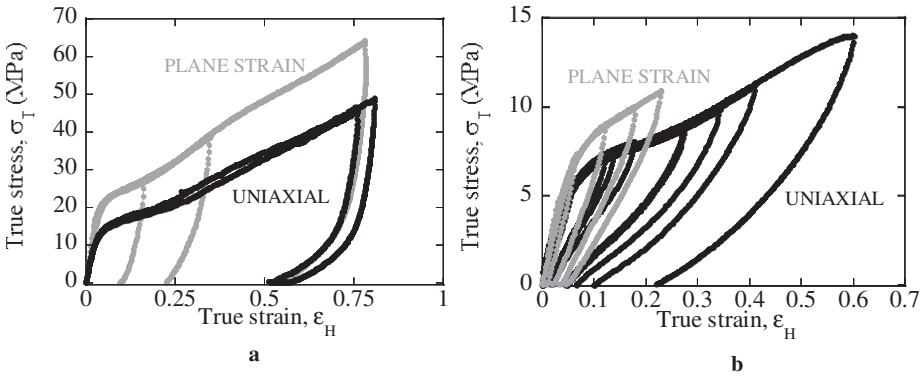

Figure 2: True stress-strain curves relevant to loading-unloading tensile tests performed on uniaxial and plane strain conditions for HDPE (a) and LDPE (b)

It can be observed, as expected, that the true stress is higher in the case of plane strain loading conditions with respect of that in uniaxial loading conditions on the overall strain range irrespective of the material. Further, HDPE is characterized by true stresses higher in both the loading conditions than those of LDPE, as expected.
In Figure 3a-b the residual strains at the end of the unloading, $\varepsilon_{H\_res,0}$, and after the recovery of the viscoelastic strain component - plastic strain, ε_{H_p} - as function of the applied strain are reported for both the materials and the stress states.

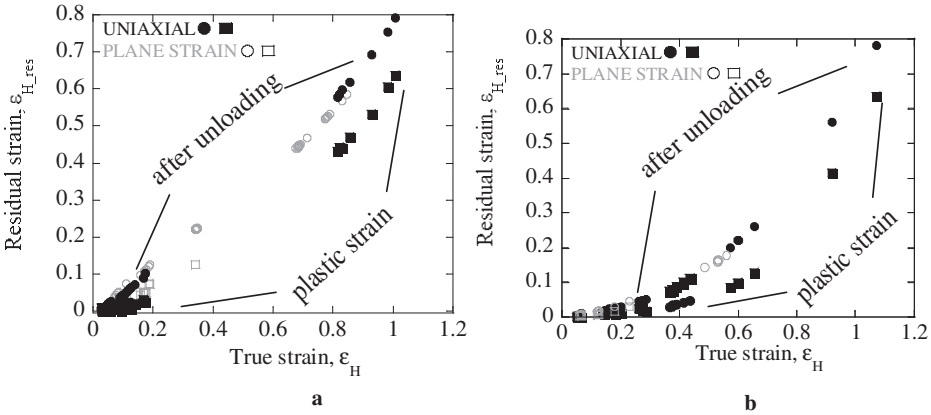

Figure 3: Dependence of the residual strain at the end of the unloading, $\varepsilon_{H\_res,0}$, and after the recovery of the viscoelastic strain component – ε_{H_p} – on the applied strain for HDPE (a) and LDPE (b).

For both the materials the plastic strain, ε_{H_p} ,was measured after a recovery time of the order of magnitude of about 10^4 s after which no significant strain recovery was observed. For both the materials the residual strain at the end of the unloading, $\varepsilon_{H\_res,0}$, and after the recovery of the viscoelastic strain component – ε_{H_p} - are independent of the stress state in the limit of the experimental error.
In Figure 4 a detail of Figure 3 reporting only the plastic strain component, ε_{H_p}, as function of the applied strain up to $\varepsilon_H = 0.25$ for both the materials and the stress states is shown.

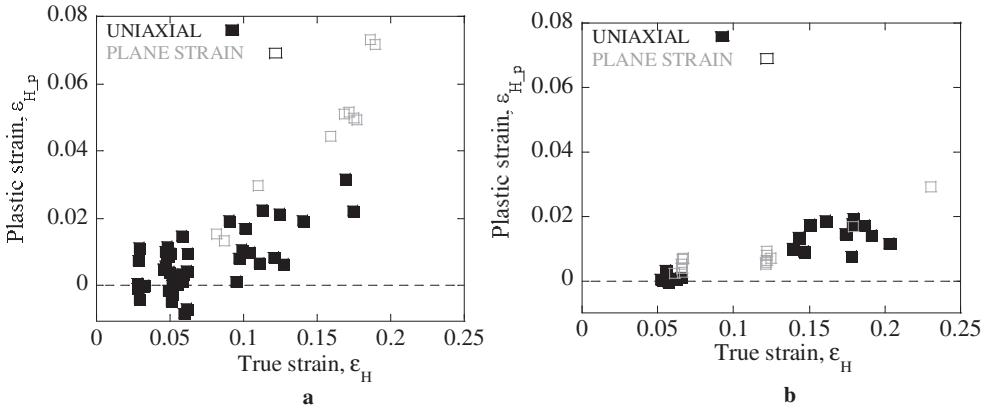

Figure 4: Detail of Figure 3.(a) Data relevant to HDPE (b) data relevant to LDPE.

Because of the data dispersion, it was not easy to perform the back-extrapolation of the plastic strain component, ε_{H_p}, as function of the applied strain to obtain the yield onset. Therefore the yield strain was determined as the mean value between that where the plastic strain oscillates around zero and that where it is definitely positive.
Irrespective of the stress state the strain at yield onset resulted to be very similar for the two polyethylenes: 0.075 ± 0.02 for HDPE and 0.08 ± 0.03 for LDPE.
These results is in agreement with the point B (yield point) determined by Strobl et al. [4-7] and by Bartczak [8].

Conclusions

The main finding of this work is that for the two polyethylenes studied the strain at yield onset does not significantly depend on the stress state.
It would be interesting to examine other stress states and to extend the research to other materials.

References

[1] Quinson R.; Perez J.; Rink M.; Pavan A., *J. Mater. Sci.* **1996**, *31*, 5,4387- 4397
[2] Quinson R.; Perez J.; Rink M.; Pavan A., *J. Mater. Sci.* **1997**, *32*, 5,1371-1379
[3] Fasce L.A; Pettarin V.; Marano C.; Rink M.; Frontini P.M., *Polym. Eng. Sci.* **2008,** 1414-1423
[4] Hiss R.; Hobeika S.; Lynn C.; Strobl G., *Macromolecules* **1999**, *32*, 4390-4403
[5] Hong K.; Rastogi A.; Strobl G., *Macromolecules* **2004,** *37*,10265-10173
[6] Men Y.; Rieger J.; Strobl G., *Phys. Rew. Lett*. **2003**, *91*, 095502-1
[7] Hobeika S.; Men Y.; Strobl G., *Macromolecules* **2000**, *33*, 1827-1833
[8] Bartczak Z., *Polymer* **2005**, *46*, 10339-10354

Ringraziamenti

Le prime persone che vorrei ringraziare per avermi aiutata a scrivere questo lavoro di tesi sono le Prof. Marta Rink e Claudia Marano. I loro suggerimenti, la loro disponibilità e anche il loro affetto sono stati degli ingredienti fondamentali per portare alla luce questo lavoro. I momenti di approfondimento e riflessione che hanno portato al compimento di questo lavoro mi hanno dato l'opportunità sia di capire più a fondo il complesso "mondo" dei polimeri semicristallini che di comprendere come stilare un lavoro scientifico. Vorrei inoltre ringraziare il Prof. Andrea Pavan i cui suggerimenti e "illuminazioni" mi hanno permesso in questi anni di entrare sempre più nella natura più intima dei materiali polimerici. Il suo sguardo esterno e la sua lunga esperienza nel mondo accademico mi hanno consentito di migliorare la mia attitudine al lavoro di laboratorio e mi hanno anche preparata forse ad un mondo in cui l'accademia ne è solo uno degli attori. Quindi ringrazio anche il Prof. Briatico e il Prof. Frassine che, con la loro critica costruttiva, hanno reso il mio lavoro più completo e mi hanno permesso di indagare altri aspetti del mondo dei materiali polimerici. Ringrazio tutti gli altri membri del gruppo ma soprattutto i miei meravigliosi colleghi che nel tempo sono diventati i miei migliori amici : Michele, Susanna, Marco, Natalia, Tommaso, Sharham, Lidia, Andrea, Emanuele, Roby, Manù, Caterina e tutti gli altri che hanno reso questi 4 anni pieni di amicizia e di allegria. Vorrei ringraziare anche tutti i miei colleghi con cui ho lavorato in Olanda: Marc, Harm, Martin, Peter, Emanuele, Lili, Enrico, e tutti coloro che mi hanno aiutato a superare le piccole grandi difficoltà che si incontrano in un Paese straniero.

Rivolgo un ringraziamento particolare al Prof. Leon Govaert che con il suo sorriso, la sua grinta e il suo sapere mi ha dato la possibilità di fare una bellissima esperienza tanto lavorativa quanto personale. Mi ha insegnato un altro modo di lavorare e di affrontare i problemi in un laboratorio di ricerca.

Vorrei a questo punto ringraziare con tanto amore la mia famiglia: papà Renato, mamma Paola e mia sorella Sara che mi hanno tanto sostenuto in questo lungo, difficile ma divertente percorso benchè lontani nello spazio ma vicini a me con il loro immenso affetto.

Un ringraziamento particolare va anche a Roberto, alla zia Nadia, a Giada, Camilla, Luca e Silvia con i due loro splendidi bambini, che mi hanno accolta in casa loro come una figlia e hanno creduto nel mio progetto talvolta più di quanto io stessa vi credessi.

E infine un grazie particolare con tutto il mio cuore al mio compagno Marcello che con il suo amore e la sua pazienza mi ha permesso di arrivare fino alla fine di questa impresa incoraggiandomi sempre a credere in me stessa e nelle mie capacità e amandomi come il più dolce degli uomini.

Acknowledgements

The first people that I would like to thank you for helping me to write this thesis are Prof. Marta Rink and Prof. Claudia Marano. Their suggestions, their availability and also their endearment have been the key ingredients to bring out this work. I would like also to thank Prof. Andrea Pavan whose suggestions and "illuminations" in these years have allowed me to enter more and more into the intimate nature of the polymeric materials. His exterior look and his long experience in the university have allowed me to improve my ability to work into a laboratory and they have also prepared me, perhaps, to enter in a world where the academy is only one of the actors. I would like also to thank Prof. Briatico and Prof. Frassine: their constructive criticism have made my thesis work more complete and have allowed me to investigate other aspects of the world of polymers. I thank all the other members of my group but especially my wonderful colleagues who over time have become my best friends: Michele, Susanna, Marco, Natalia, Tommaso , Sharham, Lidia, Andrea, Emanuele, Roberto, Manù, Caterina and all others who have made these 4 years full of friendship and joy. I would like to thank all my colleagues with whom I have worked in the Netherlands: Marc, Harm, Martin, Peter, Emanuele, Lili, Enrico, and all those who have helped me to overcome the little big difficulties encountered in a foreign Country. I extend a special thanks to Prof. Leon Govaert who with his smile, his determination and his knowledge has given me the chance to make a great job but also a great personal experience. He has taught me a different way to work and to deal with problems in a research laboratory.

I would like to thank with so much love my family: dad Renato, mother Paola and my sister Sara who have so much sustained me in this long, difficult but fun journey even though they were distant in space but near to me with their endearment.

Special thanks also to Roberto, Nadia, Giada, Camilla, Luca and Silvia with their two beautiful children, who have welcomed me into their home as a daughter and who have believed in my project sometimes more as for myself I thought.

And eventually I would like to thank you with all my heart my boyfriend Marcello who with his love and patience has allowed me to get to the end of this enterprise always encouraging me to believe in myself and in my abilities and loving me like the sweetest men.